Muons in UA1; the second level trigger and dimuon results

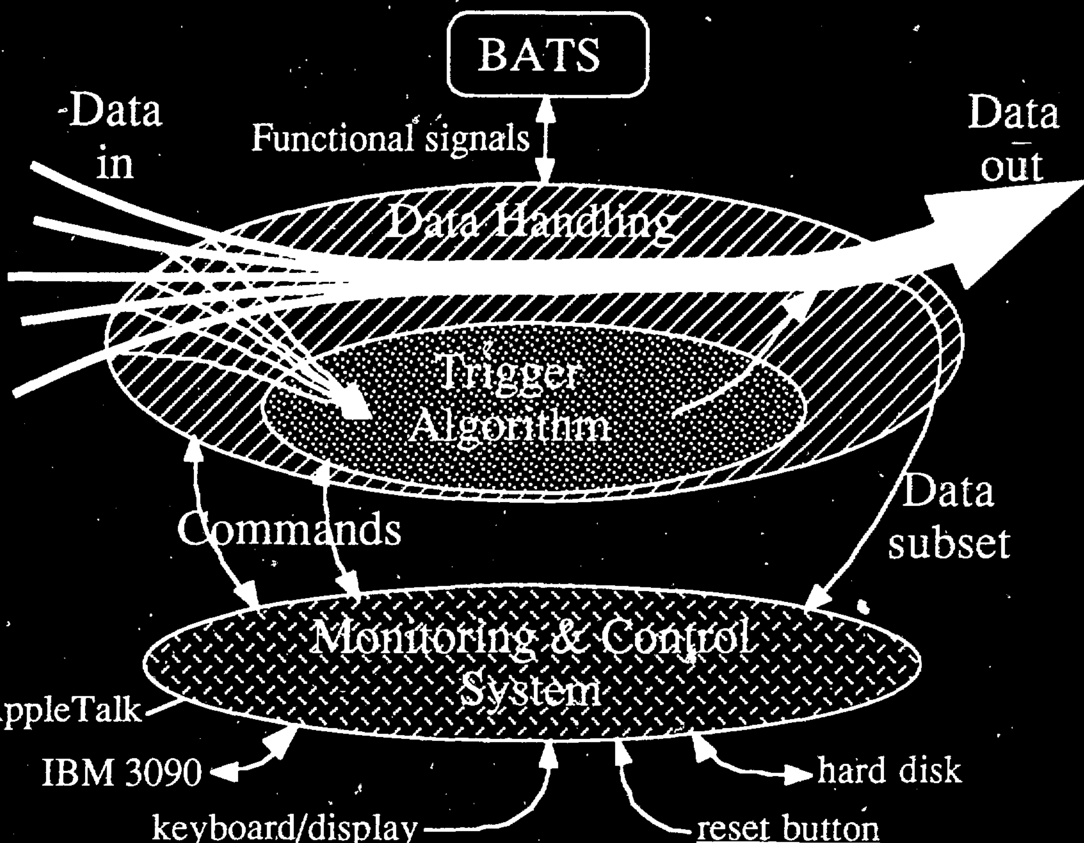

A. L. van Dijk

Muons in UA1;
the second level trigger
and dimuon results

ACADEMISCH PROEFSCHRIFT

ter verkrijging van de graad van doctor aan de Universiteit van Amsterdam,
op gezag van de Rector Magnificus Prof. Dr. P. W. M. de Meijer,
in het openbaar te verdedigen in de Aula der Universiteit
(Oude Lutherse Kerk, ingang Singel 411, hoek Spui)
op dinsdag 26 februari 1991 te 15:00 uur.

door

Adriaan Louis van Dijk

geboren te Amsterdam

Promotor: Prof. Dr. J. J. Engelen

Co-Promotor: Dr. K. Bos

The work described in this thesis is part of the research program of the 'Nationaal Instituut voor Kernfysica en Hoge Energie Fysica (NIKHEFH)'.
The author was financially supported by the 'Stichting voor Fundamenteel Onderzoek der Materie (FOM)'.

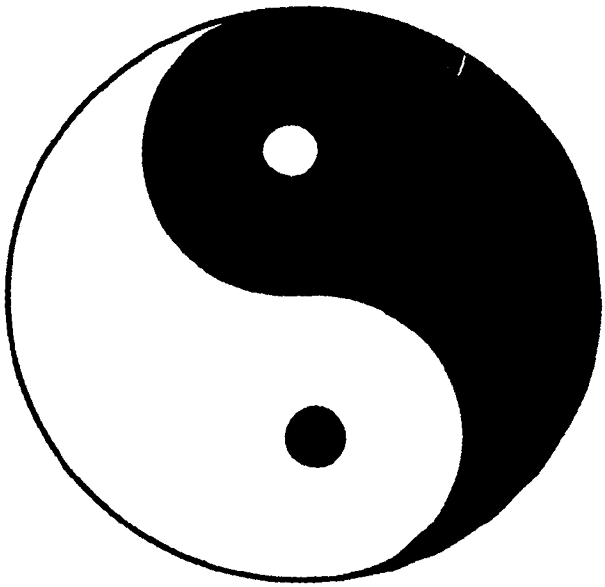

Contents

It is a contradiction to write “this page is intentionally left blank”.

I

Introduction

1.1. Proton-antiproton physics, motivation

The suggestion of converting the Super Proton Synchrotron (SPS) at CERN into a collider with contra-rotating beams was presented in 1976 by C. Rubbia et al. [1.1]. The original proposal suggested the acceleration of both proton and antiproton beams up to an energy of 273 GeV[1] and in its third year of operation this was upgraded to 315 GeV. In fact, this proposal relied heavily on ideas worked out by S. van der Meer to create intense beams of anti-matter using stochastic beam cooling techniques [1.2]. The hadron accelerators (CERN, FNAL) operational in the seventies were mainly providing proton beams ($\approx$ 400 GeV) for fixed target experiments, resulting in a rather limited center of mass energy accessible by these experiments ($\sqrt{s} \approx 28$ GeV.). Having two colliding beams would drastically increase the total amount of energy available for an interaction, namely, $\sqrt{s} \rightarrow 2 * 315 = 630$ GeV. The Intersecting Storage Rings (ISR), a collider of two proton beams operating at CERN, already had proven that it was technically possible to build such a device. However, the energy range accessible by the ISR was still about an order of magnitude lower ($\sqrt{s} \approx 30$ - 60 GeV.) than what was foreseen for the modified SPS.

Clearly, the reason for exploring a new energy range was a combination of both experimental results and theoretical achievements. The discovery of the neutral currents [1.3] and the development of gauge theories lead to an extremely elegant theoretical model, the so-called 'Standard Model' of weak and electromagnetic interactions. This model, originally proposed by Glashow [1.4] and modified by Weinberg [1.5] and Salam [1.6], is based on the ideas of gauge invariance and spontaneous symmetry breaking via the Higgs mechanism [1.7]. Many reviews are available, in ref. [1.8] a small selection is given.

There were many indirect indications that the carriers of the weak force would be very massive (80 - 90 times the mass of the proton). Therefore, it would be challenging to try and observe these carriers, the weak $W^{\pm}$ and Z^0 bosons, in a more direct way. Determination of both their mass and decay-width would enable precise tests of the predictions made by the Standard Model.

Efforts were not only made in the field of unification of the electromagnetic and weak forces. Also the strong forces were brought into the spotlight. Although theories on this subject have already been around since the 1930's, it was only in the 1970's that a more complete theory was developed, based on the same 'gauge' principles. The so-called theory of 'Quantum Chromo Dynamics' (QCD) [1.9] assumes that the mediators of the strong force form a set of eight massless gluons. These gluons only couple to quarks or to themselves; the coupling to leptons is completely absent. First experimental evidence for the existence of gluons was found at experiments at the e^+e^- collider at PETRA (Hamburg) [1.10] where events containing more than two hadronic jets were observed. Closer analysis of the data showed almost complete agreement between experiment and QCD predictions for the overall properties of these events. In principle QCD also describes $\bar{p}p$ interactions. In practice

[1]Crucial in this energy range is the production possibility of particles of around 90 GeV.

it is only possible to perform realistic calculations if the application of perturbation theory is justified. This means that there has to be a reasonably large energy transfer in the basic (strong) interaction. For example, the agreement between experiment and perturbative QCD predictions for heavy flavour production at the $p\bar{p}$ collider turns out to be remarkably good.

1.2. The CERN proton-antiproton collider

The main idea behind the SPS collider project was based on the assumption that both protons and antiprotons can be accelerated in the same ring. The similarity between the two particles, their mass and the opposite charge would even enable the use of a single set of magnets with both particles traveling inside the same beam pipe. There was no reason whatsoever to believe in a significant difference between the lifetime of the proton and the antiproton. Thus, one could build a collider by modifying an existing accelerator facility. Defining the total number of interactions as the product of cross-section and integrated luminosity, it is obvious that the luminosity itself, $\mathcal{L}$, depends on beam dimensions, number of bunches per beam (n) and particle concentrations

$$\mathcal{L} = f\,n \frac{N_1 N_2}{\sqrt{\varepsilon_y \beta_y}\sqrt{\varepsilon_z \beta_z}} \tag{1.2}$$

with N_1 and N_2 the number of protons and antiprotons per bunch, ε the emittances and β the betatron functions at the intersection point for both transverse projections. In order to reach a high luminosity, so that processes with lower cross-sections can be probed, the revolution frequency (f) should be high, while the size of the interaction region should be small ($\varepsilon.\beta$). Special focusing magnets near to the interaction regions are therefore required as well as a reasonable amount of antiprotons. In order to be able to observe particles with a mass as large as expected for the $W^\pm$ and Z^0 bosons, an integrated luminosity of at least 100 nb^{-1} was foreseen to be necessary. This corresponds to luminosities in the order of $\mathcal{L} \approx 10^{29}$ - 10^{30} $cm^{-2}s^{-1}$.

To reach these high luminosities the problem of creating sufficiently intense beams of antiprotons had to be solved. As already indicated in § 1.1, stochastic beam cooling could provide these intense beams. A dense 26 GeV proton beam is dumped into a copper target. Among the many particles that emerge there is a small amount of antiprotons. The fraction of antiprotons is $\approx 10^{-6}$. The so-called Antiproton Accumulator (AA) collects about $5 * 10^6$ antiprotons with an energy of $\approx$ 3.5 GeV per pulse of $\approx 10^{13}$ protons. These antiprotons are stored and the size of the beam is squeezed while the momentum of the antiprotons becomes very well defined. In other words, the motion of the antiprotons is 'cooled'. The technique of cooling is based on measuring the average position and momentum of the particles inside the beam. Beam squeezing is attained by kicking the particles into the right direction, with the help of magnets. Repeatedly adding new antiprotons leads to a stable high density beam stored in an additional (inner) ring of the AA. This procedure of stochastic cooling was first successfully verified with proton beams [1.12].

The organization of beam transfer and acceleration can be best explained on the basis of a sketch of the CERN accelerator complex, in figure 1.1 below:

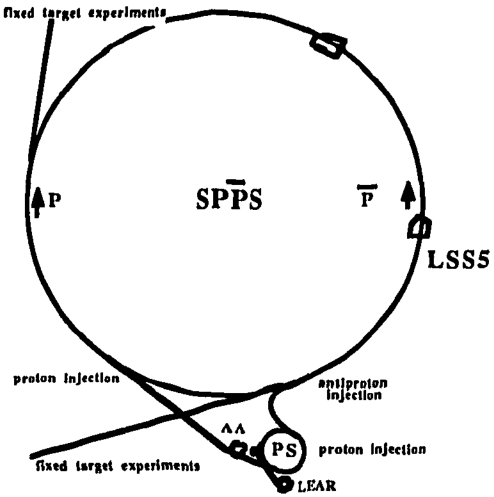

Fig. 1.1: Top view of the CERN proton-antiproton accelerator complex.

Since stacking and cooling of the antiprotons takes place in two separated rings, the transfer of the antiprotons to the Proton Synchrotron (PS) can take place at any time, while the collection of new antiprotons continues. In the PS the dense antiproton beam is accelerated to 26 GeV. After having reached stable beam conditions the antiprotons are injected into the SPS in six bunches. The proton beam undergoes a similar procedure: after acceleration in the PS, the protons are injected in the opposite direction into SPS. Finally, both beams are accelerated to 315 GeV per beam. One single revolution of a particle in the SPS takes about 23 μs. There are two large experimental areas. The LSS4 area contains the UA2, UA4 and UA5 experiments, while the LSS5 area accommodates the UA1 detector.

1.3 Collider performance and physics achievements.

After the approval of the collider project in June 1978, it took only two years until the first successful operation of the AA was reported. The PS received and accelerated its first antiprotons in February 1981. In the same year both protons and antiprotons were injected into the SPS and stable beams of 273 GeV each were achieved. Each proton bunch contained $\approx 10^{11}$ protons while the contents of each antiproton bunch was about an order of magnitude lower: $\approx 10^{10}$ antiprotons.

The two enormous UA1 and UA2 detectors became operational at the 10th of July 1981 when UA1 reported the first interactions [1.13] seen by their detector. Physics runs started in October 1982 and lasted for two months. Already over this period both UA1 and UA2 results were extremely promising. About 25 nb^{-1} of luminosity was recorded by the UA1 collaboration and serious analysis was started. Rapid data acquisition and data transfer allowed for fast preliminary analysis and it was already in the first month of 1983 that UA1 and UA2 each announced a handful of $W^{\pm}$ candidates [1.14]. This culminated in a press conference on the 25th of January where CERN officially presented the discovery of the charged weak boson. The mass of this particle turned out to be surprisingly close to the theoretical predictions, $\approx$ 80 GeV/c^2. The neutral partner was expected to be slightly heavier and more data was needed to establish its existence. A long period of running in the beginning of 1983, with improved machine performance, finally resulted in the official announcement (1 June 1983) of the discovery of the Z^0 [1.15]. Since then the performance of the collider has steadily improved as illustrated in table 1.3.1:

Table 1.3.1: Average- and integrated luminosity of the SPS collider.

Year	Average $\mathcal{L}$	Integrated $\mathcal{L}$
1982	*0.5 * 10^{29} $cm^{-2}s^{-1}$*	*18 nb^{-1}*
1983	1.6 * 10^{29} $cm^{-2}s^{-1}$	108 nb^{-1}
1984	3.6 * 10^{29} $cm^{-2}s^{-1}$	254 nb^{-1}
1985	4.0 * 10^{29} $cm^{-2}s^{-1}$	330 nb^{-1}
1987	4.0 * 10^{29} $cm^{-2}s^{-1}$	400 nb^{-1}
1988	0.5 * 10^{30} $cm^{-2}s^{-1}$	1.3 pb^{-1}
1989	1.2 * 10^{30} $cm^{-2}s^{-1}$	3.5 pb^{-1}

Besides the luminosity improvements there was a significant increase in beam lifetimes[2]. In 1982 lifetimes of several hours were recorded while in 1989 lifetimes of more than 30 hours at a luminosity of 1.2 * 10^{30} $cm^{-2}s^{-1}$ were usual. The beams were only dumped in order to increase the luminosity again (maximization of integrated luminosity) and for maintenance.

In 1987 the AA and SPS were upgraded and a new ring was added, 'ACOL' [1.11], to improve the luminosity and lifetime with an order of magnitude. Peak luminosities of 4.0 * 10^{30} $cm^{-2}s^{-1}$ were obtained resulting in an average integrated luminosity of $\approx$70 nb^{-1} per day to be compared with the 108 nb^{-1} for the whole 1983.

[2] The luminosity degrades exponentially: the decay constant is called the lifetime.

1.4. Jets, muons, heavy flavours and flavour mixing

Analysis of the data collected in the short 1982 run showed that jet production at the collider is significant. A detailed comparison of experimental data with QCD indeed shows that jet production at the collider is well described by perturbative QCD [1.16].

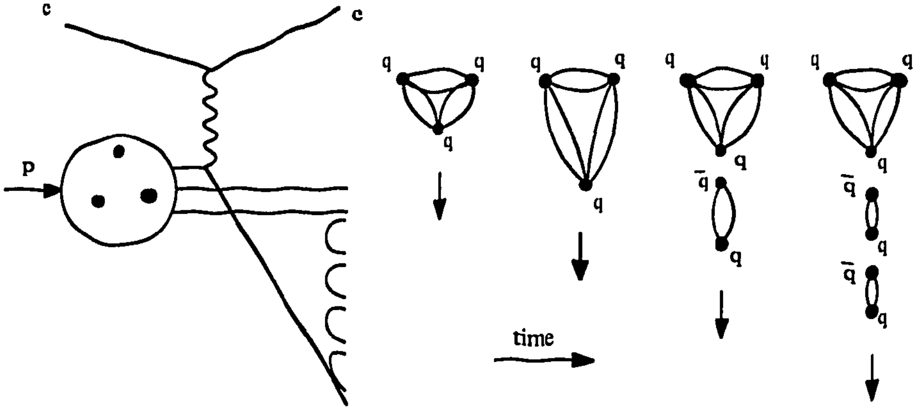

Fig. 1.2 Quark fragmentation in electron-proton scattering. The hadronization (creation of $q\bar{q}$ pairs) is sketched in the form of a chain. The right diagram shows at successive time intervals, the struck quark leaving the proton.

Jet production is the result of the hadronization of quarks (and/or gluons) that occur in the final state of a hard scattering process. Such a hadronization process is illustrated in fig. 1.2 where the relatively simple case of deep inelastic electron-proton scattering is considered. In this thesis we will concentrate on the production of heavy quarks. Detailed measurements in e^+e^- annihilation experiments have shown that heavy quarks on average lose only little energy in the fragmentation process. Thus production of high momentum heavy quarks generally leads to high momentum heavy hadrons. The decay of these heavy hadrons is studied in the much 'cleaner' e^+e^- experiments and shows that heavy flavour decay properties are very well described by phenomenological models based on the weak decay of heavy quarks. In the (3 - body) semileptonic decay of an energetic heavy hadron the lepton will take a significant amount of energy. Hence, the direction of the lepton will be strongly correlated with the original quark direction. The hadrons from the fragmentation as well as from the subsequent decay of the heavy hadron surround the lepton. This effect is certainly weaker when the heavy quarks are produced almost at rest. By demanding a significant lepton energy, which is also necessary to minimize the background from kaon and pion decays (see chapter VI), and by demanding a significant hadronic activity close to the lepton we are able to indirectly select high momentum heavy hadrons.

In the presence of hadronic activity, muons can be rather well identified, even at relatively low momenta. This is in strong contrast with electrons which suffer from a significant misidentification background due to pions and photons. Shortly after the discovery of Z^0 decays into a pair of muons, the search for dimuons has been extended down to muon pairs with a mass as low as the mass of the J/ψ particle (3.1 GeV/c^2). Besides the electromagnetic production of lepton pairs and of lepton pairs from the decays of J/ψ and Υ we expect a significant amount of dimuons from heavy flavour decays. These multilepton final states can be separated into combinations of first generation charm and bottom decays, for example:

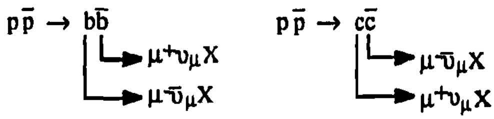

fig. 1.3 First generation muon pair production schemes.

and combinations of first and second generation bottom decays. For example:

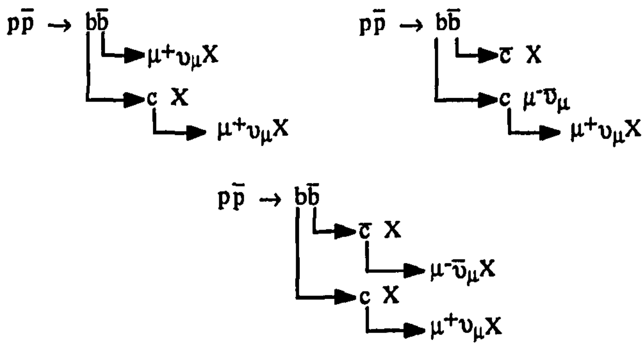

fig. 1.4 Second generation muon pair production schemes.

At each weak decay a lepton may be produced. The cross-section for the production of top hadrons is significantly suppressed compared to charm and bottom hadrons due to the relatively high mass of the top quark[3]. If the top quark mass is larger than the W mass it will decay exclusively into W's. *In this thesis we do not consider top quark production.*

The production mechanisms for like- and unlike-sign muon pairs are different. In the absence of background and mixing there is no like sign dimuon first generation production. A source of same-sign dimuon events is the combination of a first generation muon from the b-decay and a second generation muon from the $\bar{b}$-decay or vice versa.

Mixing is also a possible source for same-sign dimuons. When either a B^0-meson or the $\bar{B}^0$-meson changes into its antiparticle the lepton in the subsequent decay chain will change sign. This mixing between B^0-mesons and $\bar{B}^0$-mesons then gives rise to same-sign dimuon events where both muons are from the first generation. To enhance this effect one can impose kinematical cuts on the muon momentum and the invariant dimuon mass that remove most of the second generation muons.

---

[3]Presently the top mass limit is $m_t \geq 77$ GeV/c^2 by CDF [1.17].

1.5 Outline of this thesis.

This thesis can be divided into two parts. First there is the development, construction, testing and operation of the second level trigger for the UA1 experiment. Subsequently the analysis of dimuons is discussed.

Chapter II describes the various parts of the UA1 experiment. Chapter III describes the data acquisition as a whole and the triggers in more detail. This chapter explains the motivation, philosophy and design criteria of the second level muon trigger. Chapter IV is completely dedicated to the construction of the second level muon trigger systems and all related hard- and software. Finally, Chapter V presents its performance.

Chapters VI and VII are about data analysis; chapter VI explains the theoretical expectations while chapter VII describes the dimuon samples. Chapter VII starts with a description of the data processing and event reconstruction. After a discussion of possible background sources, the muon samples are defined. A next section discusses the mass spectrum. The following sections describe the J/ψ and Υ in detail and the last section is about b production in general, focused on the b production cross-section.

II

The UA1 Experiment

2.1. Introduction

The proposal for the UA1 experiment (named after the experimental 'Underground Area 1') was presented in 1978 [2.1]. Among another series of proposals [2.2], the UA1 apparatus turned out to become not only the most complete but also the largest detector. The SPS ring contains straight sections of which the LSS5 area (see fig. 1.1) accommodates the huge UA1 apparatus. The experimental floor is about twenty meters under ground. Part of the testing and construction of the apparatus had to be carried out at the location itself while other parts were built by participating groups in their home laboratories. During the construction period, it was foreseen to keep the SPS accelerating protons for fixed target experiments. In addition, the SPS had to be kept operational for machine development, since turning it into a collider had to be achieved in parallel with the construction of the new collider experiments. This led to the design of removable shielding between the SPS-tunnel and the so-called 'garage' were the movable detector was assembled.

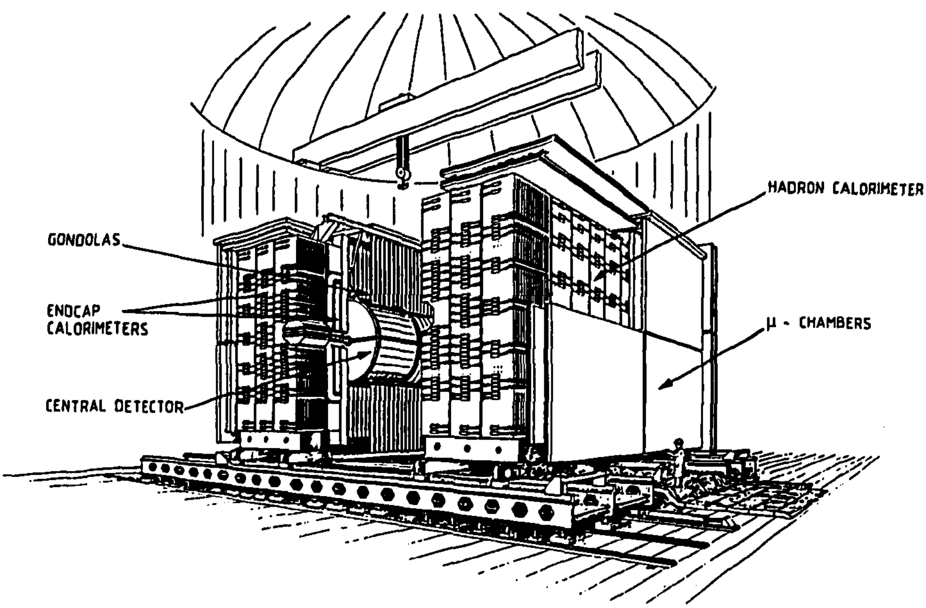

fig. 2.1: *Artist's view of the UA1 detector.*

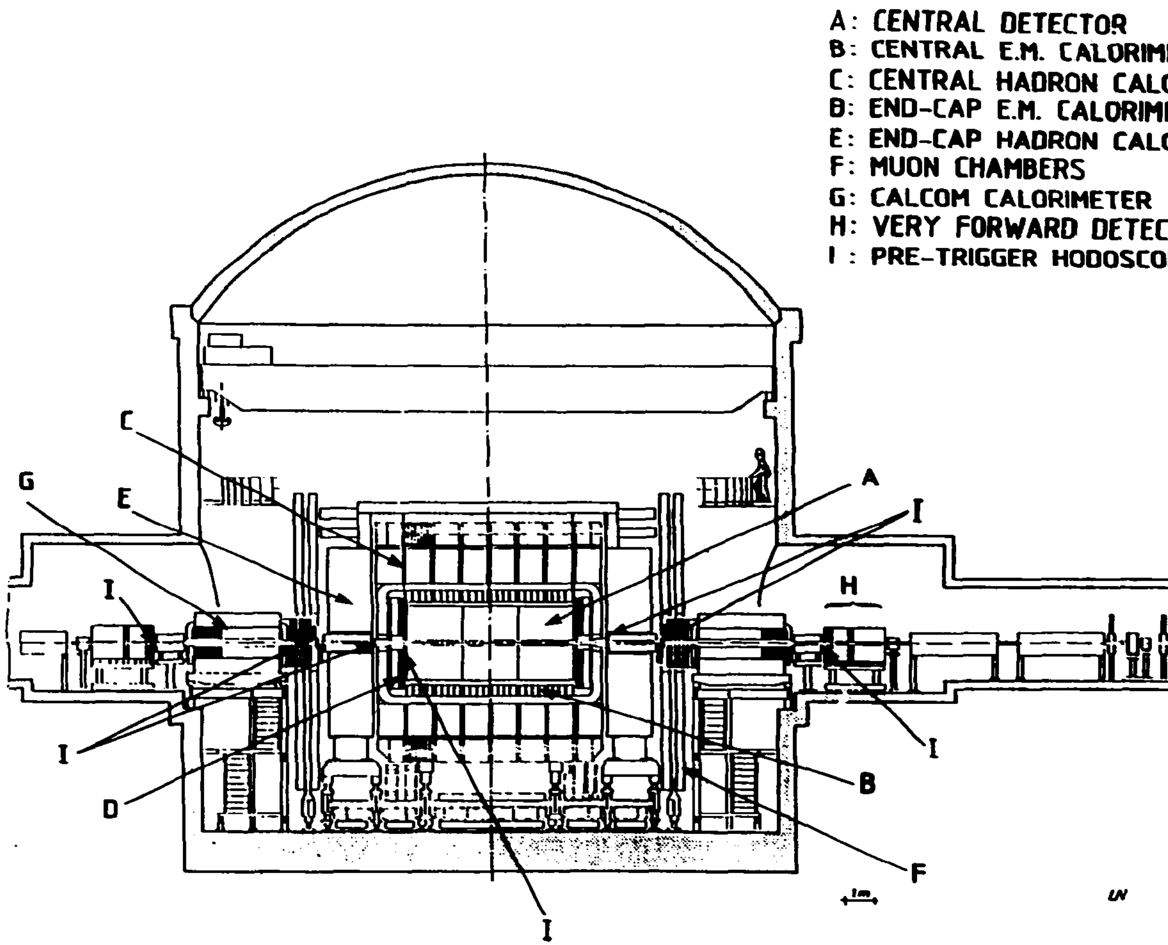

fig. 2.2: Cross-section of the UA1 detector along the beam.

Apart from a shut-down period in order to perform the excavations needed for preparing the experimental area, the new developments would not disturb the scientific program of CERN at that time too much. Cabling, gas connections etc. were designed in such a way that the detector could be operational in both the garage and at the SPS-ring. The complete apparatus is placed on a rail system so that it can be moved between the two locations.

Fig. 2.1 gives an artist's view of the opened detector while fig. 2.2 shows a cross-section along the beam. In both representations the beam pipe and transport system are clearly visible. The almost 4π coverage (polar angle from the beam direction: $\theta = 0.2°$) of the apparatus makes its possible to 'detect' escaping particles. Non-interacting particles will cause an energy-imbalance after the full event is reconstructed ('missing energy'). By this method the transverse momentum of a neutrino can be determined. The longitudinal momentum cannot be reconstructed since particles produced under small angles are not detected.

In the following sections we will briefly discuss the main features of the apparatus. Starting from the interaction region in the very center, the measurement of the momenta of charged particles is achieved by the 'Central Detector', which is placed inside a magnetic field and which will be described in section 2.3. The magnetic field is perpendicular to the beam pipe to enhance the momentum measurement in the forward region. The coil is made of aluminium (Aluminium has a bigger radiation length than copper and is cheaper). The iron return yoke of the magnetic field has been instrumented with scintillator plates and serves as the hadron calorimeter. Most particles (except muons and neutrino's) will be absorbed in this calorimeter and their energy deposition can be measured. The hadron calorimeter will be described in section 2.4. 'Minimum ionizing' muons will pass all this material provided they have sufficiently large energy. They will be detected in wire chambers at the very outside of the apparatus. These muon chambers will be described in section 2.5. Between the muon chambers and the calorimeter an additional shielding is provided against high energy hadrons leaking through the calorimeters. The shielding also drastically decreases the probability of misidentifying a charged hadron in the muon detector while it also provides an additional barrier for very low momentum muons. In this way the shielding reduces the muon rate, especially from secondary decays.

Up to 1985, the UA1 detector contained an electromagnetic calorimeter placed just outside the CD (called "Gondolas" in fig. 2.2). It absorbed electrons, photons and measured the energy deposited by these particles. This detector has been removed to create room for a new warm liquid type calorimeter (Uranium/TMP). The measurements described in this thesis were performed in the period that the new calorimeter was not in place. In this period the UA1 detector could not properly measure electrons or gamma's. The 'thinner' calorimeter was also a less efficient muon filter. Hadrons were also absorbed less efficiently.

2.2. The UA1 coordinate system.

For a further description of the detector first the coordinate system will be defined.

The origin is at the center of the detector.

The pos. X-axis (transverse to magnetic field) points horizontally in the direction of motion of the antiprotons,

the pos. Y-axis (transverse to magnetic field) points vertically up,
the pos. Z-axis (along magnetic field) points horizontally away of the SPS ring.
φ is the angle in the XY-plane, measured from the +X-axis ($0° < \varphi < 180°$ for Y>0),
λ is the angle measured out of the XY-plane ($0° < \lambda < 90°$)

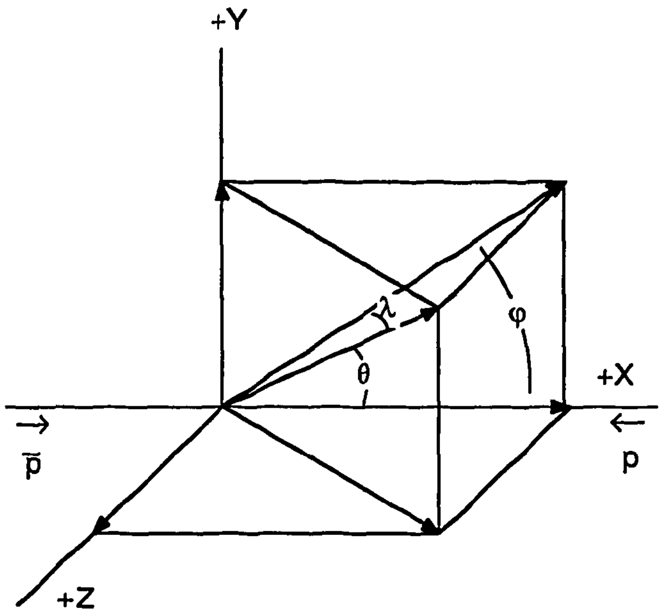

Fig. 2.3 The UA1 coordinate system.

θ is the polar angle measured from the +X-axis ($0° \leq \theta < 180°$),
ϕ is the angle measured in the YZ plane from the +Z-axis ($0° \leq \phi < 360°$),
η is the pseudorapidity calculated from the polar angle with $\eta = -\ln \tan\left[\frac{\theta}{2}\right]$,
p_t is the transverse momentum:

$$p_t = \sqrt{p_y^2 + p_z^2} = |p| \sin(\theta) \tag{2.1}$$

2.3. Central detector (CD)

The ≈ 6000 sense wires of the central detector [2.3, 2.4] form the core of the charged track reconstruction by the UA1 apparatus. The exploded view of this detector in fig. 2.4 shows the in total eight separate drift chambers, grouped in two half cylinders; two in both forward directions, two at the outer central region and another two small ones close to the beam pipe in the central region. The CD as a whole is placed in a uniform magnetic field of 0.7 Tesla, which enables momentum determination through the curvature measurement of the charged tracks via the relation (p in GeV/c):

$$p \approx \frac{0.3\, q\, B\, r}{\cos \lambda} \tag{2.2}$$

with q the charge of the particle, B the magnetic field (Tesla), r the radius of the curvature (meter) in the bending plane and λ the angle out of the plane perpendicular to the field. The total length of the cylinder is 6 meters with a diameter of 2.2 meters. The wires of the six larger modules are all organized into a series of wire planes, defining different drift volumes.

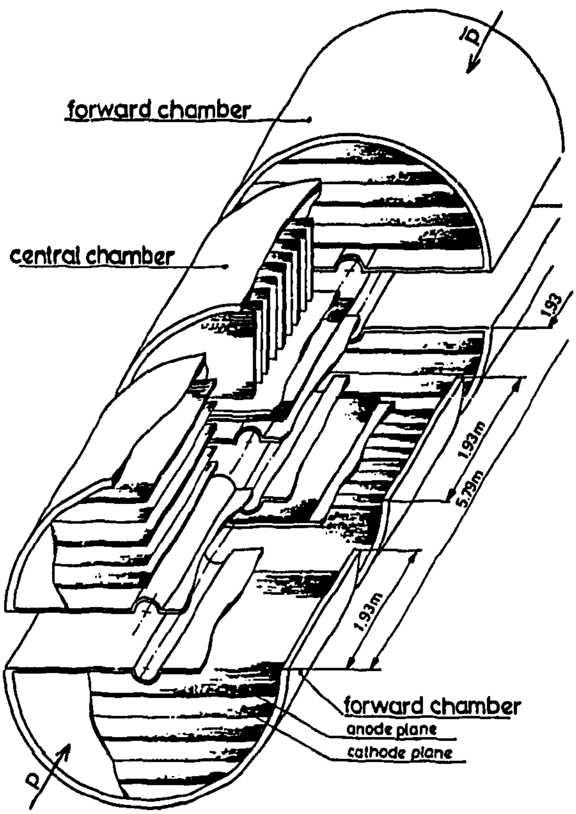

fig. 2.4: Exploded view of the central detector.

Figure 2.5 shows an example of the track reconstruction, where one can distinguish the six drift volumes in each forward module, ten drift volumes per (outer) central module and one single drift volume in each of the small chambers close to the beam pipe. Both magnetic field and wires are oriented horizontally, perpendicular to the plane of fig. 2.5. The special configuration of the planes is optimized in order to have the planes as much as possible in parallel to the 'average' track in each module.

Electrons are freed from the gas by the traversing charged particles. An electric field is created with additional field wires. This field is shaped in such a way that the electrons drift to the sense wires. Very close to the sense wires the gradient increases considerably. The drifting electrons will further ionize the gas, giving rise to an avalanche effect nearby the sense wire. Special field shaping wires control the amplification of the gas. The charge collected in this way is readout and the signal is amplified. Since the magnetic field is oriented parallel to the wires, the charged particles are only bend in the plane of fig. 2.5 (xy-coordinates).

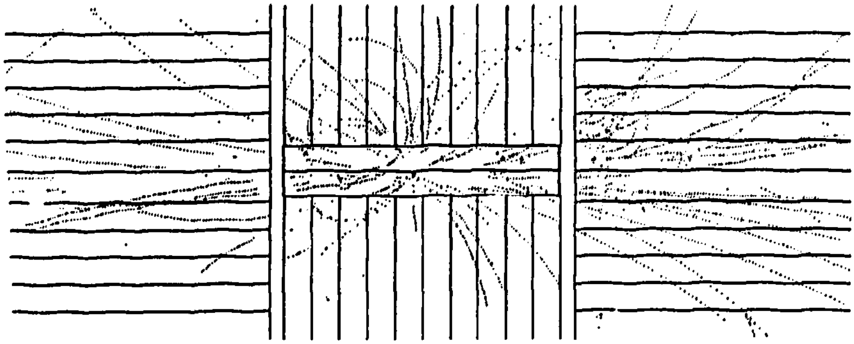

fig. 2.5: The projection of reconstructed tracks in the CD onto the bending-plane (xy-coordinates).

Measurement of the drift time, charge and position of the wire provides an excellent position determination in this plane. The position along the wire is obtained by charge division. For this the sense wire is readout at both ends. The relative amount of charge seen at the two ends provides the position of the track along the wire. The drift volumes are constructed in such a way that a maximum drift time of 3.5 μs is achieved, which is still smaller than the bunch crossing period of 3.8 μs.

The huge amount of combinatorials that appear when one tries to reconstruct a track in the CD demands a special algorithm. The basic idea behind the so-called chaining procedure (see §7.1.3) relies on the observation that neighboring points belonging to the same track are in general closer than points on nearby tracks. A parabolic path is used to build a chain of consecutive points. This leads to a typical momentum resolution of

$$\frac{\Delta p}{p^2} \approx 0.005 \ [\ \mathrm{GeV/c}]^{-1} \qquad (2.3)$$

However, the resolution for each track depends strongly on its location in the CD. The quality of the momentum determination also gives the confidence level for the charge determination. A detailed description of the algorithm can be found in ref. [2.5]. To adjust for the higher collision rate (space charge effects) in 1987, 1988 and 1989 the potential of the field wires was reduced and at the same time the amplification of the pre-amplifiers was increased. This introduced more noise and therefore made the trackfinding more difficult.

2.4. The Hadronic Calorimeter

The calorimeter consists of 'C'- and 'I'-modules. The so-called 'C-modules' cover the central regions of the detector while the 'I-modules' are placed at the ends enclosing the beampipe. Fig. 2.6 shows of a C-module. The central part of the calorimeter is made out of sixteen of these rectangular C-shaped modules, whereas the end-caps consist of six I-shaped modules each. Both types of modules are made of iron/scintillator sandwiches, with layers 5 cm of iron and 1 cm of scintillator.

Each C-module is azimuthally segmented into twelve sections and is sampled at two depths. For each sampling the light is collected by a pair of phototubes via wavelength shifters and light guides.

Note that the aluminium coil also acts as an absorber in which particles loose energy. There exists a procedure to correct for this.

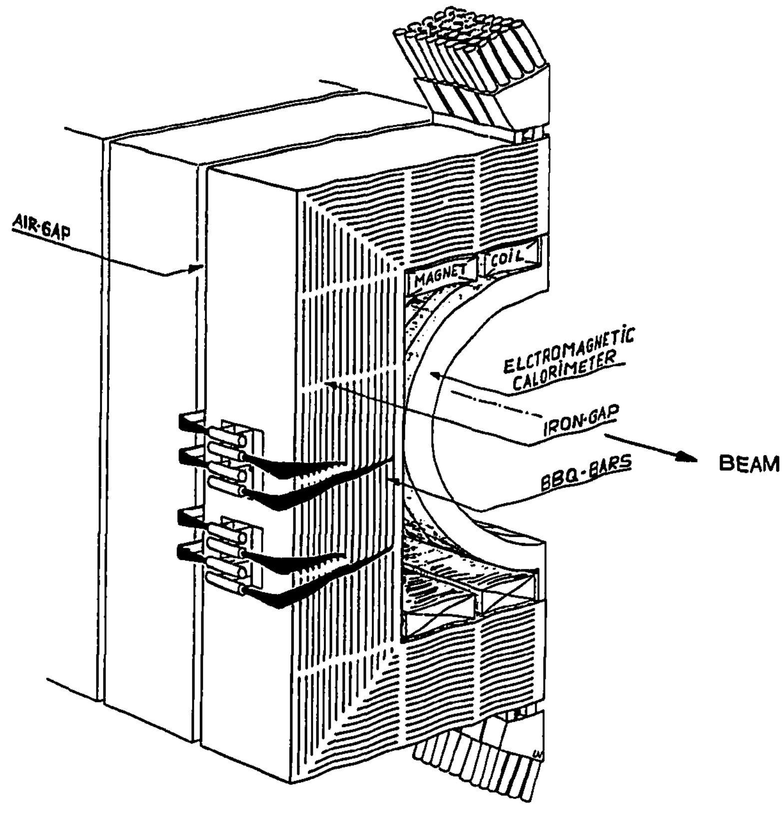

fig. 2.6. C-shaped modules of the central hadronic calorimeter.

The end-cap calorimeters (so-called I-modules, see fig. 2.7) are subdivided into six stacks. The modules closest to the beam are again subdivided into four smaller stacks since the hadronic activity in this region is bigger. Except for the difference in interaction lengths, the readout of the I's is similar to the readout of the C-modules.

The hadronic energy resolution of the calorimeter is (with E in GeV)

$$\frac{\sigma(E)}{E} \approx \frac{0.8}{\sqrt{E}} \tag{2.4}$$

The ratio of the response of electrons to hadrons is

$$\frac{e}{\pi} \approx 1.4 \pm 0.1 \tag{2.5}$$

The interaction length is

For the C-modules: 2*2.5 (at normal incidence) (2.6)

For the I-modules: 2*3.5 (at normal incidence) (2.7)

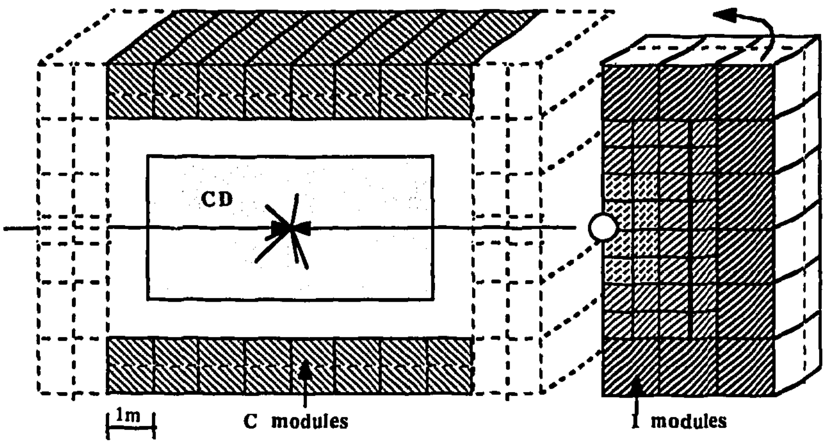

fig. 2.7: Ordering of the stacks of a hadronic end-cap calorimeter (left). The right figure shows the top or side view of the calorimeter

2.5. Muon detection system

The muon chambers [2.6] form the outermost part of the UA1 detector and cover about 70 % of the solid angle in the rapidity range of $-2.5 \leq \eta \leq +2.5$. The various gaps between the different chambers are due to construction limitations. One of the main reasons for the lack of coverage is that the original shielding of the chambers turned out to be not sufficient. The room needed for additional shielding forced the muon chambers further away from the interaction point, leaving larger gaps between the chambers. However, within the quoted rapidity range the geometrical acceptance never drops below 60 %. Except for the bottom chambers, which measure 1 x 6 meters and 5 x 6 meters, the muon detector is subdivided into units of 4 x 6 meters. Each unit contains four layers of drift tubes, two by two in orthogonal projections (fig. 2.8), except again for the bo' ɔm chambers which have only one projection. The width of a drift tube is 15 cm. Two units of four planes are stacked with a relative distance of about 60 cm. In order to resolve the 'left-right ambiguity' the tubes of two adjacent planes are staggered and form a so-called doubleplane.

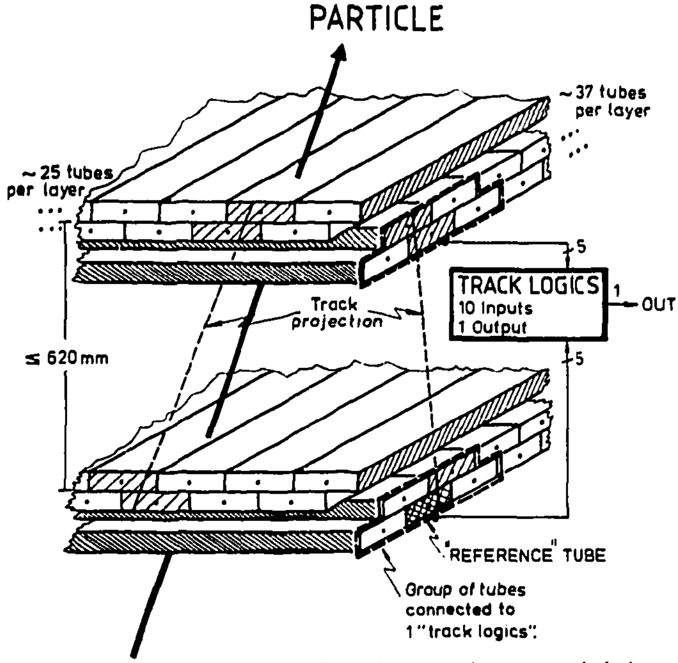

fig. 2.8: Schematic view of the muon detector. Two units of four planes are stacked whereas the tubes in adjacent planes are staggered in order to resolve the left-right ambiguity.

A cross-section of a drift tube is shown in fig. 2.9 with a muon traversing the tube under 20°. The electrons freed by a traversing muon drift to the anode wire which is shielded in such a way that only the electrons from part of the trajectory can easily reach the wire (see fig 2.9). The maximum drift time is 1.5 μs, small enough for the bunch crossing period of 3.8 μs.

In the *bottom* chambers, the charge is collected at both ends of the anode and amplified. The time difference of the signals at both ends, indicates the position of the hit along the tube. In this way a resolution of 0.3 m can be obtained. For the other chambers only the hit time is measured.

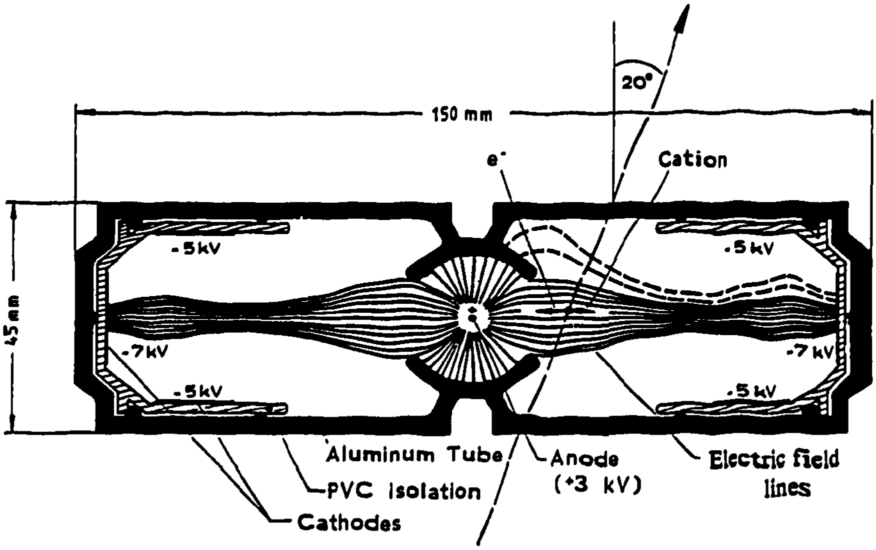

fig. 2.9 Cross-section of a muon chamber drift tube.

Figure 2.10 shows the efficiency for a single tube as a function of the muon track distance to the anode. Adding both projections, the muon will pass eight well separated tubes. If we require three hits in each projection the overall muon detector efficiency becomes 92 %.

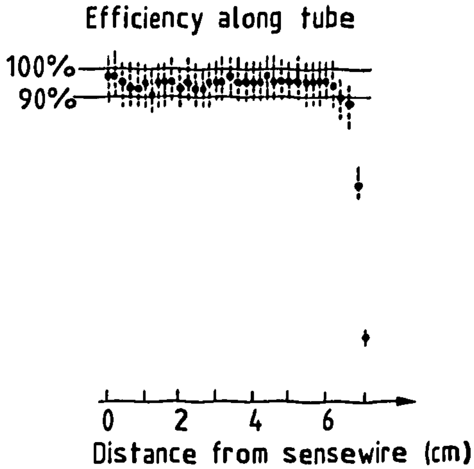

fig. 2.10: Efficiency of a muon chamber drift tube measured as a function of the distance to the sensewire (anode).

The inefficiency is mainly due to the thickness of the walls between adjacent tubes. A straight line is fitted in both projections and gives a spatial reconstruction of the muon track.

In fig. 2.11 an example of a track reconstruction is given, the drawn lines are the parts of the trajectory of the muon reconstructed in the central detector and muon chambers. The dashed line represents the central detector track extrapolation all the way into the muon detector. The muon has deposited the indicated energy in the calorimeter. Since the calorimeter acts as the return yoke of the magnet, the decelerated muon is deflected by the magnetic field and the real trajectory deviates from the extrapolated track. Also multiple scattering in the calorimeter and the additional shielding between calorimeter and muon chambers affects the muon track.

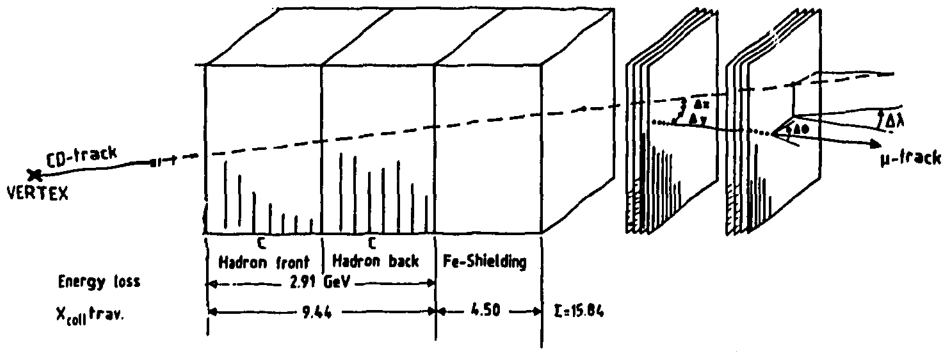

fig. 2.11: Matching of the extrapolated track measured in the CD and the muon track reconstructed in the muon chambers

Energy loss of muons is mainly determined from test beam measurements, while Monte Carlo techniques and cosmic rays provide estimates for the multiple scattering. Although both effects give rise to (energy/position) distributions that are rather broad, for most cases in the analysis of the muon data the average value of the distributions is used (the expected energy deposition in a C-module amounts to 2.0 ± 0.9 GeV). For a 'high quality' muon, the matching with the CD track has to fulfill certain requirements. The differences in positions measured along the projections of the muon chambers and the central detector track are indicated by Δx and Δy (fig. 2.11), while the angular difference in the xy-plane and the angular difference measured with respect to the normal of the xy-plane are denoted by $\Delta\phi$ and $\Delta\lambda$ respectively. These quantities are used in the selection of 'good' muons (chapter VII).

2.6. Triggering and data acquisition (1987-1990).

In the following chapters the triggers and data acquisition for the UA1 detector will be described at length. At this point, only a global description will be given.

During each beam crossing scintillation hodoscopes around the beampipe provide the so-called pre-trigger. It determines whether a proton-antiproton interaction takes place. The hodoscopes cover angles down to 0.8^0 and are therefore essentially 100 % efficient for the selection of inelastic, non-diffractive events. They provide an easy and fast discrimination against cosmic rays and beam gas interactions. The pre-trigger rate is about 100 Khz. However, this is still far from the ultimate goal of $\leq$ 10 Hz imposed by the maximum transfer speed of the data to a magnetic cartridge. These cartridges ($\approx$200 Mbytes) are used as an external storage medium at the end of the data acquisition chain.

For each pre-trigger, hard-wired trigger processors [2.7, 2.8] decide whether the event has to be accepted or rejected. In case the event is to be rejected this decision has to be made within a few μs in order to be ready for the next beam crossing. A further reduction by typically a factor 1000 in rate is achieved for the most common physics triggers. After the event has been accepted by the trigger processors, all data from the separate parts of detector are collected. Before the five main branches of data are compressed into a single stream, all analog signals have to be digitized while the amount of data is reduced as much as possible. From the original $\approx$ 2 Mbytes of information the detector delivers per event, the readout system [2.9, 2.10] only transfers about 100 kbytes. After this considerable compression the data is entered into 3081E emulators which serve to filter out interesting events. All events that were accepted by the second level triggers are written on cartridge. Interesting events, recognized as such by the emulators, are written to a so-called 'special' cartridge.

III

Data Acquisition and Triggers.

3.1 *Introduction.*

When the word 'trigger' is used in this thesis, it may mean different things. First it is used for the hardware, the crates, the processors and other modules. However it may also mean the algorithm, the program which is running on the processors. Finally the word 'trigger' may be used for the result of the algorithm, a yes/no decision indicating whether the event is considered worthwhile.

As described in Chapter II the UA1 detector consists of three main elements: the central detector (CD), the hadron calorimeter and the muon chambers. The hadron calorimeter and the muon chambers can be readout at every bunch crossing (every 3.8 μs). To read the data from the CD takes of the order of 30 ms. If this were done at each beam crossing the deadtime[4] for the detector would be unacceptably high.

During the 1988 and 1989 data taking periods the information from the muon chambers was used in a two level trigger scheme to reduce the trigger rate to values at which the CD could be read for each event without introducing too much deadtime. The primary physics goal was to search for the top quark in events containing one or more muons. The first and second level trigger searched for at least one track in the data from the muon chambers which could have originated from a real muon passing through the muon chambers and coming from the interaction vertex.

Before writing to cassette the information from the central detector is used to see if a reconstructed track in the muon chambers could be matched with a track in the CD pointing to the vertex. If this was the case the momentum of the muon candidate could be determined from the curvature of the CD track. All events containing a muon candidate with a momentum in excess of a certain value (normally $p_t \geq 4.5$ GeV/c) were written onto cassette to be analyzed afterwards.

To cope with the higher luminosity (and therefore higher event rate) and the new calorimeter, UA1 data acquisition and triggers underwent an upgrade. For the 1988 and 1989 data taking periods the readout electronics (pre-amplifiers, discriminators, digitizers, etc.) for the CD and the muon chambers were basically the same as the once used before. The ADC's for the hadron calorimeter had been replaced by the ADC's that were to be used for the Uranium/TMP calorimeter in order to have uniform readout elements for all calorimeters. All elements of the data acquisition that transport the data from the digitizers up to the cassette units had been changed for this run.

Up to 1988 a system of CAMAC crates connected through REMUS had been used to collect the data controlled by one data acquisition computer (NORD 100). The new system is based on the VME-bus, an industrial standard. The dataflow is controlled by many processors distributed over the whole system. Programs for these processors were developed on and downloaded from Macintosh PC's. A software development system,

---

4 The deadtime (in %) is defined as the fraction of the time the data acquisition is busy in such a way that the detector cannot take a new event.

MacSys [3.1], consisting of a special language (Real Time FORTRAN; RTF), a compiler, a linker and a loader was developed in the UA1 group for this purpose.

There are a few components in the UA1 detector that we have not mentioned so far. In general they also produce data that has to be dealt with by the data acquisition system. An example is the pre-trigger, a set of scintillators at several positions around the beam pipe, which provides a timing signal and a luminosity measurement for the beams. It recognizes and rejects events coming from beam-gas interactions and can be used as a trigger to collect calibration data such as minimum bias or beam crossing data (see §3.3).

In the following paragraphs the data acquisition will be described. The pre-trigger, the two muon triggers and the event filter will be treated in some detail.

3.2 Data acquisition.

For each accepted trigger data from the different detector parts have to be read, put together, compressed and written to cassette. The way this is done in principle is indicated in figure 3.1.

Originally the UA1 readout had to transfer 80 Kbytes per event at a rate of 1 every 2 seconds. During the last run in 1990 it had to be able to digest 200 Kbytes per event at a 15 Hz rate.

Two cassette units were used to write the data. While a cassette was rewound the other drive was used to record the data. Another two cassette units were used the same way to record data which were labeled "special" by the emulator farm.

3.2.1 The Data Readout

In the new system one can easily recognize two parts. One is placed right next to the detector in the pit as close as possible to the crates with readout electronics. It consists of several VME crates connected by Crate Interconnect (CI) modules (see section 3.2.3). VME-REMUS Branch Drivers (BD), are used to read the central detector and muon chamber data from the old REMUS into the new VME system. These transfers are controlled by processors in the VME crates. These processors were another in-house development of UA1: the CPUA1 based on the popular Motorola M68000 chip. Later this design was used by the DataSud company to commercialize the product. The BD gets the data in through a REMUS connector on the front panel and gives the data out on an auxillary bus, the VMX bus, on the back side of the module. This VMX bus is connected with a cable to the VMX connector of a Dual Ported Memory (DPM) in another VME crate. A DPM is a VME memory board where the memory is connected to two busses : the VME bus and the auxiliary VMX bus. So the data acquisition electronics in the pit consisted of one row of interconnected VME crates with Branch Drivers and cpu's and another row of interconnected VME crates with memories all connected by their VMX bus to the Branch Drivers. The data from the different detector components end up in different memory modules in the VME crates.

100 KB/Event average. (Up to 512KB/Event)
30 Ev/sec at Event Filter Input
10 Ev/sec into 3480 IBM Cassette

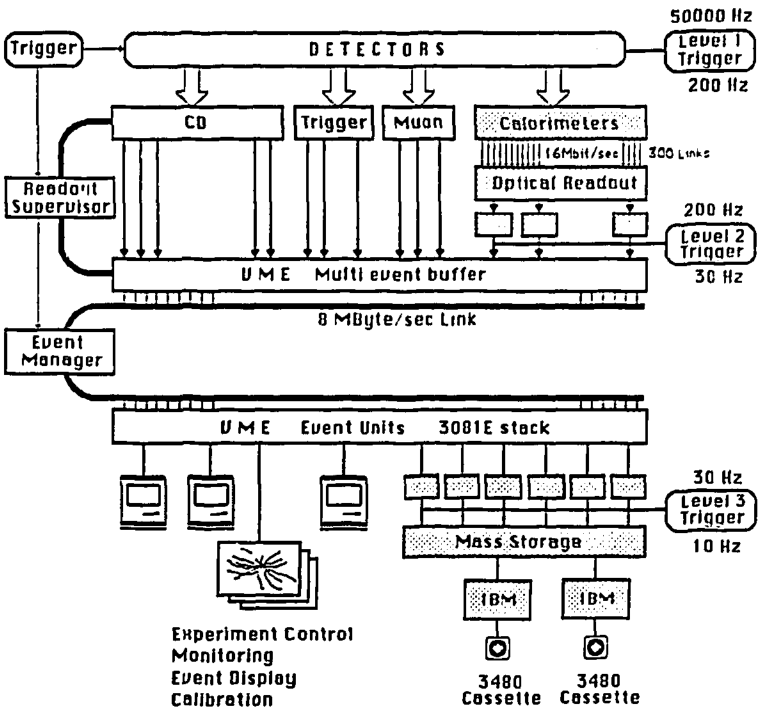

Fig. 3.1 Functional scheme of the data acquisition.

3.2.2 The Event Building

The VME bus of the crates with memories is extended all the way up to the ground floor right next to the control room of the experiment. All data from the detector are scattered over the DPM's. At the ground floor now, one cpu, called the "Event Manager", collects all the data together to form a complete event. At the same time it tests if the data coming from the different detector parts originate from the same event. It creates an event header with some information about the conditions under which the event was taken and it compresses the event by suppressing zero's where possible or compacting several data words into one computer word. Now the event is ready to be distributed over the users.

One important user is a processor which distributes the event over an IBM 3081E emulator farm. Another processor will use a copy of the event for the on-line event display. Several other processors copy the event for on-line monitoring of the detector behaviour.

3.2.3 Data acquisition hardware and standards.

Some commonly used names and abbreviations are explained below:

- The main busses/protocols that are used in the data acquisition are CAMAC, REMUS, VME, VMX and VSB.
- CAMAC is a CERN bus standard for detector readout modules.
- REMUS is a CERN standard to connect many CAMAC crates for readout. Within UA1 REMUS is mainly used for long distance (>100 m) connections.
- VME is an industrial bus standard (32 bit data- and address bus and allows a data flow up to 4 Mbyte/s).
- VMX and VSB are auxiliary busses for VME modules for connections between modules not using the VME bus.
- The (VME-) Branch Driver links REMUS to VME. The BD is a VME module. It can be controlled over the VME backplane of a crate. It has a connection to REMUS on its frontpannel and another connector for an auxiliary bus (VMX) in the backplane. It is always used in combination with a Dual Ported Memory (DPM), also a VME module with an extra connector for the VME bus. The BD can do autonomous block transfers of data from the REMUS branch into DPM in VME without other processor intervention than the start signal and an address in the DPM to where the data should be transfered. The BD also performs simple operations like word-count, event-numbering and identification.
- Crate Interconnects (CI) are VME units to connect VME crates. In each crate there must be a module connected by a flat cable or optical fiber. The CI is a passive bidirectional system. It maps address space. Therefore its presence is transparent for the users.
- CPUA1 or Robcon™ (VME020) are VME processor boards.
- MacVee[5] is an interface between a Macintosh PC and a VME or CAMAC environment. It consist of a VME module and a Macintosh module connected by (twisted pair) flat cables. The VME module acts as an autonomous unit. Therefore the presence of this interface is transparent for the user. It appears as if the VME bus is linked to the internal Macintosh bus; a VME address window is mapped into the Macintosh memory space. The speed is 2 Mbyte/s. The cable can be as long as 100 m but then precautions against electrical interference and differences in earth potential are needed.

Other modules used in the trigger are described in §4.3.1 in detail.

---

[5]The Crate Interconnect and MacVee are designed at, and for, the UA1 experiment and are now commercial products.

3.2.4 Software.

UA1Mon is designed for the Motorola 68.000 processor series, to serve as operating system on a CPUA1 or Robcon processor board. In addition to the usual features for interactive use, debugging and monitoring, an extension is available for data acquisition tasks. This includes items like autonomous data handling using the REMUS and VSB protocols. In addition UA1Mon performances hardware tests for various VME modules.

MacSys [3.1] is a complete software development system on a Macintosh PC. The system consists of a compiler, an assembler, a linker and a loader. Each of these parts can operate in a Macintosh or on a VME processor board. In addition it contains a multi window editor and a runtime library. The FORTRAN compiler (Real Time FORTRAN; RTF) is specially developed for the M68.000 processor series. The language has extensions like co-processor use, register- and absolute addressing. The special M68.010/20 features like in-core loops and cash are used by the compiler.

3.2.5 Ergonomics.

An important aspect of the data acquisition is the 'human interface'. Considerable effort is put in 'user-friendly' operation and displays (In practice, most operators are non-experts). The data acquisition gives the first possibility to analyze the performance of the detector and the quality of the data. Therefore a clear and simple presentation of the performance during data taking is necessary.

Most communication uses graphics and is self explanatory. The Macintosh PC is the UA1 standard for all 'console-like' activities. A detailed diagnostic system informs the operators about malfunctioning, errors and what to do about them. For several obvious errors there is an automatic recovery procedure.

3.2.6 Data streams.

Within UA1 2 types of cassettes are distinguished: 'Normal-' and 'Special-' cassettes.

- To *Normal* cassettes all data is written which is accepted by the second level trigger.
- To *Special* cassettes data is written which is accepted by the emulators (§3.3.3) as well. Data, that is accepted by the second level trigger as a multi muon candidate, is put on *Special* cassette also, regardless the emulator decision.

In practice, the *Special* cassettes are used for analysis and the *Normal* cassettes serve as back-up. Only for low p_t physics and for verification of the emulators, *Normal* cassettes are analyzed.

3.3 Triggers.

3.3.1 Motivation.

The need for a good trigger for the UA1 detector can be illustrated best by the difference in the total cross-section for $p\bar{p}$ interactions (60 mb) and the beauty production cross-section which is presented in chapter VII of this thesis ($\sigma(p\bar{p} \rightarrow b \text{ or } \bar{b} + X) = 3\ \mu b$ for $p_t^b \geq 6.5$ GeV/c see (7.20)). The interaction rate is, because of this σ_{tot}, 72 kHz (for the typical luminosity of $1.2 * 10^{30}\ cm^{-2}s^{-1}$) whereas the $b\bar{b}$ states are only produced at a typical rate of 3.5 Hz. So there is a factor of 20.000 between the total cross-section and the cross-section we are interested in. Of course beauty production is not the only subject one wants to study, also other heavy flavour physics and jet physics is part of the UA1 program. In the end it is the maximum speed at which one can write events to cassette (≈ 10 Hz) which determines the physics triggers one allows to run in parallel.

3.3.2 Trigger schemes.

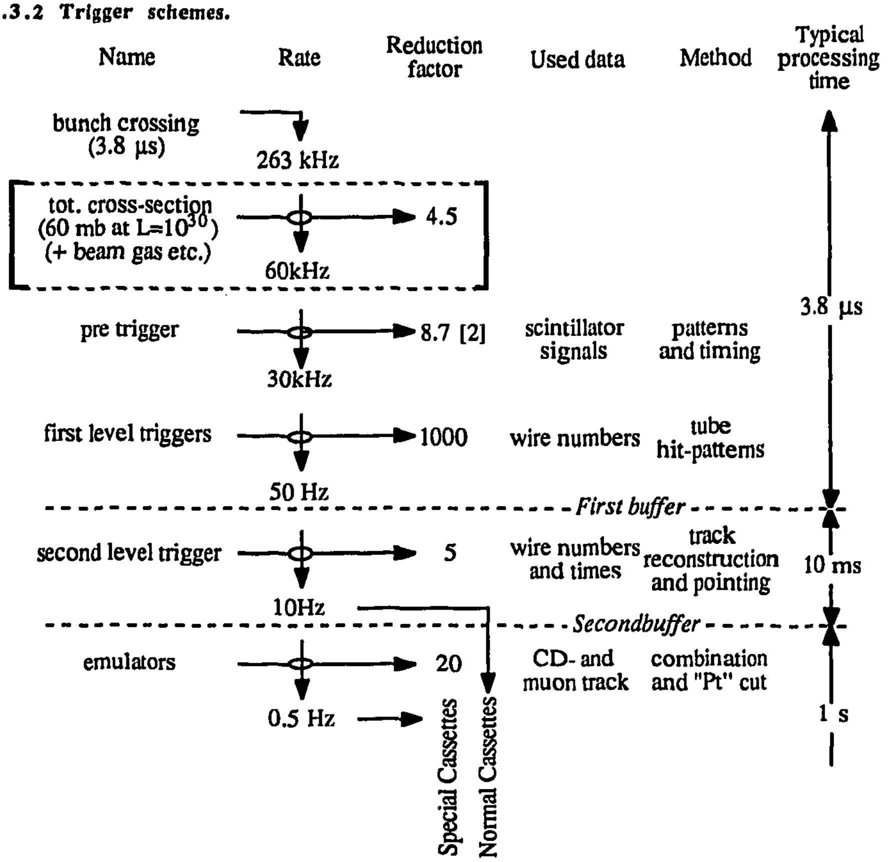

Fig. 3.2 Muon Trigger Scheme

The two level muon trigger scheme has been part of the muon trigger and readout from the very beginning. In a first stage the second level trigger was implemented in FAMP [3.3] processors, in a multi processor set up housed in (modified) CAMAC crates. The luminosity increase after 1985 by the addition of the ACOL machine motivated a complete rehash of the muon triggers. The first level was refined and speeded up, the second level was replaced by a new multi processor system (now in VME) but based on the same philosophy. The properties of the triggers is outlined in fig. 3.2.

3.3.3 The double buffer scheme.

The double buffer scheme, which was introduced in UA1 in 1987, is intimately related to the second level trigger. The second level trigger which requires processing times of the order of several milliseconds would introduce enormous deadtimes if there wouldn't be two buffers at least. While processing an event in the second buffer, the first level trigger could allow a new event to be written into the first buffer. This double buffer scheme has to be applied to all detector elements (both buffers are noted in the trigger scheme of fig. 3.2).

3.3.4 The pre-trigger.

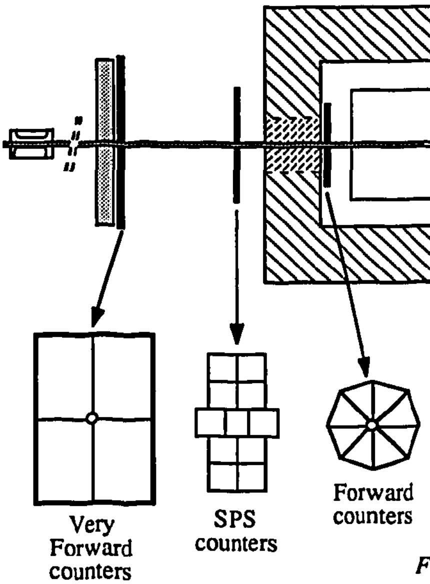

counters	rapidity	distance to vertex
V.F.	≈ 6.6-4.3	12 m
S.P.S.	≈ 5.3-3.0	6.2 m
F.	≈ 5.2-4.0	4.0 m

Fig. 3.3 Setup of the Pre-Trigger.

The lowest level trigger in the trigger scheme is the pre-trigger. It has to fire when 'something' happened at the interaction point: it should however be able to discriminate between 'something' from a proton and an antiproton in the bunches or 'something' else like beam-gas interaction or interactions from (anti-) protons not in a bunch. This should be done extremely fast because the pre-trigger will enable the readout of detector elements like the calorimeter and the muon chambers. On the data from these, the first level trigger processors have to work and decide if the interaction is worth keeping for further analysis by the second level processors. The decision has to be taken before the next beam crossing in 3.8 μs. Therefore the pre-trigger checks for 'physics' by looking at transverse energy. In addition, it only allows activity at the time the bunches cross. This discriminates events that are related with particles which are not part of the bunches. In the same way the pre-trigger veto's beam halo events.

Another task for the pre-trigger is the definition of the *time origin* (t_0) at which the collision takes place. This is needed for the conversion of drift times to space coordinates in the driftchambers.

The pre-trigger also measures the luminosity. The UA1 luminosity measurement is based on small angle elastic scattering. The cross-section for this process is known accurately.

The pre-trigger is sensitive to the collider performance (f.i. the position and size of the collision region). In this way it is used as a beam quality monitor and provides the SPS with information for beam adjustment (f.i. for the collision point, beam size, beam halo and bunching).

The pre-trigger consists of three sets of scintillator hodoscopes on each side of the collision point. The pre-trigger is a coincidence of hits at both sides of the detector which are not on a line parallel to the beam axis. The pre-trigger decision comes about 100 ns after the beam crossing. A considerable part of this time is due to the cable length.

3.3.5 The fast muon trigger.

The first level- or fast muon trigger is enabled by the pre-trigger. On an accept decision of the pre-trigger the muon chambers are read into the Multiple (drift) Time Digitizers (MTD). Rather than waiting for the drift times to be measured (may take up to 1.5 μs) a fast output of these modules is used to determine which drift tubes have been hit. This information is used by the first level muon trigger.

The principle of the fast trigger [see also fig. 2.8] is to verify if a track can be defined and associated with the vertex. This is done by checking if the data can form a track that lies within a cone pointing to the vertex area. Each tube in the plane closest to the vertex is called 'reference tube'. The information of the reference tube combined with a set of nine surrounding tubes (all tubes are represented by a bit) forms a word. The pattern of this word is checked against a look-up table for validation as a muon candidate. The look-up table has been determined beforehand and contains all possible combinations of tubes hit which could come from a track pointing to the vertex within a cone of ≈ 150 mrad for each of the two projections.

If a valid track is found, it is checked whether the corresponding segment in the calorimeter which is farthest from the vertex and closest to the muon chamber (the so called **back-stack**) has an energy deposition above a threshold. The energy deposition condition and the track validation should be in coincidence since a muon has a small energy deposition in the calorimeter. This coincidence contributes typically a factor 3 to 4 to the rate reduction. For the bottom chambers this reduction is about a factor 30 since the bottom chambers consist of only one plane.

In parallel to the first level muon trigger a first level calorimeter trigger operates. This trigger calculates global quantities like total- and missing transverse energy, and local quantities corresponding to jets. This trigger will not be further considered in this thesis.

The information from the pre-trigger, the first level muon and the first level calorimeter trigger is combined in the Trigger Processor (TP) which will now decide whether the event will be dropped or should be passed on to the second level. In the Trigger Processor (which combines the first level decisions), the table of signatures[6] of interesting physics is stored. Upon an accept signal of the Trigger Processor all the data is moved to the second buffer. The first buffer is then free for a new event from the pre-trigger. The second level trigger processors get a signal to start working on the event in the second buffer. All this should be done within 3.8 μs.

3.3.6 The second level muon trigger (I).

The Second Level Trigger will be explained in more detail in §3.4. Input for the trigger are the wire-numbers and drift-times. By using, in addition, the geometry (to get the wire-coordinates), drift-velocity and time origin (to get the position inside a tube), a track *can be*[7] reconstructed with an accuracy of ≈ 0.3 mm. A track is accepted/rejected on the basis of a criterion used for determining whether it points to the vertex. The Second level trigger reduces the rate with typically a factor 6. As is described in §5.2, the average trigger time is 8 ms including the reading and writing of the data.

Again there exists also a second level calorimeter trigger. Because it is not relevant for this thesis it will not be discussed here.

The signals from both second level triggers are combined and determine whether to drop the event or to allow it to be passed on to the third level. For the third level all the data from the detector, including the CD, is needed. So in the case of an accept, the data acquisition is signaled to readout the complete detector and to pass the full event to one of the processors of the emulator farm. In fact the readout of the CD is started before: upon a positive decision of the Trigger Processor at the first level, the readout already begins. If the second level decision is negative, the emulator farm does not process the data anymore. In dependent of the outcome of the third level calculation the event will be written to cassette.

[6]Signatures like ' 2 muon anywhere', '1 muon + a jet in the barrel region' etc.
[7]This is a Monte Carlo result based on exact knowledge of all experimental properties.

3.3.7 The event filter (third level).

The emulators form the third trigger layer. They combine the muon data with the data from the central detector. The algorithm which runs on the emulators is derived from the off-line reconstruction program. In the latter all points in the CD are used for trackfinding. In the emulators only those parts of the CD are analyzed that correspond to a track which has been found in the muon chambers. All combinations of tracks in that part of the CD and muon chambers are tried. The decision whether a track in the CD corresponds to a track in the muon chambers is based on the χ^2 of the fit of a line through all points of both tracks.

In addition a loose p_t cut (of the order 5 GeV/c) is applied. For a multi muon event this cut is weakened to $\approx$ 1.5 GeV/c for each of the muon candidates.

3.4 The second level trigger (II).

3.4.1 The trigger principle.

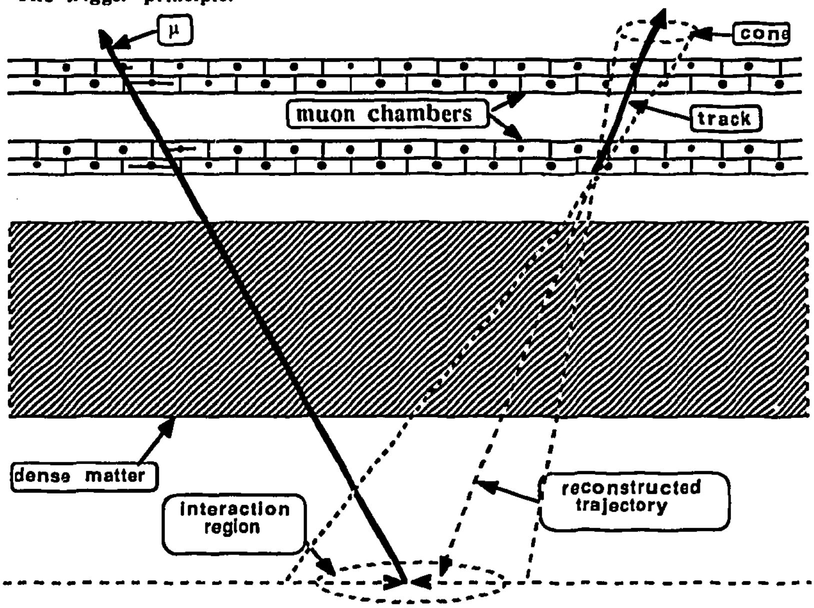

Fig. 3.4 The trigger philosophy.

In principle the second level trigger rejects events which do not contain a muon (of sufficiently high p_t) pointing to the vertex. The second level trigger uses drifttimes and can therefore reconstruct space points with much higher precision than the first level trigger. The precision of space points at the first level trigger is of the order of half the width of a drift tube (±7.5 cm), whereas the second level trigger reconstructs a track to within 1-2 mm.

The direction of a track in the muon chambers can be used as a rejection criterion (see fig. 3.4). A high p_t muon should not be deflected too much by the magnetic field or affected by multiple scattering. Therefore it is sufficient to reconstruct a straight track and determine whether it points to the vertex region. If a track points to the vertex it is not necessarily a direct muon, it still can come from a pion/kaon decay, shower leakage or from a cosmic ray. But any track that does *not* fulfill the requirement will *not* be of interest, and will be *rejected.*

Two different criteria has been used: one called the '*narrow cone*' ($\approx$ 70 mrad) for single muon events and a looser one called the '*wide cone*' for dimuon events. The wide cone is 3 time larger than the narrow cone.

3.4.2 3 point tracks.

The pointing criterion is checked for all relevant combinations of tracks in the two projections. In the bottom chambers only one projection is used. The algorithm also takes into account projections where from the 4 planes of drift tubes, one is missing. With a probability of about 5% that a track misses the sensitive volume of a drift tube, it makes that about 30% of the events has at least one projection with 3 planes only. This represents an appreciable amount of data. Tracks with only 2 hits in a projection are considered not analyzable.

IV

The Second Level Trigger Construction.

After having introduced in the previous chapter, in the context of UA1, data acquisition and trigger layout, the second level muon trigger will be described now in great detail. A considerable fraction of the NIKHEF contribution to the UA1 experiment went into the design, the construction and the operation of this part of the experiment.

4.1 Ideas behind the trigger.

4.1.1 Parallelisms in the setup.

Reaching a trigger decision based on the pointing of a track, is practical and fast. Many operations can be performed in parallel since a track corresponds to a local phenomenon in a muon chamber. The data is handled by the first level trigger in 28 parallel streams and also the two projections of a muon chamber are dealt with in separate data streams. These data streams are read-in by the second level.

Other places where things are done in parallel:

- The trigger calculation is performed by several processors simultaneously.
- The data collection and trigger calculation are decoupled and proceed simultaneously.
- The VME processors and the Macintosh act simultaneously.
- The writeout of the second level data and results to the third level is independent of the other activities.

The decoupling of data acquisition and trigger calculation is quite natural. Both can be done simultaneously and asynchronously. This is possible because after the raw data is read in, this data is locally stored in dual ported memory and therefore accessible to all processors.

The parallelisms described so far are reflected in the specific choice for the setup. The second level muon trigger consists of a VME crate with six Robcon processors based on the MC68020 processor (see §4.3), large memories and control units (see fig. 4.3 for the set-up). Of the six processors, four (CPU 1-4) read the data in parallel from the muon chambers through a chain described below. The data (typically 500 words, each word containing a wirenumber and a drifttime) are stored in the Reordering Memories. After all data has been read, the same four processors that read the data will now use the data to work out the trigger decision. One processor (CPU 0) is called the 'master' CPU. It supervises the trigger calculation. Another processor (CPU 5) is called the 'controller' for historical reasons and is there because the data acquisition of the muon data is done from the trigger crate. To combine the trigger and data acquisition in the same crate was a 'bad' decision but determined by the history of UA1.

In the processing of the data, use is made of the fact that muon tracks are local entities. A single processor can work on one track while another processor is working on another track. Even within the processing of one track independent jobs can be distinguished which in most cases can be performed in parallel. To make use of this, the trigger program has been divided into several 'tasks'. Each processor may take tasks from the tasklist[8] and execute them and may also create new tasks and put them onto the tasklist. In a systematic study it was investigated whether many small tasks were better than fewer bigger tasks. Another parameter which was studied, was the number of CPU's sharing the tasks. The result will be described below.

4.1.2 Interrupt.

There are two ways of operating a trigger processor: one is 'on call', the other is 'on interrupt'.

If the trigger runs 'on call' it basically is executing a sequence of instructions one of them being a check on a flag indicating, to start reading the data and executing the trigger algorithm.

Since it is important to issue the trigger as soon as possible once there is valid data in the muon chambers (valid means accepted by the first level trigger) it is better to operate in interrupt mode. Upon arrival of an interrupt signal the CPU is interrupted in whatever it was doing to first execute a preselected set of instructions (f.i. the trigger algorithm) before it is allowed to go on with what it was doing. Our processors had interrupt possibilities at several levels built into the hardware.

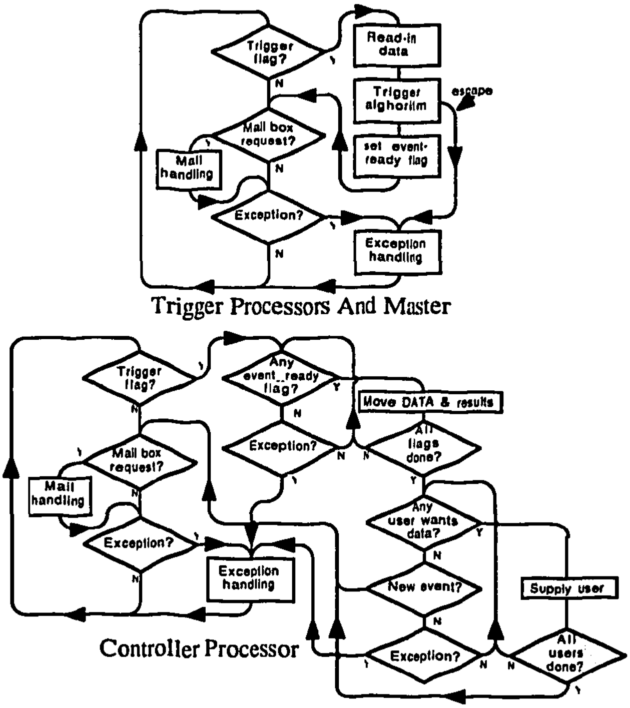

Fig. 4.1 Main loop scheme.

[8] The tasklist for the task-bookkeeping; it holds the activities by the CPU's and what should be done next. Tasks and tasklist are described in §4.4.2.

Several schemes for interrupt handling have been tried. One approach is to treat the whole of the data readin and trigger calculation as an interrupt. This gave rise to problems in situations in which the trigger was aborted or at the occurrence of fake interrupts. To recover and restore the stack is quite problematic in cases of bus errors or system interrupts[9].

Another approach is to perform the readin part of the data acquisition 'on interrupt' and the trigger calculation 'on call'. This leads to problems for the synchronization of the data read-in and the trigger calculation.

In the end a mixed scheme was adopted (fig. 4.1). One processor (the 'master') is sensitive to interrupts. On interrupt it sets a flag in memory on the VME bus for the other processors, and remains insensitive to more interrupts until after the trigger has been completed. In the Main-loop, in each processor, this flag is checked and when it is set, the data readin is started. This approach makes the system *easier to debug* than an approach that directly uses interrupts. Also this approach is easiest for simulation on a Mainframe[10].

4.1.3 Semaphores.

Semaphores are important in a multi processor environment. A semaphore is a flag which marks that a specific data block is in use. A user should wait until an earlier user has finished using the data.

In the assembler language of the MC68000 family of processors a special indivisible instruction TAS (Test And Set) exists to manipulate semaphores. This requires a series of bus actions at which no other user can *interfere*.

4.1.4 Communication.

In the communication three partners play a role: the second level processors, the physicist and the rest of UA1. Between the processors, flags at predefined positions in the memory are used. A Macintosh is used to monitor the trigger performance and to control the system and is the interface to the physicist. Between the data acquisition and other trigger processors of the detector and the second level trigger signal cables are used (see fig. 4.2). The different techniques for communication are described below:

The *triggerlog* is an array of data in VME memory accessible by all processors and the on-line Macintosh and contains information about the performance of the trigger. The Macintosh continually monitors the content of this array and displays extracts on the screen. The Macintosh is used to send commands to the trigger. An aspect of the triggerlog is its list of exceptions (like bus- and address errors). These errors are booked, if possible with the processor identity and position in the software, before the VME environment is reset and the trigger is re-initialized. Most items in the triggerlog are not protected with semaphores since they mostly represent statistical information.

To be able to talk to the trigger the physicist may use a set of commands which can be sent at any time to any one of the processors in the crate. Such commands may be drastic such as, 're-initialize everything' or 'start/stop'. Also it may just change the amount of debug output produced by one processor. It may require an

---

[9]Even in a correctly working system bus errors and system interrupts appear with a rate of several per minute. Therefore an automatic recovery procedure is needed to reduce the deadtime contribution.

[10]The trigger algorithm is developed on an APOLLO workstation and tested on an IBM mainframe.

event to be transfered to the Macintosh to be displayed on the screen. A command is a string of numbers describing the sort of command, the processor it is meant for, parameters which go with the command (such as debug level) and the way the processor should reply. Each processor in its main loop checks the so-called '*mailbox*' an array in its own dual ported memory, where the commands are written by the Macintosh. In principle CPU's can also mail commands to each other but this feature is not used.

A reply from the processor to a command may be 1) 'reply on request' or 2) 'reply when done' or 3) 'no reply'. The Macintosh may time out after a command has been sent with a reply requested and nothing happens. A special 'dummy' command requires 'no action just reply' from a processor and is used to test if that processor is still running.

The communication between processors works by *flags* in memory at predefined addresses. Upon initialization these addresses are calculated by each processor from parameter values in the program.

A special form of communication between the processors is used for synchronization: the *meeting point* formalism. In the case of just two processors this is a simple handshake: one processor sends a command to another with the request to reply upon reception. The meeting point protocol is that any processor wants to shake hands with all other processors in the system and requests from all processors to 'hold' until all processors have presented themselves. There are a few instances in the data acquisition and trigger where meeting points have to be used. If any one processor doesn't work properly it may not present itself at a meeting point. The process will then continue after a time out and an error message will be issued.

4.1.5 Debugging.

Debugging a process on a parallel processor system is more complex than debugging a sequential process on one CPU, for several reasons:

- In a parallel system the time sequence of the actions is lost.
- Tasks in our parallel system can be generated by several sources and work on several pieces of the data.
- The different processors have to interact with each other.

The four main tools used in debugging are:

- Each processor is connected to a display which, upon request, provides intermediate results.
- Each processor writes flags in Common Memory (described in §4.3.1) when the algorithm passes certain points. These flags, typically one word, identify the point as well as the processor. (f.i. to check the sequence of the tasks while processing).
- A Bus-Tracer (described in §4.3.1) 'visualizes' the bus actions and can trigger on special bus configurations (f.i. to find unforeseen processor interactions and hardware orientated exceptions).
- At the occurrence of an error, a message is written in the triggerlog. If possible the message is accompanied by the number of the processor and the point in the algorithm. Hardware orientated errors like bus-, address- and interrupt- errors are also listed with the position in the algorithm. This is important because in general after such an error the algorithm is re-initialized automatically. By using the triggerlog information, the origin of these errors can be traced.

4.2 Control signals and BATS.

The interaction of the trigger with the rest of the experiment proceeds through NIM signals. The implementation of the second level triggers and the double buffer scheme increased the complexity of the traffic of the control signals, to a point at which handling by just NIM logic was not feasible anymore. The main reasons are that the reliability is poor and that it is difficult to debug and there is hardly no flexibility.

To control the inter-detector communication signals plus the double buffer, the BATS (Buffer And Trigger Sequencer) was introduced: a VME crate with processors and Input/Output registers. All control signals are connected to these I/O registers and a processor steers the output signals upon a change in the combination of the input signals. In essence, a readout/trigger/data acquisition cycle of the detector can be described as a fixed sequence of states of the detector. A state of the detector is completely determined by the control signals. In a look-up table we have on one hand the (incoming) control signal combinations of one state and on the other hand the (outgoing) control signal combinations needed to move the detector to the next state.

Such a sequence of states has to be defined for each mode of operation: data taking, calibration, cosmic ray measurements etc. It must be clear that the bulk of the work which went into the preparation of the look-up tables consisted of finding all the exceptional- or error states of the detector in case one of its components fails.
A second processor checks the behaviour of the control signals and monitors quantities like error rates and deadtime contributions. BATS is able to detect illegal states and hang-ups and can reset *all* data acquisition electronics. BATS is booted and controlled by a Macintosh.

The communication between the second level trigger and BATS during a trigger cycle uses 5 signals (fig. 4.2):

Move First buffer (MF) signal from BATS:	The trigger cycle starts; first the muon data is read from the first into the second buffer.
First buffer move Done (FD) signal to BATS:	The trigger signals that the raw data is read so the first buffer is free.
Accept/Reject signal to BATS:	The trigger decision.
Clear Trigger / Move Trigger (CT/MT) signal from BATS:	The trigger is requested to clear the event or to prepare its readout.
Trigger Done (TD) signal to BATS:	The trigger is finished and ready for a new event.

The trigger and BATS are 'tightly bound' because these 5 signals should come in a well defined sequence. A different sequence is considered as an error. Nevertheless the trigger algorithm is designed such that no hang-up will occur as a consequence of this error.

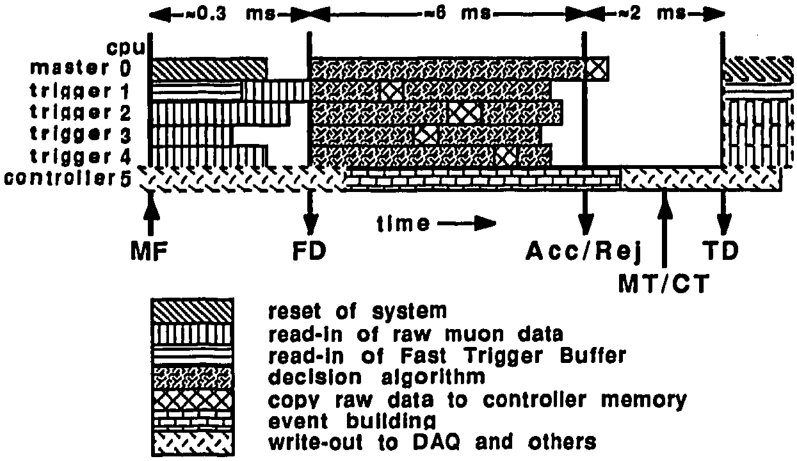

fig. 4.2; Trigger signals. For an explanation of the symbols, see text.

Other signals are:

Initialize (INI) signal from BATS:	The trigger is requested to abort, reset and initialize.
Initialize done (ID) signal to BATS:	The trigger has finished initialization.
Reset signal to BATS:	The trigger is in trouble and requests a reset/initialization of all UA1 elements.

If one wants to test the trigger without the rest of UA1, one only has to connect the TD and MF signal, the Accept and MT signal, and the Reject and CT signal before going to BATS (TD → MF, Accept → MT, Reject → CT). This way the trigger 'runs around' either on zero or on data written into the second buffer beforehand. This option turned out to be crucial in the development stage. A similar way of operating the trigger was possible including the readout of the muon chambers. Also this option was used frequently to debug both systems and to check the cables and electronics.

A set-up was made, using NIM logic and a VME I/O-register by which the trigger system could be set in such a mode by one single command from the Macintosh.

A very powerful control item is the Macintosh reset button. Upon usage of this button *all programs* in the Macintosh and the VME processors are reloaded and started *from scratch* and through the BATS a reset of all other UA1 elements is generated. All the programs and constants are on the Macintosh hard disk. After a reset they are first loaded into Common Memory and then loaded into the Dual Ported Memory of the processors. Next the programs are linked and initialized by the processors themselves. This procedure takes about two minutes. However the second part of copying into DPM and initialization, takes less than a second. This is done upon an INI signal.

4.3 The hardware.

The muon trigger consists of 12 racks of electronics for the first level and 2 racks for the second level. The main part of the second level muon trigger is a VME crate, 6 FAMP (CAMAC) crates and 2 NIM crates with electronics. Some additional hardware is used for test-, control- and monitor purposes (scalers, terminals, switches, power supplies, water cooling and a coffee machine). Of the most important units a short description is given below:

4.3.1 The modules.

- **Processor:** Our VME processors (type ROBCON™-VME020 [11]) come from the Robcon firm in Finland. This computer consists of a 68020 (25 Mhz) CPU with a 68881 floating point co-processor, a 68562 I/O handler and 2 Mbyte Dual Ported Memory.
- **Macintosh II:** is used for program development and as boot- , control- and display facility for the trigger. The Macintosh is connected to several VME crates, has an ethernet connection to the CERN computers and an AppleTalk connection to printers, and all other UA1 Macintosh's.
- **MacVee:** (see also §3.2.3); serves as an interface between a VME environment and a Macintosh PC.
- **FAREM:** Famp REMUS Interface; this unit serves as an intermediate (first-in first-out) buffer in which read/write actions can be performed simultaneously.
- **FAXNIX:** FAMP VSB interface (developed by NIKHEF).
- **MTD:** Multiple (drift) Time Digitizer [4.2].
- **MTD controller:** readout controller for a crate of MTD's [4.3].
- **VME register:** (NIM) I/O unit in VME.
- VME Branch Driver/VMX DPM memory (see also §3.2.3): used as REMUS→VMX→VME interface. This combination of modules autonomously reads a data stream and stores the data in DPM.
- Common Memory: memory in VME visible for all VME processors and the Macintosh.
- **Dual Ported Memory:** this memory is visible from two busses. On the processor boards there is 1 Mbyte DPM visible by VME, and the MC68020. Also these units are used in combination with a Branch Driver.
- Battery Backup Memory: this is memory that keeps the data after a power drop. It is used to save the programs and bases of constants and serves for fast initialization.
- Reordering Memory: reads muon data from the MTD controller. At read-in the data is sorted by wirenumber and time. This implies that neighboring wires correspond to neighboring datawords and avoids time consuming sorting routines.
- Crate Interconnect: (§3.2.3) this is a bidirectional interface between VME crates. The units map a part of the address space of one crate into another.

[11] This board was initially designed in UA1 and is now a commercial product.

- VMETRO Bus Tracer: a VME module that samples the bus activity and stores into memory. At a pre-programmed condition (f.i. bus error) the tracer stops and displays the 2048 last bus steps preceding the trigger condition.

4.3.2 Set-Up and Data Flow.

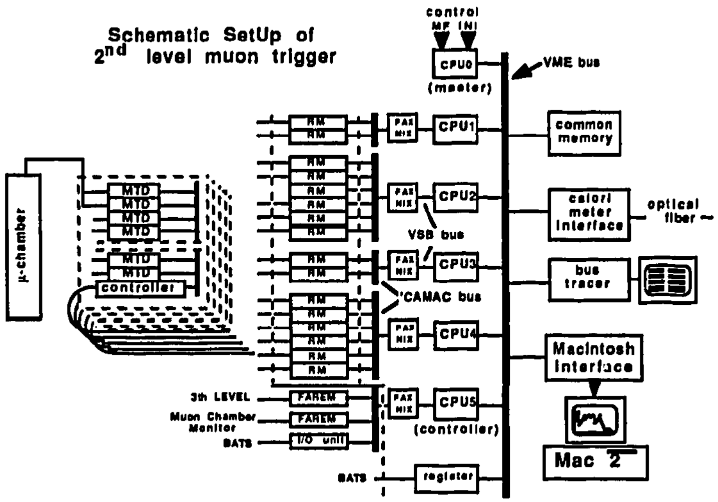

fig. 4.3. Schematic overview of the hardware.

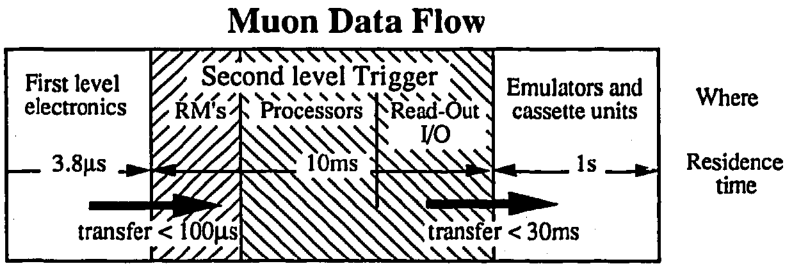

fig. 4.4. Muon Data Flow.

Figure 4.3 gives a simplified scheme of the set-up while fig. 4.4 gives a scheme of the dataflow. Both schemes show the 3 buffers that the data pass; the first buffer consists of the MTD's, the second buffer is the second level system and the third buffer is at the level of the emulators. The second buffer consists of three stages: i) the Reordering Memories and ii) the DPM's of the trigger-processors and iii) the data is combined into an event and written into the output buffer (FAREM).

Upon a signal from the pre-trigger (the BATS MF), the muon chambers are read out by MTD's. These units transform the signals into wire numbers and drift times. A MTD controller collects the information of a group of MTD's. Such a group corresponds typically to four muon chamber projections (planes)[12]. The MTD controller transfers these data to a reordering memory within 100μs (typically 1μs/word).

The RM's are the second buffer in the scheme. The processors 1-4, which are connected to the readout, set a flag when they notice that all data has been transfered from the MTD crates into the RM's. Simultaneously, a Branch Driver reads the so called Fast Trigger Buffer (FTB). This Fast Trigger Buffer contains the result of the first level muon system and should be saved on cassette too. After the readout of the FTB has been completed, CPU 5 sets a flag. When all five flags are up it means that all data has been copied from buffer 1 into buffer 2 so that a new event may be accepted by the pre-trigger. The processor which is the last to finish the readin, is the one that sends the FD signal to BATS by the VME I/O register. This cannot be done by the controller processor since the controller might still be busy with the readout of the previous event (see fig. 4.2).

Now the actual trigger calculation may start. Any number of CPU's may take part in this calculation but most of the time it was done by CPU 0-4. A simple flag, which could be controlled from the Macintosh, determined which CPU's were on. Default, however, was all CPU's in the crate except the controller.

During the trigger use could be made of the fact that the data were stored in the RM's according to increasing wire number and time. Another very useful feature of the RM's is that they can be directly interrogated for the presence of a hit, expected by the trigger algorithm, by writing the corresponding wire number into the RM. The RM then returns the hit next to (or of) the interrogated wire number.

During the trigger calculation, the CPU's 1-4 have to read once more their RM's but now to copy all data. This is done at the first occasion at which the CPU is waiting (either because the trigger calculation is finished or because there is no intermediate result available for further processing). The controller copies these data words and combines them with a data block containing trigger information into what is now called a muon event. Also during the trigger calculation, a data block in common memory is updated, which at the end of the trigger calculation contains the trigger result and the tracks that were found. At the end of the trigger calculation the controller copies this data block, adds it to the muon event and sends out the Accept/Reject signal to BATS.

The controller holds the muon event until a decision has been made by the BATS to either read the event (MT) or to clear it (CT). If it receives an MT signal the data is copied into a memory (FAREM) where the Data Acquisition can access it and combine it with the data from all other detector parts. Only at this point it sends the TD (trigger done) signal to BATS to say that the second buffer is free now for a next event. While waiting for an MT or CT the controller can also (on request and regardless of the trigger decision) make a copy of the muon event for monitoring the chamber performance or for analysis and display on the Macintosh. If a next event is there, the controller finishes what it is doing and then starts to combine the data of the next event.

[12]The projections of the muon chambers are grouped in such a way that the two projections of the same chamber arrive at different trigger processors; this favours parallelism.

4.4 Software.

There were some guidelines for the software:

- All software is written in FORTRAN (RTF).
- All trigger software must be able to run on the processors, on the Macintosh and on the IBM or APOLLO.
- The programs are identical for all VME processors.
- The trigger software is independent of the number of processors. Increase of the number of processors should not imply changes in the software.
- All arrays have a power of 2 as size (for speed up reasons).
- There are *no* endless loops; all loops have a time-out and check for a reset flag (§4.2).
- If the program is polling on a flag in a processor, it must be in the DPM of *that* processor. This minimizes bus access and is therefore faster. In addition this is easier for debugging the program.

Usage of the same software on- and off-line is made possible by an initialization routine that identifies the environment and provides the addresses of global variables. In principle the IBM or APOLLO serves as a development and testing environment for the trigger algorithm. The Macintosh serves as a tool for the development of the data handling-, monitoring- and of control software.

The software can be divided in three parts (of about equal sizes):

- The *data handling.*
- The *trigger algorithm.*
- The trigger *monitor & control.*

Figure 4.5 shows this structure schematically and the next paragraphs describe these parts in detail.

The *trigger algorithm* is defined as the set of routines that analyze the muon data resulting in an accept/reject decision.

The *data handling* is all the software concerning the data-flow (data read-in, event building).

The *monitor and control system* is everything needed to control and monitor the other two parts (f.i. the event display). This part only works on the Macintosh and forms the interface to the physicist.

These three software parts are to a large extent decoupled from each other. This decoupling is important since it preserves the possibility to test the trigger algorithm on a different computer. The data handling system can run without trigger. This is needed for calibration/cosmic ray runs and is handy for development of the trigger algorithm. And finally the monitor and control system is independent of the other two parts in such a way that it can boot and (re-)start them in all situations.

All systems are designed to recover automatically from almost any error or exception without human interference. This includes errors like bus- and address errors.

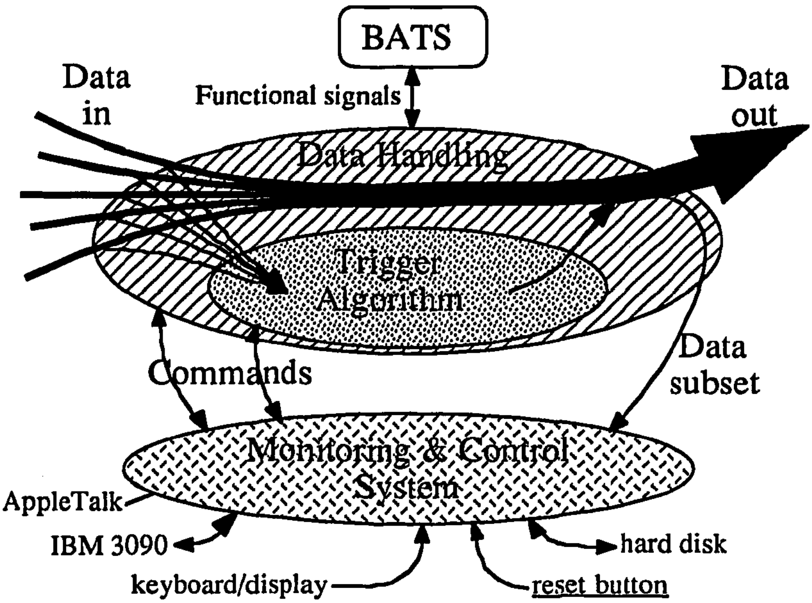

fig. 4.5; Global structure of the trigger systems.

4.4.1 The data handling.

The data handling software performs 4 basic actions:

- Event building
- Write-out
- Communication with BATS
- Communication with the monitoring and control system

The trigger algorithm is independent of and embedded in the data handling system. This makes the trigger algorithm flexible and easy to update. The readout of the data from the first level is dedicated to the trigger algorithm. This is because the readout of the Reordering Memories is done by the trigger processors in parallel with the trigger calculation.

The eventbuilding routines are again a separate package independent of the read and trigger routines. These routines are only used by the controller CPU. This CPU polls on flags from the other CPU's indicating that they have finished with the trigger calculation. If that is the case the controller will copy the data and combine this information into an 'event'. Besides this data there are other blocks like the result of the first level trigger. If all data are copied then the controller will copy the overall trigger results from common memory and send out the Accept/Reject signal to BATS.

An event is copied to the data acquisition system upon request (MT from BATS). In that case it is written into the FAREM from where it can be read at any time by the data acquisition system. It may however also serve other users like the *monitor & control.system* which requests an event for analysis. In that case the event is copied to a part of memory from where it can be read by the Macintosh. As soon as the controller finds the MF signal of the next event it will stop the writeout phase. However the controller will complete a writeout if it had already started.

4.4.2 The Trigger Algorithm.

Introduction.

To be able to test the trigger in the parallel processor version, the possibility had to be created to run the same algorithm on the same events on another computer in order to compare the results. This forced us to write the whole algorithm in a higher level language (FORTRAN). Indeed the trigger algorithm contains only standard FORTRAN. Some routines which were only called when running in the VME crate contained a few non-standard real-time FORTRAN statements but these routines were not part of the trigger algorithm as such, but had to do with the data handling.

The basic source of the code was developed with PATCHY (a CERN code management program) on an APOLLO workstation. In PATCHY a switch can be set to generate a program to either run on the APOLLO, the IBM or in VME. In any other mode than running in VME, the program would read events from a file. In the VME version of the program a switch can be set to either read the events from the Reordering Memories or from a fixed data set in common memory. Via the Macintosh it is easy to copy the file containing the test events from the APOLLO or IBM to this fixed data block in VME memory. By this procedure many events were processed using the same program running on the APOLLO and IBM and one or more processors in parallel in VME.

The Tracking.

The main activity of the trigger algorithm is the reconstruction of tracks. This is done by fitting a line to points in the 4 planes of a muon chamber. The possible number of combinations (and with this the trigger time) grows quadratically with the number of points (in a module).

Track finding is done in the coordinate system of the module. First both projections are handled independently while in a later stage of the tracking the results are combined. By making this independent tasks, they can be done in parallel. Moreover, time can be gained by rejecting (all) points as soon as in one of the two projections no track can be found.

The four planes are numbered 1-4 with number 1 closest to the interaction point (see fig. 4.6). The program loops over all hits in plane 1 which is now called the *reference* plane. It then loops through all hits in plane 3 and looks if the line through the points in plane 1 and 3 roughly points to the center of the detector. If a pair of such points is found the algorithm looks for all points in planes 2 and 4 that *could* roughly lie on a line through the vertex. For this the intervals in the plane 2 and 4 are calculated where the points are expected. From all combinations of points in the planes 1 and 3, the 'straightest' track with four or three hits is selected. Tracks with four hits are preferred over tracks with three hits. A track is accepted if the hits in the planes 2 and 4 are less than 5 mm from the fitted line. For each accepted track the number of points, the positions of the hits and the deviations from a straight line are stored in a data block called the **tracklist**. This procedure is followed twice, the second time with plane 4 as the reference plane and the first loop through plane 2.

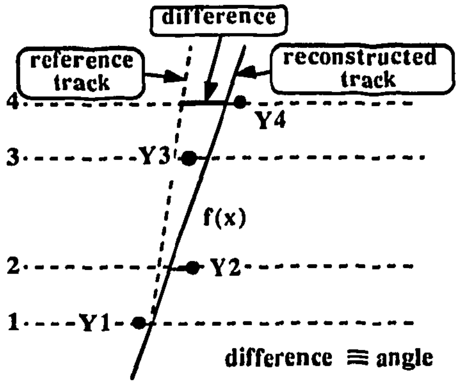

Fig. 4.6 The tracking.

Next the tracklist is cleaned up by comparing the one dimensional tracks with each other. The two main rules that are used for this comparison are:

- From tracks with the same number of points and one point different, the straightest is kept.
- If a 3 point track has its 3 points in common with a 4 point track, then the 3 point track is rejected if the 4th point is less then 3 mm away from the line fitted though the 3 point track. Such cases can occur as the consequence of the left-right ambiguity in reconstructing the points.

After the clean-up of the **tracklist** all one-dimensional track candidates in the same muon chamber are combined in space. For each combination the angle of the one dimensional track is compared with the cut angle. This cut angle (≈ 70 mrad for single muon events, 'narrow cone', and ≈ 210 mrad for dimuon events, 'wide cone') has been determined by Monte Carlo and forms the selection criterion. The two projections are combined into candidate tracks.

The (task-) Manager.

The trigger calculation is split into tasks. Each task does an *independent* part of the calculation like the determination of a hit pattern, fitting a line or combining lines into a track. A task consists of one subroutine called by the task manager (naturally these subroutines can call other subroutines but not one that is called by the manager itself). If a processor has finished the manager decides which task to perform next. The task manager works with a **tasklist**, a list of jobs to be done. The tasklist also contains a pointer to data on which the task works. Also in the tasklist a preference for a specific processor may be indicated. This is sometimes useful to minimize bus traffic.

Several schemes for the manager were tried. The simplest version was opted for in which the manager runs in all processors and works on a 'first-in first-out' basis. More intelligent ways of distributing the tasks were studied. This does not pay off in trigger time and renders the system difficult to debug. The main reason against more sophisticated designs is the addition of overhead to the overall processing time. Suppose that a manager routine has 100 simple FORTRAN statements and 2 statements are executed in 1 μs. Then each time the manager is called will take 50 μs for the subroutine body plus $\approx$12 μs for the CALL-RETURN action. If the manager is called a 100 times per event the overhead is $\approx$ 6.2 ms. Divided by typically 6 processors, this represents $\approx$ 30% of the trigger time. In practice, this gets even worse since sophisticated manager routines work with several semaphores and bus-accesses by which waiting time is added.

Task scheduling

The tasks (identified by a number) and pointers to their input parameters (like a number in the track list) are stored in a tasklist in /TASLIS/[13]. At the start of an event (MF signal) this list is initialized by the Master processor. There are two sets of entries in the list, each linked by pointers. The first set is a linked list of all available tasks, ready to be executed. The second set contains all free entries in the list. While a task is executed it is in neither list. A counter keeps track of the total number of available plus active tasks.

To add a new task a subroutine is called that removes a free entry number from the 'empty' list and fills in the entry with the number of the new task and its parameters. Then it adds the entry to the available tasklist and increments the task counter. When all tasks in the system are done, the task counter is zero.

The Tasks are:

- 'Read Data': This task reads the data from the RM's. Next it orders the data into blocks. Each block represents a projection of one chamber.
- 'Read Group': This task reads a data block from the previous task and unpacks the raw data into wires and times. If the data belonging to one projection satisfies certain requirements (see §4.4.4) it will store the datawords in /WIRELIST/.
- 'Put Hits': This task reads an element of the /WIRELIST/ and translates the data into coordinates. The result in stored in /HITLIST/.
- 'Track in 1 dim': This task searches for one dimensional tracks in /HITLIST/ as described above. Results are stored in /TRACKLIST/.
- 'Track Fit': This task performs a fit on tracks in /TRACKLIST/ and calculates positions and directions.
- 'Track Rejection': This task combines two one-dimensional tracks into a two-dimensional track and looks whether it satisfies the criteria for the single- or dimuon trigger. Validated tracks are stored into /SEMOUT/. /SEMOUT/ is the data block, carrying the triggerresult and is kept with the data. All other intermediate results are normally lost.
- 'Bottom Track Rejection': This task does the same as the previous task but only for the single projection of a bottom chamber.

---

[13] In this thesis we use the notation "/NAME/" for a COMMON data block in common memory.

- 'Read Rawdata': This task reads *all* raw data of a crate of RM's. It combines these data and puts them into DPM after which the controller processor can transfer it. This task is performed *once* by each processor, at the first moment that the processor is waiting for an empty TASKLIST. This task is necessary because the 'Unpack Data' task only considers that part of the raw data, that is interesting for the trigger calculation. Also this task makes it easier to run the data acquisition independently of the trigger.

During the execution of these tasks, a list is kept of all projections being processed. If a projection is rejected, the projection of the same muon chamber in the other direction, is not considered anymore.

The division of the algorithm into these tasks is a process of optimization with respect to the trigger-time. More tasks will introduce more overhead, more calls to the manager and more moving around of data. Less tasks disfavor the parallelism.

4.4.3 The Trigger Monitor and Control system

This part mainly runs on the Macintosh. The program is looping continuously and checks flags. Commands can be given manually or can be generated automatically.

Action of the system can be triggered by:

- the general reset (button)
- input from keyboard or mouse
- an error or exception from the trigger algorithm or data handling system
- the monitoring system itself
- a timer interrupt

The trigger control is done by sending commands to the processors as described before, using the mailbox. Extensive use is made of the Macintosh windowing system to facilitate the use of the commands.

The monitoring of the trigger is done by use of the triggerlog (see §4.1.4). Numbers of events rejected/accepted are displayed on the screen at fixed time intervals, together with other numbers like efficiency and trigger time. A picture of the monitor display is given and explained in fig. 4.7. The monitor is able to detect abnormal situations (f.i. low (≤10%) acceptance over the last 1000 events). In case that a processor is not responding on the monitor requests a reset will be generated.

Data Acquisition and trigger mode (data taking, calibration, test etc.).

```
Date/Time : 15/06/1989 21:26:03
ROMODE=         3 TRGSEL=       -1
BATSTR=       DAS FWAREA= new:F3+
 2nd level Cal.Trigger= Active
```

Number of times that the communication signals occurred (scaler). The numbers are checked for consistency (f.i. #INI=#ID or #MF=#MFD).

```
   INI=       128        ID=      128
    WS=       128
    MF=     25798       MFD=    25798
    MT=      6237
    CT=     19482        TD=    25719
 FATAL=         0    OSCIL=         0
MU SPY=     25790   MC SPY=         4
```

Acceptance separated into event types. These numbers are checked for a 'normal' behaviour of the trigger.

```
ACC. SINGLE MUON=       4703   18.23%
ACC. DI MUON    =        313    1.21%
ACC. 2nd Cal.TRG=         86    0.33%
ACC. TRG.PRC.JET=       1217    4.72%
ACC. REJ. EVT.  =        209    0.81%
TOTAL ACCEPTANCE=       6257   24.25%
TOTAL  REJECTION=      19541   75.75%

RAW MU TRG=  23871;1MU ACC=19.70%
RAW ≠ET    =    814;≠ET ACC=10.57%
```

Trigger time etc.

```
trigger frequency 15.8hz
  local Dead time 14.6%
  av.trigger time  9.2ms
  av.waiting time 38.7ms
```

This line states that all processors are functioning well. If not the monitor will generate a reset.

```
CPU=OK    0T   1T   2T   3T   4T   5T
```

Fig 4.7 Monitoring output.

Some information about the second level trigger (f.i. trigger rate, acceptance) is sent via an AppleTalk link to the general UA1 status display approximately every 30 seconds.

During a run errors are booked in an error log and some histograms are filled (trigger time, acceptance in eta-phi space, acceptance per module etc.) which are only displayed on request. Every 2 hours this information is copied to the Macintosh hard disk together with additional run information.

It was foreseen that a version of the trigger algorithm would also operate on the Macintosh. This would serve as an 'on-line' check by re-determining the trigger decision and by comparing both decisions. However, soon after the introduction of the second level trigger, this system appeared to be so reliable and stable that such a check was considered not necessary. The on-line monitoring of key-variables and fast Express-line[14] checks appeared to be sufficient.

[14] The Express-line is formed by people on 'shift'. They provide a fast detector performance check by analyzing data directly after they have been written. The second level system was integrated in this analysis.

4.4.4 Cuts on the data.

During the trigger calculation, several cuts and boundaries (f.i. array sizes) limit the amount of raw data that is processed. One of our rules had to be that under all circumstances the structure of the dat (datawords/markers/wordcounts/...) should be preserved. This meant that in case of f.i. array overflow, complete projections or even chambers had to be left out (accompanied by the proper error messages of course). This rule was applied throughout all software concerning the second level trigger.

Below a list is given of some of the most important cuts on the data.

- A RM is 2k words deep and the data inside a RM is organized in two groups. During the readout of the RM for event building only 256 words per group are read.
- A FAREM, the interface to the data acquisition system (third level) and the muon chamber monitor, is 8k words deep. If the total amount of data (including markers, word-counts and trigger results) becomes more than 8k words, some of the data may be lost and a warning is issued.
- Only 3 hits per wire are accepted if they are separated by at least 32 ns.
- A projection is accepted if there are more than 3 hits and less than 26.
- Hits of which a the corresponding time lies outside the interval -40 ns $\leq t \leq$ 1.4 μs around the beam crossing time are not used. They are considered to originate from cosmic rays.
- If a new task is generated and the tasklist, which has 128 entries, is full, this task is skipped and an error is generated.
- The one dimensional track list has 16 entries per projection. If more tracks were found, an error is generated and these tracks are skipped.

V

Performance of the trigger.

5.1 Reduction.

Averaged over the whole run in 1989 (3 months) the trigger reduces the event rate to:

≈ 7% if the first level muon trigger does *not* use calorimeter[15] information.

≈ 14% if the first level muon trigger uses calorimeter information.

≈ 20% if the first level muon trigger is combined with a jet requirement.

In all cases the dimuon rate is about 1.2% of the event rate presented to the second level trigger.

The trigger is sensitive up to $|\eta| \approx 1.7$.

5.2 The trigger time.

In this section we distinguish the cycle time, being the time between the MF (start) signal and the TD (end) signal (as shown in fig. 4.2), and the trigger time, being the time that the algorithm needs for the trigger decision.

In a multi-processor trigger, the trigger time is sensitive to the task scheduling and the number of processors. The sequential code was optimized by running it off-line on the APOLLO on events from a file. In fig. 5.1 the average trigger time as a function of the number of processors is given for a set of 600 real events (not necessarily containing a muon). This test was performed reading the data from memory in VME so the readout time of the RM is not taken into account. This affects the results: when reading the data from RM the trigger is generally slightly faster because not all data has to be read using a special feature of the RM's.

The trigger time in fig. 5.1 is measured from the MF signal (which in this case means: read an event from memory) until Accept/Reject. It does not include the data acquisition by CPU 5.

number of processors	time [ms]
1	15.4
2	10.0
3	7.4
4	6.0
5	5.7
6	5.5

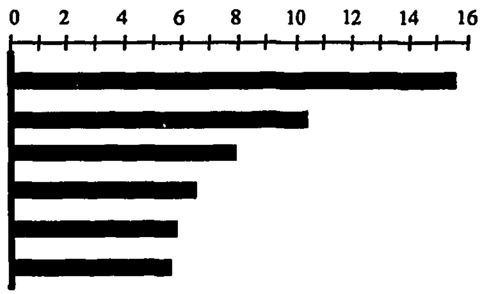

Fig. 5.1 Trigger time as a function of the number of processors.

The structure itself of calling the task manager, initializing the tasklist etc. takes 1.8 ms. This is measured by running on empty events. Fig 5.1 clearly shows the gain of a multi processor trigger compared to a

15With this the coincidence of the calorimeter back-stack and a muon track is meant as described in §3.3.5.

single processor set-up: a factor of 3. This is not a general result but is only valid for our second level muon trigger. The time difference between a 5 and 6 processor setup is already quite small. This is due to a combination of three effects: bus saturation, waiting for active semaphores and the presence of indivisible tasks. With the bus tracer one can see that in the 6 processor setup the average bus occupation is around 20% and peaks in the middle of the trigger cycle. On average, 40 tasks per event are executed. Of course, the 6-processor performance gets better for more complicated data such as events with more then 200 tasks, and these are not exceptional. For these events, the tracking task (TRACK1) is called about as often as all other tasks together.

The performance is also studied for a situation in which the tasks are split up into smaller ones. This did not improve the trigger time; the benefit of parallel processing then cancels against the additional overhead (the manager itself and the CALL-RETURN sequence for every task) and the waiting for semaphores. The more or less *natural* separation of the algorithm into the tasks as mentioned in the previous chapter seems an optimum.

The studies, mentioned above, inspired us to use a 6 processor setup in which the 6th processor is dedicated to event building and readout. This is more efficient than to let the 6th processor participate also in the trigger algorithm

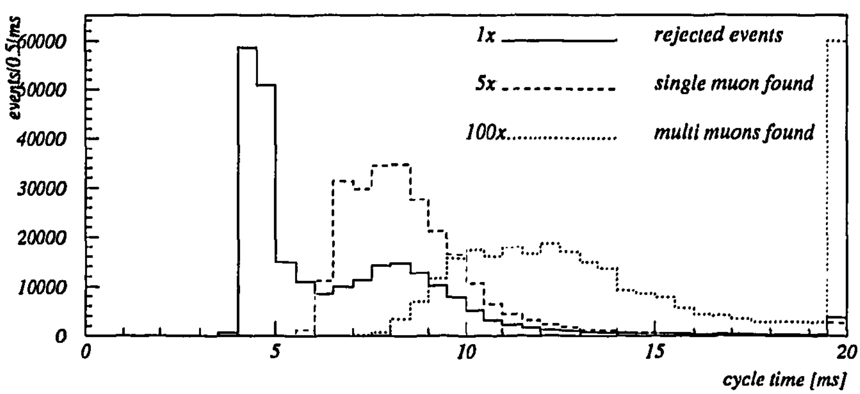

Fig. 5.2 Cycle time distribution.

Fig. 5.2 shows the distribution of the cycle time for rejected events and accepted single- and multi muon events for a typical sample of the 1989 run (the highest bin contains the overflows).

The minimum trigger time is 4 ms. Of this, 1.8 ms is the minimum time taken by the algorithm and 2.0 ms (2µs/word) is a typical writeout time. The time the Reordering Memories need to readin the data from the MTD's is typically 50 µs (1µs/word parallel over 17 branches). Table 5.1 gives the average cycle time for the 1989 run.

Table 5.1 Average cycle time for the 1989 run.

decision	cycle time [ms]
reject	7.3
single muon	8.9
multi muon	14.0
weighted average	7.8

5.3 Deadtime.

The deadtime is measured by the BATS which also specifies the various contributions. For a luminosity of $2*10^{30}cm^{-2}s^{-1}$ and the UA1 detector running on an inclusive muon trigger with all detector elements and triggers operational, the overall deadtime is ≈20%. The main contribution (≈8%) is due to the readout of the Central Detector. The double buffer system adds ≈5% to the deadtime, the VME readout (event filter) contributes also ≈5%. The second level trigger contributes ≤1% and the contribution from BATS itself is also ≤1%.

5.4 Reliability.

Reliability is a measure for the stability (i.e. up time) of the trigger hardware and software and the correctness of the trigger decision.

Many features are built in to recover automatically from most errors occuring on-line. This resulted in a the rate at which the trigger crashed of the order of once a fortnight and in most cases the monitor & command system automatically restarted the system. In fact the only cause[16] for which the trigger stopped was when one of the processors physically died.

Our faith in the trigger results is based on a comparison of the trigger results from the on-line multi processor trigger with the off-line code as it runs on the IBM as part of the UA1 reconstruction program. The off-line code has been tested with Monte Carlo generated muons and with real events from previous runs. Also events are visually scanned to verify the trigger result. However, this is a time-consuming activity (ca. 5 events/hour) and this is only done in exceptional cases.

There can be three reasons to accept an event. First, the trigger program may find one muon track candidate of good quality[17]. Second, it may find more than one muon track candidate of medium quality and in the third place, an event can also be accepted for both reasons at the same time. In addition the trigger can accept events with 'the benefit of the doubt', for example in cases information is lacking. With in addition the possibility to reject an event, the trigger decision is thus a choice from 5 possibilities.

[16]The trigger is resistant against any corrupt data and even a RM failure after which the trigger automatically continues without that data stream. In all these cases 'a bell rang' for the operators.
[17]see §4.4.4: with good quality is meant a straight track that is pointing to the vertex within the cut-angle.

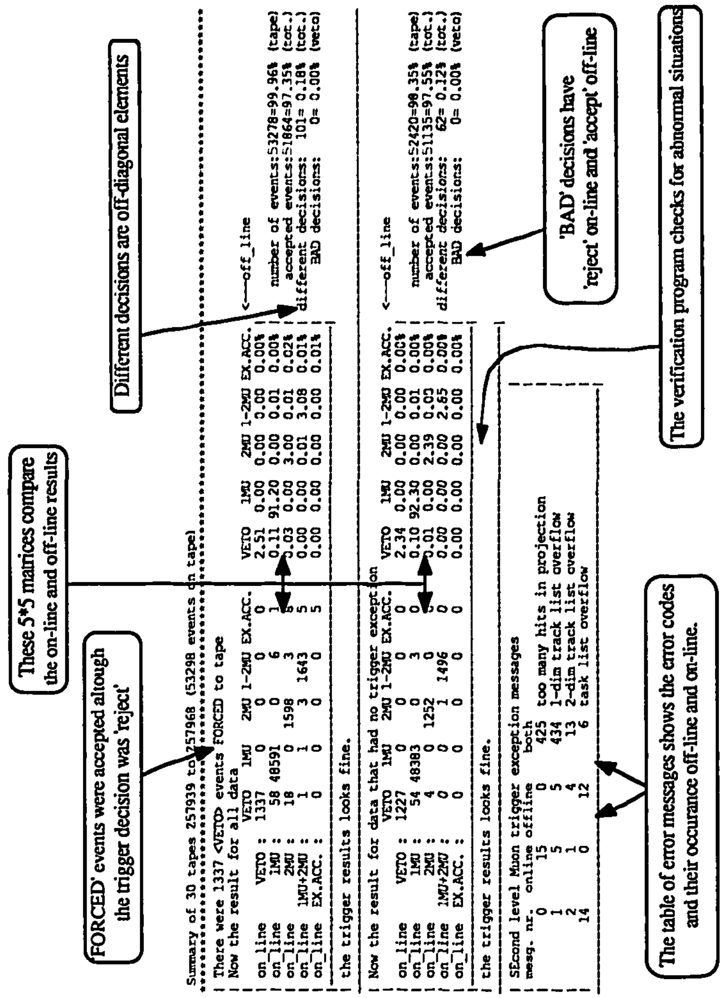

Fig. 5.3 Comparison of the on-line and off-line decision with the 30 tapes Z57939 to Z59768. (53298 events)

The comparison between the on-line and off-line trigger results can be represented by a 5 by 5 matrix. In the ideal case this is a diagonal matrix. Fig 5.3 shows this comparison for the data of 30 cassettes. The non-diagonal elements are an indication of unexpected[18] behaviour of the on-line trigger. A "BAD" decision is defined as one that had a "VETO" on-line but not off-line (Such events were written to cassette as part of the 1% of the rejected events that were still accepted for monitoring purposes or by a 'second level trigger off' dedicated run).

[18]The on-line and off-line results are not identical by definition: the structure of both machines (f.i. the accuracy of the numbers) can provide a difference in the results. However this difference is expected to be less than a fraction 10^{-4} of the events.

All "BAD" cases which were found were related to special events like cosmic showers. During a run, the comparison is done every few hours with in addition a one page report on exceptions and acceptances.

5.5 Efficiency from Monte Carlo.

The efficiency of the trigger as a function of the p_t of the muon has been calculated by generating single muons using a Monte Carlo program.

Events from this Monte Carlo program were processed through the UA1 detector simulation program. This program also accounts for multiple scattering, muon chamber efficiencies etc. The output of this program are wire/time data words just like the raw data.

The off-line muon trigger code has been used to process these data and the results are shown in fig. 5.4 and 5.5. Plotted is the ratio of the reconstructed muon tracks over generated muon tracks as function of p_t.

In the results below '*narrow cone*' refers to the criterion for a high p_t muon track candidate while with '*wide cone*' we mean a di-muon track candidate (§3.4.1).

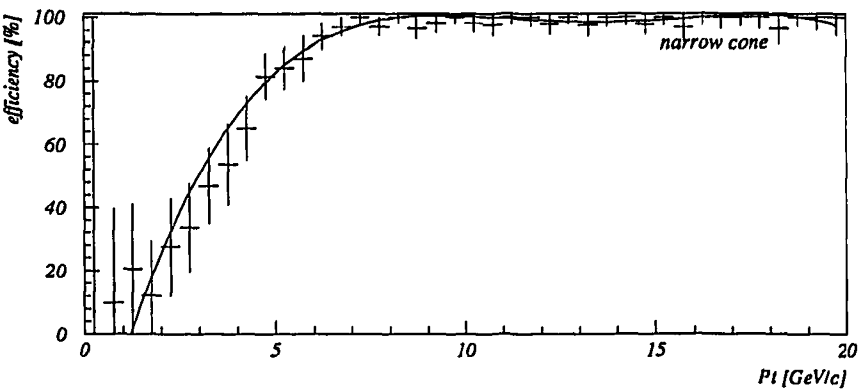

Fig. 5.4 Efficiency for the narrow cone by Monte Carlo.

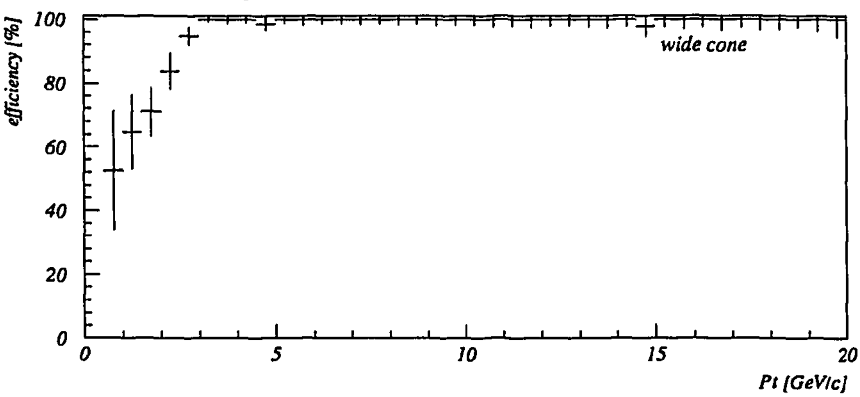

Fig. 5.5 Efficiency for the wide cone by Monte Carlo.

The simulation resulted in a calculated efficiency of:

Narrow cone:	$\geq 98.8 \pm 0.4\%$	for $p_t \geq 7$ GeV/c
Wide cone:	$\geq 99.5 \pm 0.2\%$	for $p_t \geq 4$ GeV/c
	(statistical errors only)	

5.6 Efficiency from data.

From the special data which are taken to study the difference between on-line results and the off-line reconstruction we can also calculate the efficiency of the trigger as a function of p_t of the muon.

Therefore the data had to be processed including the full Central Detector reconstruction to calculate the muon momentum. The results of the comparison with the on-line result are shown in fig 5.6 and 5.7. Plotted is the ratio between the number of muon tracks found in the off-line reconstruction and the on-line trigger result. This method is the most realistic one but suffers from low statistics.

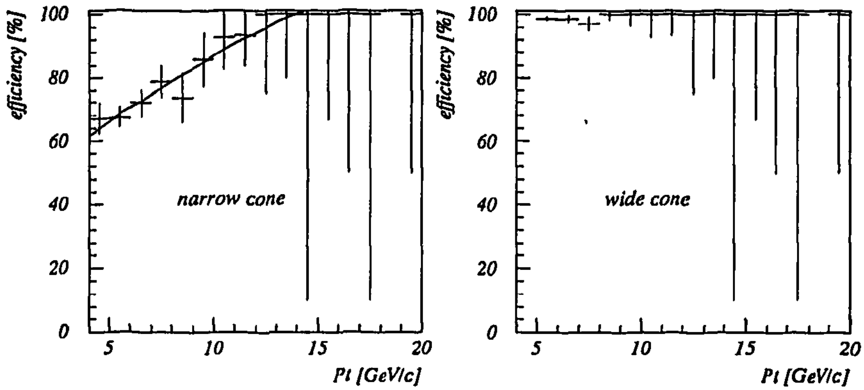

Fig. 5.6 Efficiency by real data.

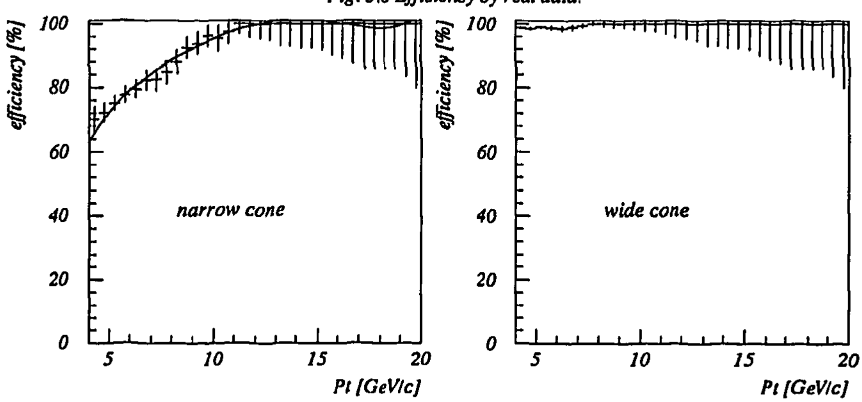

Fig. 5.7 Efficiency by real data summed for all events above a P_t.

The statistical errors in these histograms are calculated from

$$\Delta\varepsilon = \sqrt{\left[\frac{\sqrt{\#DIFF+1}}{\#IN}\right]^2 + \left[\frac{(\#DIFF)\sqrt{\#IN+1}}{\#IN^2}\right]^2} \ [*100\%] \tag{5.6}$$

This formula takes into account the correlation between in- and output rate. In this formula #IN is the input number of events to the trigger and #DIFF is the number of events which are rejected.

In spite of the ***identical*** results of the on-line and off-line algorithm, there is some difference in efficiency between simulated- and real data, as shown in fig. 5.8. This could have two reasons:

1) The simulated muon sample is clean with respect to additional activity like noise, cosmic rays, leakage, hot-spots and spikes.

2) The off-line selection overestimates the efficiency: it is known (during scanning we learned that some of these events were cosmic rays and kinks) that there is a class of events which does not pass the trigger criteria but passes the 'off-line' selection criteria. The 'pointing requirement' of the trigger turns out to be much stronger. Moreover, the timing information poses more stringent criteria in the trigger algorithm than in the off-line selection.

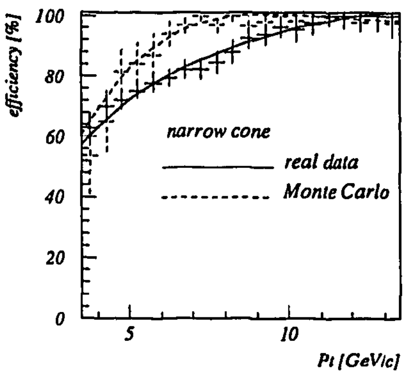

Fig. 5.8 Comparison of real data and MC.

The following numbers are the "final" results (with the present knowledge of the detector) for the efficiency of the second level muon trigger.

selection	data sample	muon p_t	trigger efficiency
Narrow Cone (single μ)	Real Data	$p_t \geq 8$ GeV	91.0 ± 6.0 %
		$p_t \geq 10$ GeV	96.0 ± 4.0 %
	Simulated Data	$p_t \geq 7$ GeV	98.8 ± 0.4 %
Wide Cone (multi μ)	Real Data	$p_t \geq 3$ GeV	98.0 ± 1.0 %
	Simulated Data	$p_t \geq 4$ GeV	99.5 ± 0.2 %

Fig. 5.9 Trigger efficiency.

The quoted errors are statistical only.

The systematic error is estimated at ±2%.

5.7 Conclusions.

- The second level muon trigger has successfully operated during the 1988 and 1989 runs.
- The efficiency is better than 91 % ($p_t \geq 8$ GeV) for single muon events and 98 % ($p_t \geq 3$ GeV) for multi muon events.
- The reduction for single muon events is 14 to 20% depending of the first level trigger parameters.
- The reduction for multi muon events is 1.2%.

In addition we quote the following numbers

- ±45% of the di-muon triggers also satisfied the single muon criterion.
- The contribution of the second level trigger time to the total UA1 dead time was less then 1% for $\mathcal{L}=2*10^{30}cm^{-2}s^{-1}$.
- The average processing time is 7.8 ms.

VI

Muon physics.

6.1 Introduction.

The standard Model

Our present knowledge of the fundamental laws of nature can be summarized in a theoretical framework generally known as the 'Standard Model' [6.1]. The fundamental spin $\frac{1}{2}$ fermions are six leptons and six quarks. They can be grouped in doublets of three families:

leptons

ν_e	ν_μ	ν_τ
e	μ	τ

quarks

u	c	t
d	s	b

Although the t (top) quark has not yet been discovered, its existence is plausible and there is indirect evidence[19]. There exist four fundamental interactions which are mediated by the exchange of a boson (integer spin).

- The electromagnetic interaction, mediated by the massless photon (γ).
  The photon couples to electric charges.
- The weak interaction, mediated by the massive vector bosons W^+, W^- and Z^0.
  These bosons induce transitions in 'weak isospin' and 'weak hypercharge' space.
- The strong interaction, mediated by eight massless gluons (g).
  The gluons couple to a charge called 'colour'
- Gravity, mediated by the graviton.
  Gravity is not yet described in the framework of a relativistic quantum field theory.

The electromagnetic interaction is known since a long time. It is described by a gauge theory called Quantum Electrodynamics (QED). Quantum Chromodynamics (QCD) was developed in analogy to QED. Rather than to electric charge the particles couple to 'colour', existing in three types. As only quarks and gluons carry colour, leptons do not feel strong interactions. The quarks are grouped either in mesons, which consist of a quark and antiquark carrying a colour and its anti-colour, or in baryons which consist of three quarks carrying complementary colours.

The electromagnetic and weak interactions are simultaneously described in the Glashow-Salam-Weinberg theory [6.2].

---

[19]There exists a relation between the top quark mass and the flavour mixing parameters. The experimental limits for mixing indicate the presence of the top quark.

The 'physical' states d, s and b are a mixture of the weak eigenstates d', s' and b'. Weak interactions of quarks can therefore occur between different families, a charm quark can decay into a strange quark or (less likely) into a down quark. The mixing is described by the Kobayashi-Maskawa matrix [6.3]

$$\begin{bmatrix} d' \\ s' \\ b' \end{bmatrix} = \begin{bmatrix} V_{ud} & V_{us} & V_{ub} \\ V_{cd} & V_{cs} & V_{cb} \\ V_{td} & V_{ts} & V_{tb} \end{bmatrix} \begin{bmatrix} d \\ s \\ b \end{bmatrix} \tag{6.1}$$

The Z^0 mediates neutral current interactions e.g. $\nu p \rightarrow \nu X$. Neutral current transitions between members of different quark families are suppressed. The physical states Z^0 and γ are mixtures of the third component of the weak isospin and the weak hypercharge. This mixing is parametrized by the Weinberg angle θ_W.

The theory requires at least one physical scalar particle called Higgs. The Higgs field is necessary to make the $W^{\pm}$ and Z^0 bosons massive by spontaneous symmetry breaking. The Higgs particle has not yet been discovered.

Although the Standard Model describes our knowledge of nature very well, it is generally not believed to be the ultimate theory. It needs 18 parameters which have to be determined experimentally: 6 quark masses, 3 lepton masses, 3 Kobayashi-Maskawa angles and a phase, the electromagnetic coupling, the Weinberg angle, the vacuum expectation value of the Higgs field and the Higgs mass, and the QCD scale. A more fundamental theory should predict their values. Also there is no obvious reason why there are three families of quarks and leptons. Finally, gravity is not included.

Many parameters of the Standard Model can be measured at Hadron Colliders such as the Sp$\bar{p}$S at CERN where at a center of mass energy of hundreds of GeV/c^2 processes occurring at the quark level can be observed. For example: by measuring high energy muons and more specifically dimuons, one may study processes involving the heaviest (un)known quarks (heavy flavour production). Muons (and jets) are a unique tool to look for the as yet unobserved top-quark. In the dimuon channel several resonances like the J/Ψ and Υ can be studied. The Z^0 particle was discovered by measuring dileptons at the p$\bar{p}$ collider at CERN. Flavour mixing can also be studied in the dimuon channel. Everything stated about (di)muons generally also holds for (di)electrons, but in this thesis only muons will be discussed.

6.2 Di-muon sources

Heavy flavour

Quark-antiquark pairs are produced by several processes like $p\bar{p} \rightarrow q\bar{q}'$. In all the cases the quarks may decay into another quark plus a muon and neutrino, directly or after a cascade (according to fig. 1.3 and 1.4).

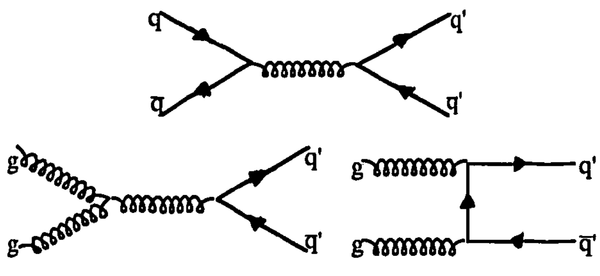

Fig. 6.1 3 Examples of Feynman diagrams for heavy flavour production.

Drell-Yan

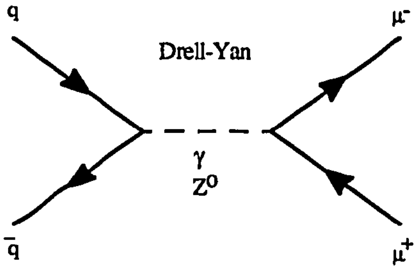

Fig. 6.2 Feynman diagram for Drell-Yan muon pair production.

The Drell-Yan process is the annihilation of a quark and its antiquark into a lepton pair. Lowest order calculations, based on γ exchange, predict a cross-section:

$$\frac{d\sigma}{dm} = \frac{8\pi\alpha^2}{3} F(\tau) \frac{1}{m^3} \qquad (6.2)$$

in which α is the fine structure constant and m is the dilepton invariant mass. The scaling function[20] $F(\tau{=}m^2/s)$ describes the probability to find a quark-antiquark pair of mass m at center of mass energy $\sqrt{s}$.

The signature of such events is a pair of opposite sign leptons, which are not accompanied by any hadrons (apart from the hadrons of the underlying event[21]). Hence the muons from a Drell-Yan process should be 'isolated' (An exact definition of isolation will be given in the next chapter).

---

[20] In the presence of scaling violations, the F has to be modified, i.e. becomes m dependent.

[21] The underlying event is that part of the event which is associated with the remaining parts of the protons which did not take part in the hard collision.

J/Ψ and Υ

Resonance production of dimuons is expected through the Υ and J/Ψ states. Such mesons, corresponding to a bound $c\bar{c}$ (=J/Ψ) or $b\bar{b}$ (=Υ) state, can in principle be produced by the Drell-Yan mechanism, if the virtual photon converts into a bound quark-antiquark state. They can also be produced by strong interactions and this is expected to be one of the main sources at the collider. Another important source of J/Ψ's could be the decay of beauty mesons. A branching ratio b → J/Ψ+X of about 1% has been measured [6.4]. As for dimuons from ordinary Drell-Yan processes, these muon pairs are unlike-signed and isolated. In the dimuon mass distribution they appear as resonances above the Drell-Yan and heavy flavour continuum.

Theoretically, a $t\bar{t}$ bound state is not excluded. At present this state is not observed. From the lower limit for the top mass [6.5], the expectation that the decay width will be large and the expectation that the branching ratio for the dimuon channel will be around one percent, makes this state difficult to observe at the CERN Sp$\bar{p}$S collider.

6.3 Flavour mixing.

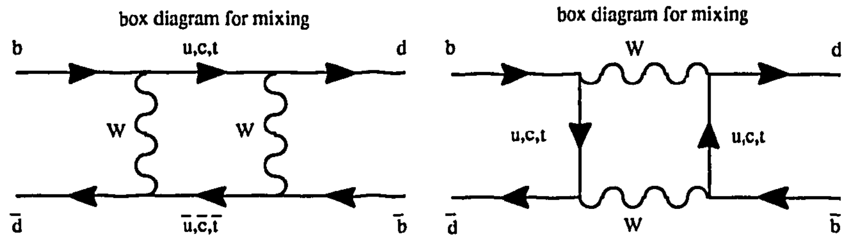

Fig. 6.3 Feynman box diagrams for oscillations of $b\bar{d}$ mesons.

The decay of neutral kaons has so far been a unique tool for studying second-order weak interactions. Since weak interactions need not conserve flavour quantum numbers, transitions between $K^0 = (\bar{s}d)$ and $\bar{K}^0 = (\bar{d}s)$ are allowed. As is well known, the mass eigenstates are not K^0 and $\bar{K}^0_?$ but linear combinations: K^0_S and K^0_L. The mass difference between these states, ΔM, result in a time-dependent phase difference between the K^0_S and K^0_L wave functions and a consequent periodic variation of the K^0 and $\bar{K}^0$ components. Thus $K^0 \leftrightarrow \bar{K}^0$ oscillations are observed, with a period given by 2π/ΔM. An excellent review of the physics of the K^0 system can be found in [6.6]. Since the discovery of the new quark flavours, charm and beauty, it is natural to consider the possibility of oscillations in the case of neutral D and B mesons [6.7]. Mixing is observable in the K^0 system only because the lifetime is comparable to the oscillation period. The D^0 mesons have a short lifetime compared with the expected oscillation period. It is therefore not surprising that no mixing has been observed in the D^0-$\bar{D}^0$ system [6.8].

The recent observation that beauty particles have relatively long lifetimes [6.9] suggests that oscillations may be observed in the B^0-$\bar{B}^0$ system. The degree of mixing (r) can be expressed as the probability that a B^0 meson oscillates into a $\bar{B}^0$ relative to the probability that it remains a B^0:

$$r \equiv \frac{\mathrm{Prob}(B^0 \rightarrow \bar{B}^0)}{\mathrm{Prob}(B^0 \rightarrow B^0)} \cong \frac{(\Delta M/\Gamma)^2}{[2 + (\Delta M/\Gamma)^2]} \tag{6.3}$$

assuming $\Delta M << \Delta\Gamma$; $\Delta\Gamma$ is the difference between the decay width of the B_h^0 and B_l^0 states, $B_{h,l}^0 = (B^0 \pm \bar{B}^0)/\sqrt{2}$ and CP violation is neglected. Oscillations may occur for the two neutral meson states $B_d^0 = (\bar{b}d)$ and $B_s^0 = (\bar{b}s)$. The B_h^0 - B_l^0 mass difference can be calculated according to box diagrams using the experimentally determined values of elements of the Kobayashi-Maskawa matrix [6.3].

Experiments at e^+e^- colliders have recently placed limits on $B^0 \leftrightarrow \bar{B}^0$ oscillations. CLEO and ARGUS have deduced substantial oscillations in the $B^0 \leftrightarrow \bar{B}^0$ system by measuring the rate of like sign dileptons from samples of $B\bar{B}$ events on the Y(4S) resonance. However they have no sensitivity to oscillations in the $B_s^0 \leftrightarrow \bar{B}_s^0$ system since the Y(4S) is below the threshold for producing $B_s^0 \bar{B}_s^0$ pairs.

VII

The (di-) muon sample.

7.1 Data collection.

In section 7.1 we describe the data collection and event reconstruction. Section 7.2 presents the data sample with a discussion of the background sources. In section 7.3, some quantities used for further analysis are investigated. Next, the J/Ψ and Υ signals will be discussed.

7.1.1 Luminosity & triggers.

Roughly $3*10^7$ events were collected during the 1987, 1988 and 1989 runs. To store all detector information 25.000 cassettes (≈4.500 Gbyte) were written. The 1987 run was dedicated to 'Minimum Bias[22]' events, to study the detector behaviour. At the same time, the collider was tuned for higher luminosities ($2*10^{30}$) and 6 on 6 bunch operation. In 1988 an integrated luminosity of 1.4 pb^{-1} was recorded at a center of mass energy of 630 GeV. In 1989 another 3.5 pb^{-1} was accumulated. Due to the absence of an electromagnetic calorimeter, the 1988 and 1989 runs were dedicated to muon physics. Events of the data samples discussed in this chapter contain at least two muons (typically 1.2 % of all triggers).

At the first level, two main muon triggers could be used:
For "low" luminosities, $\mathcal{L} \leq 10^{30}\,cm^{-2}s^{-1}$:

$\left\{\begin{array}{l}\text{1 muon in the F3 area}\\ \text{or 2 muons anywhere.}\end{array}\right.$

For "high" luminosities, $\mathcal{L} \geq 10^{30}\,cm^{-2}s^{-1}$:

$\left\{\begin{array}{l}\text{1 muon in the F3 area combined with a jet[23] of } E_t \geq 10\ GeV/c^2 \text{ anywhere}\\ \text{or 1 muon in the barrel chambers } (|\eta| \leq 1.6)\\ \text{or 2 muons anywhere.}\end{array}\right.$

Furthermore one major calorimeter trigger was used:
For "very low" luminosities, $\mathcal{L} \leq 0.2\ 10^{30}\,cm^{-2}s^{-1}$,:

$\left\{\begin{array}{l}\text{a jet of } E_t \geq 10 \text{ GeV anywhere (for background studies).}\\ \text{In this case the second level } \mu \text{ trigger and the event filter were disabled.}\end{array}\right.$

The F3 area corresponds to those tubes that roughly lie inside the range $|\eta| \leq 2.2$. The main reason for excluding the very forward regions ($|\eta| > 2.2$) from the inclusive muon trigger is the very high background from beam fragments. Inclusions of these areas would introduce a significant rise in trigger rate and consequently would cause less efficient data taking.

In practice only events that passed the emulator 'FILTER' are used for the analysis. This reduces the 1988 data sample to 440.442 events on 666 cassettes; the data sample from 1989 contains 740.906 events on 953 cassettes.

---

[22]Minimum Bias events are taken with very weak trigger constraints and serve as reference data for detector performance and calibration.
[23]At the trigger level, a jet is defined as a cluster of calorimeter cells representing a cone in eta-phi space.

7.1.2 Definitions.

In this paragraph, several quantities used in the analysis are defined:

Mass:

The invariant mass of a dimuon pair is defined as:

$$m = \sqrt{(E^1+E^2)^2 - (p_x^1+p_x^2)^2 - (p_y^1+p_y^2)^2 - (p_z^1+p_z^2)^2} \tag{7.1}$$

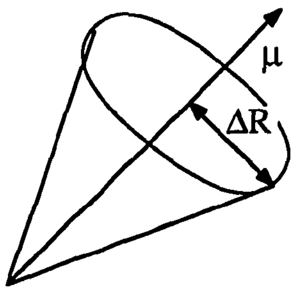

fig. 7.1 Cone definition.

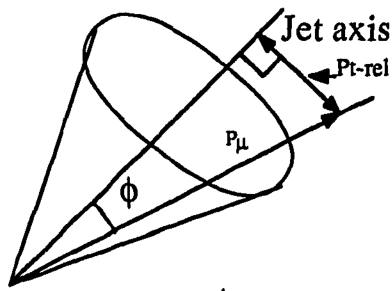

fig. 7.2 p_t^{rel} *definition.*

Cone:

A cone is defined in η - ϕ space. Its origin is at the vertex (fig. 7.1). The cone size ΔR is:

$$\Delta R = \sqrt{\Delta\phi^2 + \Delta\eta^2} \tag{7.2}$$

Isolation:

Isolation is a concept used in relation to a muon. It is defined as the energy (measured in the calorimeter) and momentum (measured in the CD) of particles in a cone of size ΔR around the muon. Isolation is used to differentiate between the physical processes from which a muon may originate. It is expected that muons from heavy flavour decays will be close to, or inside a jet while muons coming from Drell-Yan, J/Ψ or Υ have little activity around the muons, hence are isolated.

Three definitions for the isolation are used:

$$I \quad = \quad \frac{\Sigma E_t}{3} + \frac{\Sigma P_t}{2} \qquad (\Delta R=0.4 \text{ or } 0.7) \tag{7.3}$$

$$S \quad = \quad \sqrt{\left(\frac{\Sigma E_t}{3}\right)^2 + \left(\frac{\Sigma P_t}{2}\right)^2} \qquad (\Delta R=0.4 \text{ or } 0.7) \tag{7.4}$$

$$S^{2\mu} \quad = \sqrt{\left(\frac{\Sigma E_t^{\mu 1}}{3}\right)^2 + \left(\frac{\Sigma E_t^{\mu 2}}{3}\right)^2} \qquad (\Delta R=0.4 \text{ or } 0.7) \text{ (footnote 24)} \tag{7.5}$$

[24] The variable $S^{2\mu}$, is also known without the root and factors $\frac{1}{3}$, but in this paper defined in 7.5 for compatibility with 7.4 and 7.3.

For an ideal detector I and S should give the same value but they differ due to statistical effects and detector accuracy. About $\frac{1}{3}$ of all particles in a jet, are electrically neutral and are not detected by the CD. The calorimeter is sensitive to both, neutral and charged particles. To balance the contribution of the E_t and P_t measurements, factors 1/3 and 1/2 are used.

P_t-relative:

P_t relative is defined as (see fig. 7.2):

$$p_t^{rel} = |p^{\mu}| \sin \phi \tag{7.6}$$

p_t^{rel} serves as a measure for the distance between a muon and a jet.

Missing E_t.

Conservation of energy would require cancellation when adding transverse energies vectors as measured by the calorimeter cells in all directions. This supposes that the detector is hermetic for transverse energy measurement. An unbalance in this energy sum is called missing E_t ($\not{E}_t$) and is the signature for an escaping neutrino. In the case of a muon event, this variable is corrected for the muon energy. The muon momentum as measured in the CD is used to correct the energy sum.

7.1.3 Event reconstruction and identification.

Preprocessing.

In the reconstruction, a data management scheme, HYDRA [7.1] is used. The first reconstruction step, called 'preprocessing' mainly converts the data into this HYDRA format. In addition, calibrations are applied.

- In the CD, the t_0 values are subtracted from the measured drift times, and the coordinate along the wire is obtained from the ratio of charges at its two ends.
- In the calorimeter, pedestals are subtracted and ADC counts are converted into raw energies.
- The calorimeter data is corrected for 'problem channels' (dead photomultipliers).
- The muon chamber information is only copied.

Reconstruction in the CD

The track reconstruction in the CD [7.2] is the main part of the reconstruction procedure, not only because it requires a large fraction of the computer time, but also because the CD immediately visualizes the event structure and is indispensable for the reconstruction of muons.

The first step is the search for track segments in individual drift volumes. Tracks are searched for only in the drift plane of the CD. A chaining algorithm is used that makes use of the fact that points belonging to a track are in general closer together than random combinations. The points of a chain have to lie on a straight line locally, i.e. groups of at most eight consecutive points in a chain have to pass certain quality criteria in a straight line fit. This rejects cases in which two tracks overlap or a track changes curvature due to particle decay. Chains on a common circle line are combined to track segments in a drift volume. This procedure is repeated for all drift volumes.

The first step is nearly independent of calibration constants, drift velocity and drift angle. In the next step these constants are applied to those points of the track segments, which are used to combine track segments from different drift volumina. Then the tracks are refitted using the information of all points. The least-squares method is used to fit circles in the xy-plane and straight lines in the sz-plane, where $\vec{s}$ is a tangent vector to the trajectory.

Finally the information from all tracks is used to reconstruct the vertices. While the horizontal and vertical beam position are known to about 200μm, the location of the interaction point along the beam can vary by ±50 cm due to the length of the bunches. Therefore the intersection points of all tracks with the beam axis in the xy-plane are calculated to find the vertex or vertices. All tracks compatible with a vertex within 3σ are associated to the vertex and refitted, using the vertex position as additional information.

Reconstruction in the Calorimeter

The reconstruction of the barrel and endcap calorimeters is done by

$$E_j = \sum_{i=1}^{2} C_{ij} \cdot Q_i \tag{7.7}$$

In which E_j is the energy of the j- th cell, C_{ij} a calibration constant belonging to the i- th photomultiplier of the j- th cell and Q_i is the signal from the i- th photomultiplier. In situations in which the photomultiplier signal is bad (photomultiplier is dead or the pre-amplifier is oscillating), that photomultiplier is skipped and the signal of the complementary photomultiplier is taken.

Reconstruction in the Muon Chambers

Since there is no magnetic field in the muon chambers, trajectories of particles passing them will be straight lines. Track finding is performed in the projections. In the ideal case, four points of a track will be measured per projection, but points can be lost by inefficiencies or dead regions. Therefore only three hits are required to reconstruct a track. Tracks are found by choosing two planes as pivot planes, initially the two outermost planes, and looking for additional hits in the intermediate planes. A hit is accepted, if its distance from the line connecting the outermost points is less than 5 mm. Once an additional hit has been found, the angle dependent calibration function is used, and a straight line is fitted to the points using a least-square method. If the χ^2 of this fit exceeds 50 per degree of freedom, the track candidate is discarded. After all hit combinations of the two pivot planes have been considered, an other pivot plane is chosen and the procedure is repeated.

In the second step, the tracks in projection are combined to tracks in space. With only two projections (in the same module), there is no possibility to decide which projected tracks belong together. So every track in one projection is combined with every track in the other one. To obtain the final parameters of the space tracks, the tracks in projection are refitted, using the information from the other plane to take into account the propagation time of the signal along the wire. [7.3]

Identification of Muons

Due to the mass of the calorimeter and the additional iron/concrete shielding, all tracks in the muonchambers most probably originate from muons. To qualify as muon, a track in the muon chamber has to have a corresponding track in the CD. The momentum of the muon is then determined from the (corresponding) CD track. Combinations of (an extrapolated) track in the muon chambers and all tracks in a sector of the CD around this candidate muon track are considered. For each combination the matching of the 2 tracks in coordinate space and r-φ space are calculated. χ^2_{ang} and χ^2_{pos} serve to find the combination of (muon chamber and CD) tracks which come from the same muon. At the time just after or during a run when the full calibration of the detector is not yet available "loose matching" is applied in order not to loose muon candidates. When time goes by and the alignment of the separate detector elements is better known a more severe requirement "tight matching" is used to identify a muon. For the analysis presented here a third criterion was used to find the "most probable" combination of a muon chamber and CD track. This method is based on a maximum likelihood fit: from all combinations of CD tracks and muon chamber tracks, the 'most probable' combination is selected [7.4]. This method gives better results for dimuons if the muons are close to each other.

Identification of Jets

The aim of the jet reconstruction is to measure the momenta of quarks and gluons. The average direction and the total momentum of the fragments, will be correlated to the original parton. So a parton will be visible as a concentration of energy within a certain cone.

The method to reconstruct the jets is as follows:

- Each calorimeter cell is assigned an energy vector.
- The cells with a transverse energy of $E_t \geq 1.5$ GeV are ordered according to the E_t.
- The cell with the highest E_t initiates the jet finding algorithm.
- All cells within a cone of $\Delta R=1$ are added to the 'initiator'.
- From the remaining cells the highest is the next 'initiator'.
- all cells with $E_t < 1.5$ GeV are added to the nearest jet.
- etc. etc.

Beside the initiator threshold, the method requires the cone size as an input parameter. The choice of $\Delta R=1$ was inspired by jet studies; a "typical" jet lies within this cone.

Identification of 'Neutrinos'.

The UA1 detector has been designed to cover the complete 4π solid angle for energy measurements. Therefore missing Et can be used to identify a neutrino. Transverse energy and not energy is used in the analysis since energy close to the beam escapes detection.

$$E_t^{miss}\ (\not{P}_t) = -\sum_i E_t^i \tag{7.8}$$

In reality, particles escaping through cracks and measurement errors lead to a finite energy sum even if no non-interacting particles are present. Therefore the missing energy measurement is only accurate for "high" P_t neutrino's, say $P_t \geq 15$ GeV/c.

7.2.1 Selections and Samples.

7.2 Selection criteria.

From the reconstructed data, several samples are created with a 'Technical', 'Loose', 'Semi-tight' and 'Tight' selection[25]. For these samples different selection criteria are used and sometimes different calibrations. Moreover the time at which they became available after the data-taking is different. The 'Tight' selection uses the strongest criteria, the most accurate calibration constants but became available only 7 months after the end of the 1989 run. There are single muon samples for studies such as W/Z analysis and top search. The dimuon samples consist of two major ones: the general sample and the J/Ψ sample. Out of the general sample, subsamples are created for topics as the Υ and top search.

The 'Technical' selection is done immediately after the run and used to reduce the data. In addition it serves to study the selection criteria and to understand the selection software. To process the 1988/89 data, a substantial part of the selection software had to be rewritten. This was needed since the detector had been modified and the old track-extrapolation software was considered inadequate.

Although other analyses used weaker selections, the data used in this thesis have in general passed the 'Tight' selection.

For the general dimuon sample with 'Tight' selection the following criteria are used:

- The CD tracks from both muons have to originated from the *same primary* vertex.
- The CD track quality must obey:
  number of points in the xy plane ≥ 20.
  The projected track length ≥ 20 cm.
  The χ^2 from the residuals in the xy plane ≤ 3.0.
  The χ^2 from the residuals in the z plane ≤ 9.0.
- The events have to pass the Kink- Cosmic- and leakage[26] rejection routines.
- The $\chi^2_{average} = 0.5 \bullet (\chi^2_{angle} + \chi^2_{posistion})$ from the CD- muon chamber matching < 15.0.
- $p_t^{\mu 1} \geq 3.0$ GeV/c, $p_t^{\mu 2} \geq 3.0$ GeV/c.

Note that this selection does not contain a mass cut or a rapidity cut.

For the J/Ψ sample, these criteria are also used except that the P_t cuts are replaced by a mass cut of $2.0 \leq m^{\mu\mu} \leq 4.5$ GeV/c^2 and the vertex is not necessarily a primary one. By the exchange of these cuts, the J/Ψ

[25]In this paper we use *selection* for a set of cuts and *sample* for a collection events.

[26]A kink is a discontinuity in the direction of a charge track due to the decay of a kaon or pion into a muon.

sample is about 4 times larger. The J/Ψ sample discussed in §7.3 is not selected with the final ("tight') matching.

We expect the dimuon sample to contain muons from heavy flavour production, Drell-Yan production and decay of vector bosons. The heavy flavour events will appear as a continuum with peaks for several resonances especially the J/Ψ and Υ will be clear. Besides these mechanisms we expect a substantial amount of events in witch one or more muons originated from a pion or kaon decay. There are other background sources, however we expect their contributions to be small compared to the pion and kaon decays.

7.2.1 Muon Background sources

Muons from the decay of π's and K's in flight [7.5]

Charged pions and $K^{\pm}$ mesons predominantly decay into muons and form a serious source of background since real muons are involved. Fortunately the lifetime of both mesons is relatively long ($O(10^{-8}$ s)). The probability that a decay occurs within a traversed distance L is given by the following expression

$$\text{Prob.}(\text{meson} \rightarrow \mu^{\pm}\nu_{\mu}) = \int_0^L \frac{m}{p\,c\tau}\,ds \tag{7.9}$$

with m the mass of the meson, τ the meson lifetime, p the meson momentum and c the velocity of light whereas the traversed distance is the integration variable. The probability of a decay very close to the interaction vertex is small due to the large values of cτ namely: $c\tau(K^{\pm}) = 370.4$ cm and $c\tau(\pi^{\pm}) = 780.4$ cm [7.6].

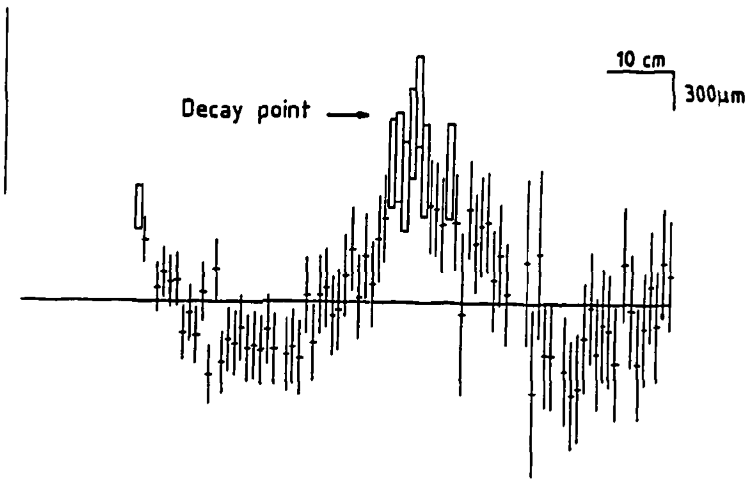

fig. 7.3: *Residuals of the reconstructed CD tracks in the decay $K \rightarrow \mu\nu$.*

Many of the decaying mesons give rise to mis-measurements of the muon momentum in the CD. This occurs when meson and muon tracks are fitted to one single track as is illustrated in the track residual plot of a reconstructed kaon decay (fig. 7.3). Two circular segments are combined and form a so-called 'kink'. In practice the background due to these kinks can be removed as long as the decay occurs not too close to the edges of the CD. For the less massive pion, kinks will be much less pronounced and more difficult to detect. High momentum mesons, which only rarely decay, but which produce high momentum muons form another dangerous background. With a specially written Monte Carlo program the detector response to pions and kaons decaying in flight into muons was studied. The contribution to the dimuon sample from this background varies strongly with the cuts applied and will be listed along with the discussion of the data.

Cosmic rays

Since the UA1 detector is only shielded by ~ 5 m of earth one expects a significant flux of cosmic rays. However, cosmic rays will in general not go through the interaction vertex and will only very rarely pass the detector at exactly the time when the apparatus is triggered by a beam crossing. Timing[27], association with the vertex and the fact that cosmic rays give very stiff tracks in the CD, provide good discrimination possibilities. Therefore the background due to cosmic rays can be removed by software to within 1% [7.7].

Leakage of hadrons through cracks

Light guides, cabling, mechanical supports etc. cause cracks in the iron shielding between the calorimeters and the muon chambers as well as in the calorimeters themselves. The geometrical acceptance in the muon selection was reduced to exclude CD tracks pointing at cracks or regions with a relatively small amount of material between the CD and the muon chambers. It was checked that these fiducial cuts effectively remove leakage through cracks [7.8].

Non-interacting hadrons

Nuclear collisions causes hadrons to lose their energy in the material of the calorimeters and in the shielding of the muon chambers. This in contrast to muons which lose energy[28] due to ionization. On average, hadrons must traverse about 8 interaction lengths between CD and muon chambers. Test beam measurements show that the probability for each hadron (π's, K's) to reach the muon detector is less than 10^{-4} [7.9]. The background due to non-interacting hadrons is typically two orders of magnitude smaller than the previously discussed background from pion and kaon decays and is not considered to be significant.

---

[27] The property that, in general, cosmic rays are off-time with the beam-crossings, already gives a reduction by the second level trigger.

[28] In the UA1 detector, a muon has an average energy loss of 2.0±0.9 GeV.

Leakage of hadronic showers

Although most of the incident hadrons are fully absorbed in the calorimeters or in the shielding, very energetic hadrons may give rise to showers of secondary hadrons that are energetic enough to escape from the material. Charged hadrons can trigger the muon detector since the hardware trigger allows for a rather wide cone in which the muon chamber track has to point back to the vertex. In general shower leakage can be easily discriminated since it causes many hits in the muon chambers. In the cases were only very few hadrons escape from the shielding, the requirements of tight matching with CD tracks and association with the vertex are enough to remove this sort of background. Measurements with 2 - 10 GeV pion test beams together with the matching constraints show that the fraction of pions that will be misidentified as muons is less than 10^{-4} [7.9]. More energetic hadrons will deposit energy in the calorimeters in excess of what is expected for minimum ionizing muons.

Mis-association of CD tracks to tracks reconstructed in the muon chambers

Wrong matching of the track reconstructed in the muon chambers with a track reconstructed in the CD may introduce a mismeasurement of the muon momentum [7.10]. This source of background is studied *before* the muons from pion and kaon decays are removed from the data sample and was found to be much smaller than the 'direct' background due to $\pi^{\pm}$ and $K^{\pm}$ decays (~ 5 %) [7.5]. Removal of pion and kaon decays would introduce an error in the background analysis. In all the cases where mis-association occurs the rejection criteria for kinks etc. would be applied to the wrong CD track.

7.3.1 The general dimuon sample. The dimuon mass spectrum

Using the criteria of §7.2.1 the data from the 1988/1989 runs have been reduced to a set of 2810 dimuon events with $p_t^{\mu 1} \geq 3$ GeV/c and $p_t^{\mu 2} \geq 3$ GeV/c. Fig. 7.4 shows this sample as function of the dimuon mass.

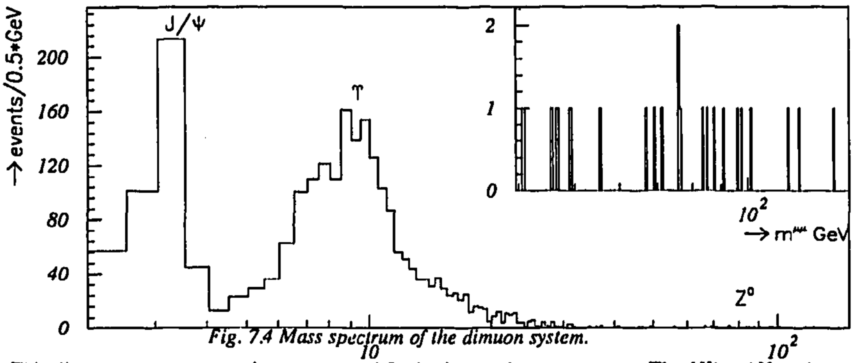

Fig. 7.4 Mass spectrum of the dimuon system.

This dimuon mass spectrum is not corrected for background or acceptance. The J/Ψ and ϒ peaks can clearly be seen above the heavy flavour and Drell-Yan continuum. The events above 50 GeV are Z^0 candidates with Drell-Yan events as background. The absence of a peak can be explained by the resolution of the detector: high P_t tracks are poorly measured. Only scanning and correcting on an event by event basis, will improve the distribution.

Resolution versus the number of points on a muon track.

Compared with the 1985 analysis, the dimuon mass spectrum demonstrates a decrease of the resolution of our detector. Since this is partly due to the different behaviour of the CD, the effect of the number of points on a muon track in the CD track is studied. In the selection a CD track is only accepted as a track if a minimum of 20 points are measured on that track.

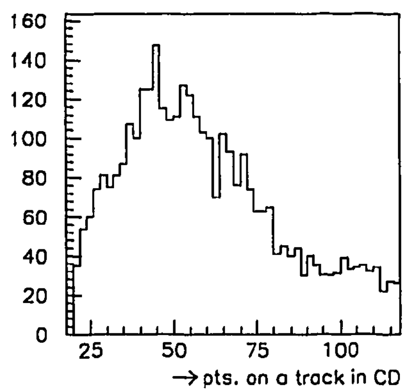

Fig. 7.5 Number of points on a CD track.

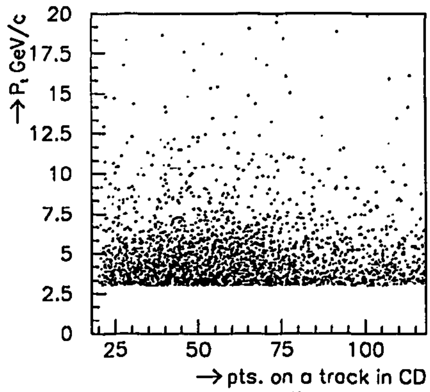

Fig. 7.6 Number of points on a CD track vs. P_t of that track for events with $P_t \geq 3$ GeV/c

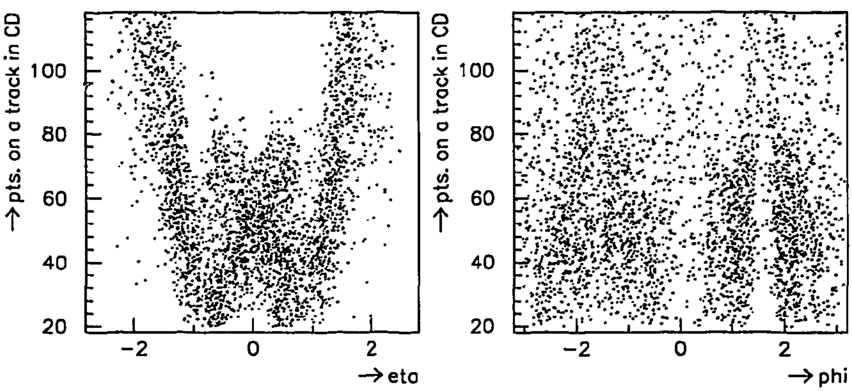

Fig. 7.7 The number of points on a CD track in relation to rapidity and phi

Fig. 7.5 shows the distribution of the number of points on a CD track. From this figure it can be seen that most muons have around 50 points per measured track in the CD. The long tail towards higher number of points is caused by lower energy muons which make relatively long tracks in the CD. Very few tracks have less than 20 points per track. In order to look for systematic effects the number of points per track was also displayed as function of eta and phi (Fig.7.7). These distributions ought to reflect the wire geometry in the CD (a track at large rapidity will in general pass more wires then at low rapidity). No systematic deviations could be found. Fig. 7.6 shows the number of points on a CD track versus the P_t. This plot, and also the plot in fig. 7.5, do not show any systematic effect. Also there is no correlation between the number of points on a CD track and the invariant dimuon mass, $\Sigma(P_t)$ and $\Sigma(E_t)$. It may be concluded that the selection cut of at least 20 points on a CD track is a reasonable choice.

Missing E_t.

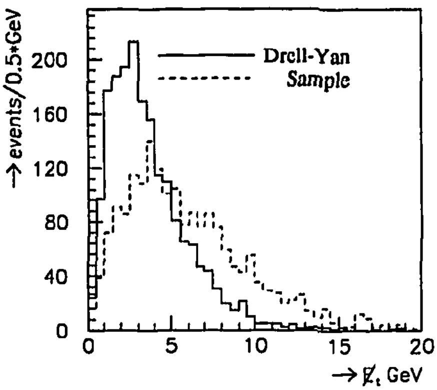

Fig. 7.8 Missing E_t for the dimuon sample and a Drell-Yan Monte Carlo (Both samples have the same number of events).

Next we investigate wether the missing E_t is a useful quantity to separate heavy flavour events from Drell-Yan and Υ events. Fig 7.8 shows the missing E_t distribution for events from the dimuon sample and a Drell-Yan Monte Carlo (scaled to the same number of events). In both cases only events with an invariant mass of $m^{\mu\mu} \geq 6$ GeV/c^2 are used. One expects no missing energy component for events from the Drell-Yan or Υ mechanisms, and at the parton level there is none in the events from the ISAJET Monte Carlo program. However, after the detector simulation one expects missing E_t even in Drell-Yan events, due to detector effects (energy smearing, cracks). One would expect, however, that this missing energy component would be less pronounced as in the case of processes where a real neutrino is involved such as heavy flavour decays. A clear difference between the two data sets in fig. 7.8 can be seen, but it is impossible to identify a value for missing E_t which could be used as a cut to isolate events from the Drell-Yan process. Apparently, in these dimuon events, the missing E_t is not much correlated to a neutrino but is coming from the detector resolution, statistical effects and the loss of energy into the beampipe. A conclusion is that this quantity is of no use in analyzing the *dimuon* samples.

Isolation.

In the 1985 analysis a powerful tool for identifying events was the isolation. Isolation can also be used to discriminate between muons from heavy flavour decays and muons from the Drell-Yan process or from decay of the J/Ψ or Υ. In the case of a b decay: $b \to c\ \mu^- \bar{\nu}_\mu$ one expects the muon and the jet from the c quark to go roughly in the same direction. However in the process $p\bar{p} \to \Upsilon \to \mu^+\mu^-$ one expects à priori that the muons are isolated i.e. not accompanied by energy nearby. In principle isolation can also be used to (partially) separate $b \to \mu^-\ \nu_\mu\ X$ and $c \to \mu^-\ \nu_\mu\ X$ since the muon from a c decay will on average be closer to the jet then for a b decay.

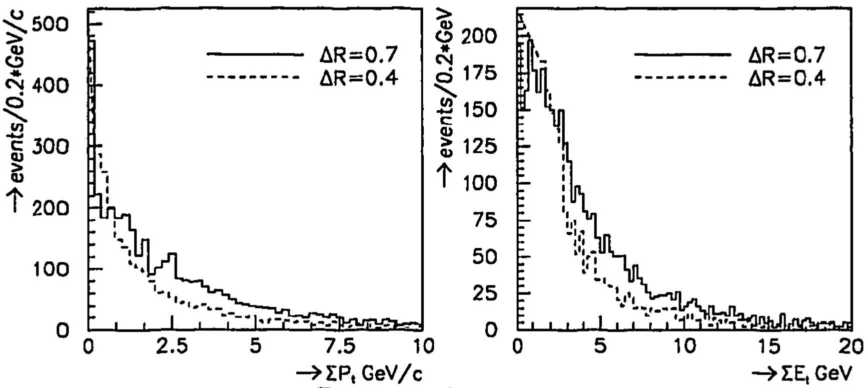

Fig. 7.9 $\Sigma(P_t)$ (left) and $\Sigma(E_t)$ (right) for both cones.

In the previous (≤1987) analysis a cone of ΔR=0.7 was used in the definition of isolation. In the present analysis a smaller size, ΔR=0.4, fits better the granularity of the calorimeter of the upgraded UA1 detector[29]. Therefore new and old results are not directly comparable.

In fig. 7.9 distributions are shown for the $\Sigma(P_t)$ and $\Sigma(E_t)$ for both cones around any of the muons from events of the dimuon sample, as measured in the CD and calorimeter. From neither of the four distributions subsamples can be recognized of isolated and non isolated events. To enhance the power of the isolation criterion the $\Sigma(P_t)$ and $\Sigma(E_t)$ ought to be combined (see def. of isolation) but here there seems to be a problem. In fig. 7.10 $\Sigma(P_t)$ versus $\Sigma(E_t)$ is plotted for both cones. In a perfect situation one expects a distribution around a straight line whose slope represents the fraction of charged particles in a jet. Fig. 7.10 shows little correlation between $\Sigma(P_t)$ and $\Sigma(E_t)$. Apparently the CD and calorimeter measurements are not correlated in this energy range. An explanation could be that the energy measurement for such 'low' P_t particles is too inaccurate in our detector. Furthermore it certainly doesn't help that the electromagnetic part of the energy flow is badly measured because of the absence of an electromagnetic calorimeter (and the presence of the coil).

[29] In those days it was expected that parts of the calorimeter would replace the old one during the cause of the run.

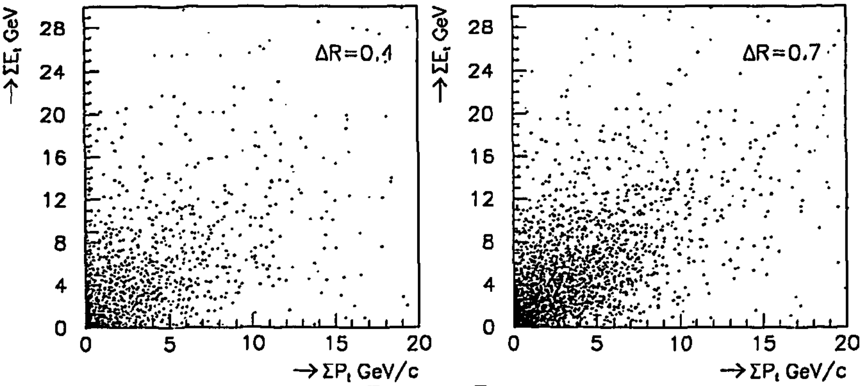

Fig. 7.10: $\Sigma(P_t)$ versus $\Sigma(E_t)$ for both cones

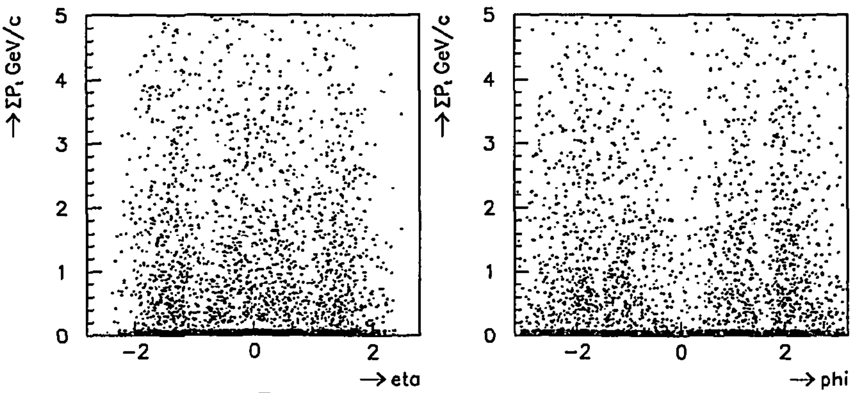

Fig. 7.11: $\Sigma(P_t)$ vs. rapidity (left) and phi (right) for a cone of ΔR=0.4.

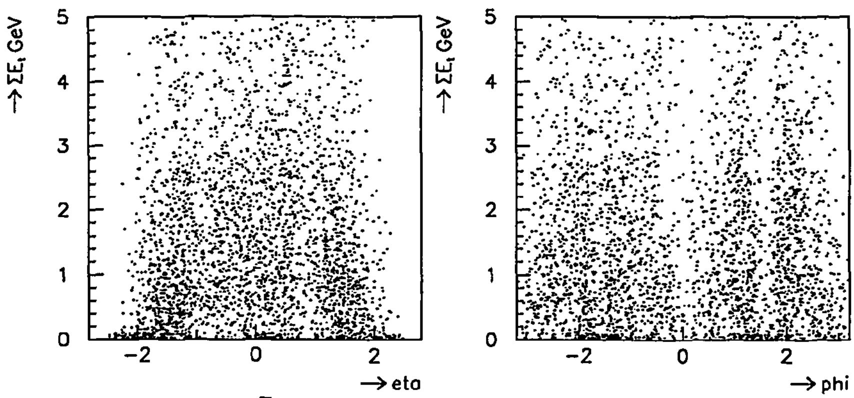

Fig. 7.12: $\Sigma(E_t)$ vs. rapidity (left) and phi (right) for a cone of ΔR=0.4.

To search for systematic effects $\Sigma(P_t)$ and $\Sigma(E_t)$ are shown against rapidity and phi in Fig. 7.11 and 7.12. These plots show some structure but this is not related to the lack of correlation in fig. 7.10. Note that in fig. 7.11 the influence of the coil is not present.

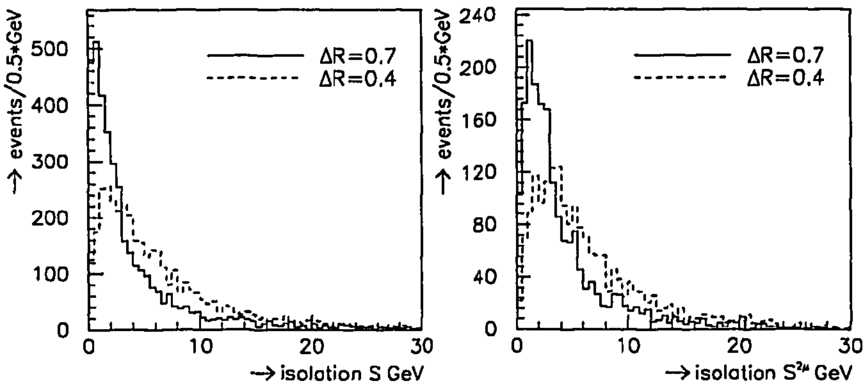

Fig. 7.13: S and $S^{2\mu}$ for cone sizes of ΔR=0.4 and ΔR=0.7.

Fig. 7.13 shows the isolation variables[30] S and $S^{2\mu}$ for cone sizes of ΔR=0.4 and ΔR=0.7. Comparison with the 1985 analysis shows that the shape of these curves is similar although less peaked around zero. Fig 7.14 shows the isolation $S^{2\mu}$ for the sample (solid line) and a Drell-Yan Monte Carlo calculation (dotted line) scaled to the same number of events. By definition Drell-Yan events produce muons which are isolated. Indeed all P_t or E_t activity can be found in the first 2 or 5 bins respectively of the distributions. This comparison gives a feeling where a cut could be made when using the $S^{2\mu}$ isolation. This plot shows that the isolation can be used to separate Drell-Yan events from heavy flavour events but compared with the 1985 analysis this separation is less effective. This plot suggests a cut of $S \leq 3$ GeV/c for selecting isolated events.

[30] It is verified that the isolation variable I has the same shape as the variable S. However on an event by event basis I and S differ due to the discrepancy of the relation $1.5\ \Sigma(P_t) = \Sigma(E_t)$ as indicated by fig. 7.10.

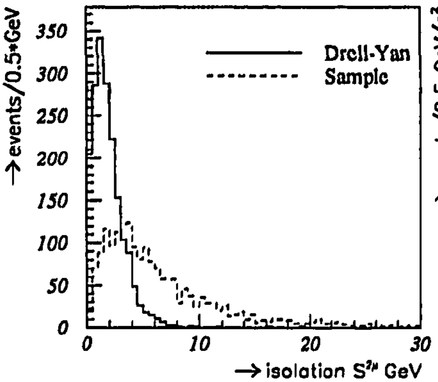

Fig. 7.14: $S^{2\mu}$ for Drell-Yan and Sample.

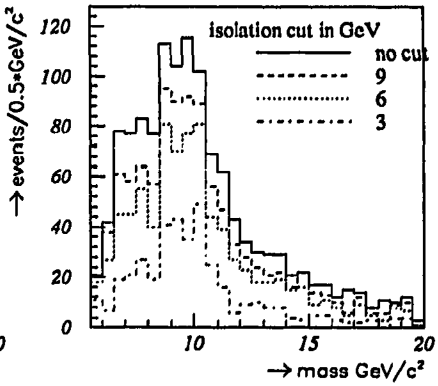

Fig. 7.15: mass of unlike sign dimuons for an isolation of 9, 6 and 3 GeV/c^2 (solid line = no cut).

Fig. 7.15 shows the mass spectrum of dimuons again but now only the unlike sign dimuons and starting at 6 GeV/c^2, so the J/Ψ is left out. The peak in the mass spectrum is the Υ resonance. Other contributions come from heavy flavour decays and Drell-Yan processes. A selection of isolated events $S^{2\mu} \leq 3$ GeV should enhance events from Υ decay and Drell-Yan, making the peak more pronounced. This effect is not as strong as in the 1985 analysis. Nevertheless it has been decided to make use of the isolation for this purpose.

7.3.2 *The J/Ψ sample.*

To study the J/Ψ resonance a special selection of events was made from the inclusive muon sample, as mentioned in §7.2.1. Only unlike sign pairs are selected, an additional mass cut of $2 \leq m^{\mu\mu} \leq 4.5$ GeV/c^2 was applied and tight matching was not required. These criteria resulted in a sample of 2194 events.

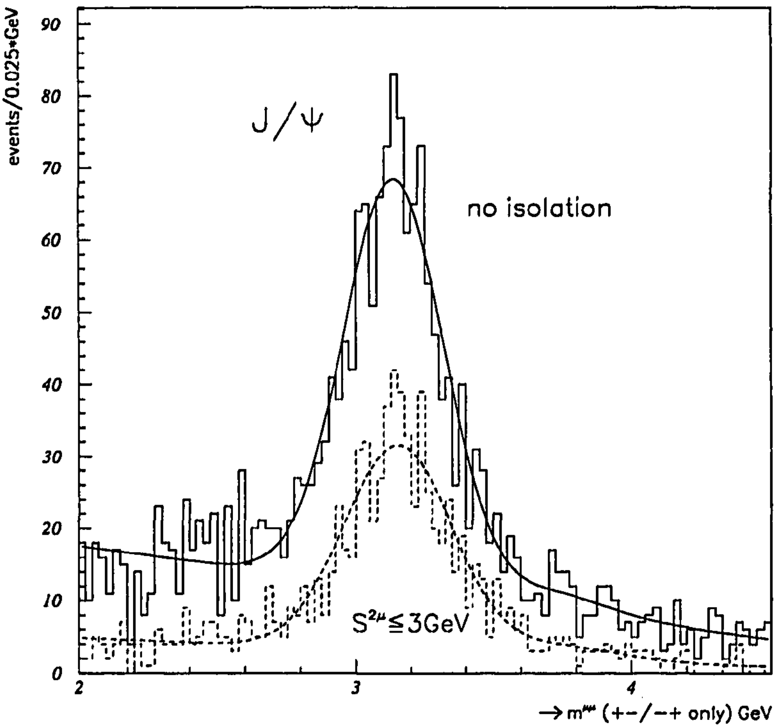

Fig. 7.16: The dimuon mass distribution of the J/Ψ sample together with a fit to the data. The dotted line is the sample after an isolation cut of $S^{2\mu} < 3$ GeV.

Fig 7.16 shows the dimuon mass distribution of the J/Ψ sample. In this figure two graphs are shown one for the sample as it was selected with the criteria listed above and one with an additional isolation cut of $S^{2\mu} \leq 3$ GeV. In both plots a curve is used to fit the data in order to determine the J/Ψ fraction. Ideally one would determine the shape of the background of the contribution of $q\bar{q}$ and from Drell-Yan with a Monte Carlo program and then use these distributions to fit the data. This would determine the contribution from J/Ψ alone and would lead to a determination of the cross-section for J/Ψ production at the collider. At the time of the preparation of this thesis this Monte Carlo program was not finished and could therefore not be used. In stead a fit is performed on the data assuming that $q\bar{q}$ and Drell-Yan form a linear background to the J/Ψ peak. The fitted curve is defined as the sum of two Gaussian shapes, for the J/Ψ and Ψ' with a linear background. All parameters are left free. The widths of both Gaussians have to be the same because they are dominated by the detector resolution. This restriction is necessary for the stability of the fit since the Ψ' contribution is small compared to the J/Ψ and background. The results of the fit are shown in table 7.1 and 7.2.

$$\begin{cases} \mathrm{Gauss}_1 = \dfrac{\mathrm{EXP}\left[-\frac{1}{2}\left(\frac{X-\mathrm{Mass}}{\sigma_e}\right)^2\right]}{\sigma_e\sqrt{2\pi}} \\ \mathrm{Gauss}_2 = \dfrac{\mathrm{EXP}\left[-\frac{1}{2}\left(\frac{X-\mathrm{Mass}-\mathrm{Delta}}{\sigma_e}\right)^2\right]}{\sigma_e\sqrt{2\pi}} \\ \mathrm{Background} = \dfrac{1.0-\mathrm{Constant}(X-3.25)}{2.5} \\ \mathrm{Prob.} = \mathrm{Norm}\,[\,(1-\mathrm{Fract})\,\mathrm{Gauss}_1 + \mathrm{Fract}\,\mathrm{Gauss}_2\,] + (1-\mathrm{Norm})\,\mathrm{Background} \end{cases} \tag{7.10}$$

Table 7.1 Results of a fit to the mass spectrum of J/Ψ sample.

Mass	3.146	±0.008	3.142	±0.008	3.097	fixed	3.13	± 0.01
Delta	-----	-----	0.589	fixed	0.589	fixed	0.41	± 0.12
σ_e	0.18	± 0.01	0.18	± 0.01	0.19	± 0.01	0.17	± 0.01
Norm	0.47	± 0.02	0.49	± 0.02	0.51	± 0.03	0.48	± 0.03
Fraction	0.00	fixed	0.04	± 0.03	0.06	± 0.03	0.07	± 0.04
Constant	0.44	± 0.04	0.47	± 0.05	0.45	± 0.05	0.46	± 0.04

Table 7.2 Results of a fit to the mass spectrum of J/Ψ sample, with an isolation cut $S^{2\mu} \leq 3$.

Parameter	single peak		fixed mass difference		fixed masses		all parameters are left free	
Mass	3.17	± 0.01	3.16	± 0.01	3.097	fixed	3.16	± 0.01
Delta	-----	-----	0.589	fixed	0.589	fixed	0.63	± 0.13
σ_e	0.20	± 0.02	0.19	± 0.01	0.19	± 0.02	0.19	± 0.02
Norm	0.63	± 0.03	0.66	± 0.03	0.70	± 0.03	0.66	± 0.03
Fraction	0.00	fixed	0.05	± 0.02	0.09	± 0.02	0.05	± 0.02
Constant	0.47	± 0.08	0.57	± 0.08	0.53	± 0.09	0.58	± 0.09

A second adjustment is made by fixing the mass difference of the J/Ψ and Ψ' to the published value [7.6]. This should remove any error in the absolute energy measurement. A third adjustment is made while keeping the masses of the J/Ψ and Ψ' fixed to the published [7.6] values of the world average. The numbers show a small enhancement of J/Ψ events due to the additional isolation cut. The Ψ' over J/Ψ ratio is stable at 0.08. This ratio does not represent the ratio of the cross-sections since the acceptances are not the same. A Monte Carlo acceptance calculation should give the definite answers.

At present no cross section calculation is available: since the J/Ψ sample consists of rather low P_t muons, the upgraded detector requires a completely new acceptance calculation. The acceptance calculation for the 1985 analysis can not be used for this purpose.

By looking at a sample of like signed dimuons in this mass range (mainly background), it is clear that the background can not be described by a linear function. This implies that such a description for the background is also not valid for the J/Ψ sample since background is invariant under the sign of the muons. The final results of this analysis will be published [7.11]

7.3.3 The Υ sample[31].

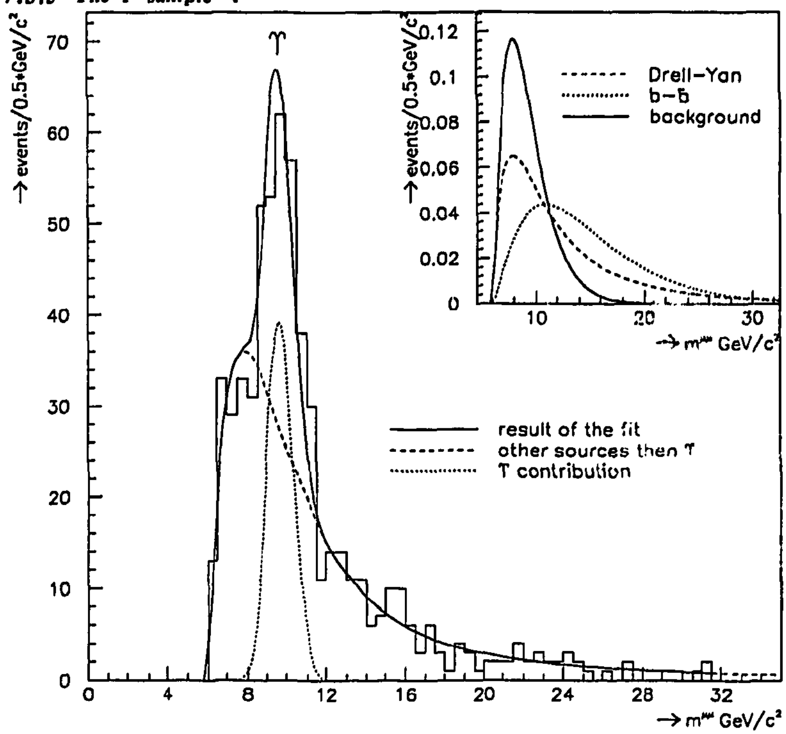

Fig. 7.17 Dimuon mass spectrum from the Υ subsample together with the fit. (The inset shows the shape of the contributions to the fit normalized to 1 event)

To study the Υ a subsample has been created from the total dimuon sample with the additional selection of *unlike* sign events, with isolation $S^{2\mu} \leq 3$ and mass $6 \leq m^{\mu\mu} \leq 35$ GeV/c^2. This selection should enhance Υ

[31]The results presented here are preliminary. For more details and final results the thesis of Alexander Moulin (Aachen) and a UA1 publication will become available.

and Drell-Yan events with respect to heavy flavour events. Also the process $p\bar{p} \to Z^0 \to \tau^+\tau^- \to \mu^+\bar{\upsilon}_\mu\ \upsilon_\tau\ \mu^-\ \upsilon_\mu\bar{\upsilon}_\tau$ could give events in this selection but the rate is expected to be smaller then 1 event and is neglected. The Υ sample consists of 585 events and is shown in fig. 7.17 as function of the dimuon invariant mass.

The following sources of dimuons contribute to the sample: Υ, Drell-Yan, heavy flavour and background events. To calculate contributions from the Υ, a maximum likelihood fit has been performed with the Monte Carlo[32] curves for the shape of the Υ, Drell-Yan, $q\bar{q}$ and background. The curve for background is calculated from real single muon data with a simulated second decay muon superimposed. The curve for the Υ is made up of 3 Gaussian shapes, at the mass of Υ, Υ' and Υ'' with widths of 0.5 GeV and a ratio of 1.0 : 0.3 : 0.15 in normalization. The result of the fit is rather insensitive to these ratios. The width of 0.5 GeV represents the resolution of the experiment.

Table 7.3 Fit of the Υ.

Source	#events	#events
Υ	116 ± 18	119 ± 18
Drell-Yan	239 ± 58	213 ± 58
$b\bar{b}$	143 ± 83	186 ± 64
background	87 ± 46	47 fixed

The results listed in the middle column are from a fit where all parameters are left free whereas for the right column the numbers come from a fit in which the background is kept at a fixed value. The second adjustment is expected to be better because the background of 87 events is considered too big. An estimation based on the 1985 analysis and other 1990 analyses suggests a value of 47. The second fit shows that the result for the Υ is not sensitive to the value for the background. In these fits, the Drell-Yan and $b\bar{b}$ are correlated while the Υ is not correlated to the other 3.

The Drell-Yan contribution comes out twice as big as in the 1985 analysis. This is not yet understood. One explanation is the similarity in shape of the Drell-Yan and $b\bar{b}$ contributions. This causes an uncertainty in the fit. Also the shape of the Drell-Yan and $c\bar{c}$ contribution are expected to show similarity [1985 analysis]. Due to the decreased power of the isolation cut a bigger $b\bar{b}$ contribution and a none-zero $c\bar{c}$ contribution could be a consequence. In the end more Monte Carlo calculations will have to clarify these points.

To have a better discrimination between the contributions from Drell-Yan and background in the fit one could study the sample of like sign dimuons in the same mass range. In this sample there is no Drell-Yan nor Υ. If one may assume that background for like sign and unlike sign dimuon events is the same this provides us with an additional handle on the background contribution for the Υ sample.

[32] The situation for the analysis of the Υ is better than for the study of the J/Ψ because some Monte Carlo data samples are available. The ISAJET [712] code has been used to generate Υ Drell-Yan and heavy flavour events which were subsequently passed through the detector simulation and analysis using the same cuts as for the data sample. The curves for these contributions can also be seen in the insert of fig. 7.7 normalized to 1 event.

7.3.4 The $b\bar{b}$ sample.

Semi leptonic decays of beauty quarks are the dominant source of high P_t muon pairs at the collider. So far dimuons from $b\bar{b}$ production were considered as background in the paragraphs where the J/Ψ and Υ were discussed. In this paragraph, however, we will concentrate on a determination of the fraction of dimuons from $b\bar{b}$ in a subsample of the general dimuon sample. This subsample was selected by applying a mass cut of $6 \leq m^{\mu\mu} < 40$ GeV/c^2 and demanding that both muons come from the same *primary* vertex. With this mass cut dimuons from the J/Ψ are removed as well as events originating from Z^0 decays. Also dimuons from beauty-charm cascades are suppressed this way.

The background sources for this subsample are the same as the ones discussed for the general dimuon sample. The main contribution to the background comes from pions and kaons decaying in flight into muons plus a (very) soft neutrino. This background was simulated by using single muon data and adding artificially a pion or kaon decaying in flight. This 100% background sample was then filtered through the analysis program with the same cuts as were used for the data, resulting in a set of events which will be discussed below. All other sources of background such as non-interacting hadrons, shower leakage and cosmics are negligible compared to the decay background.

The dimuon subsample is expected to contain, besides muons from $b\bar{b}$ and from decay background, events from Drell-Yan processes and Υ decays. It is possible to separate events from those last two classes from heavy flavour events by the use of non-isolation: a muon track is not generally expected to be embedded in a jet for Drell-Yan pairs and Υ decays although for the present detector configuration this criterion is not as powerful any more as it used to be for the old configuration as was discussed in §7.3.1.

For compatibility with earlier publications on this subject [715], the following[33] isolation definition is used in this and the next paragraph:

$$S^{2\mu} = \left(\sum_{\Delta R=0.7} E_t^{\mu 1} \right)^2 + \left(\sum_{\Delta R=0.7} E_t^{\mu 2} \right)^2 \qquad (7.11)$$

[33] compare with 7.5; $S^{2\mu} = 9(S^{2\mu})^2$

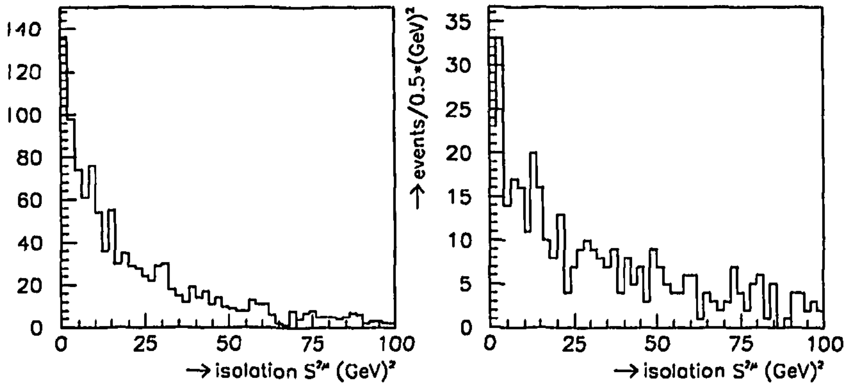

Fig. 7.19 and 7.20 $S^{2\mu}$ for unlike (left) and like sign events (right).

Another illustration of the deterioration can be seen in fig. 7.19 and fig 7.20 where isolation $S^{2\mu}$ is plotted separately for the unlike-sign and like-sign dimuons from the subsample. The cone size for the definition of isolation was ΔR=0.7. No like-sign dimuons can be produced through Drell-Yan and Υ decays. Some like-sign dimuons must be in the sample from $b\bar{b}$ decays where one b decays semileptonically and the other one decays into a c quark first and then the c quark decays semileptonically. From Monte Carlo calculations we know that this sort of decays amounts to ≈ 30% of the decays where both b's decay semileptonically into muons. In the 1985 analysis a clear excess could be seen in the unlike-sign distribution for events with an isolation $S^{2\mu} \leq 9$ (GeV)^2. This effect is no longer visible in fig. 7.19 and 7.20.

In spite of the fact that isolation is no longer a strong argument the cut of $S^{2\mu} \leq 9$ (GeV)^2 has been applied to the data in order to suppress events from Drell-Yan processes and Υ decays.

7.3.5 Beauty production cross-section.

To get an impression of the fraction of dimuons from beauty, events originating from charm decays should be removed. The relative transverse momentum p_t^{rel}, between the muon and its accompanying jet can be used to separate beauty and charm jets on a statistical basis. Since beauty particles are relatively heavy, the decay of the muon tends to have a larger p_t^{rel} than for charm particles.

The subsample of non-isolated ($S^{2\mu} \geq 9$ (GeV)^2) dimuon events was used in which a charged particle jet was clearly identified in the CD. At least one $p_t \geq 1$ GeV/c track other than the muon was required in the jet. The jet axis was required to lie within $\Delta R \leq 1.0$ of the muon. The E_t of a jet had to be at least 7 GeV.

The sample of events passing these criteria was compared to samples of Monte Carlo generated dimuon events from $b\bar{b}$ and $c\bar{c}$ which were processed through the detector simulation program and subsequently filtered through the same selection criteria as the data.

The first set of generated events using the ISAJET Monte Carlo program only became available at the very final stage of the preparation of this thesis. The detector layout has to be known very accurately and generating these events consumes large amounts of computer time. The production of these samples had therefore to be done outside CERN (in Lyon) and was somewhat delayed.

A thorough analysis in the context of this thesis is impossible but the distributions and a preliminary fit to the data allow for a first impression of beauty production measured during the 1988 and 1989 runs.

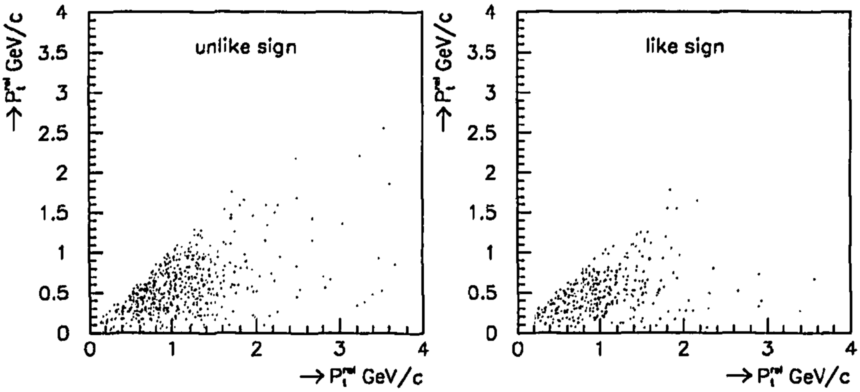

Fig. 7.21 p_t^{rel} vs. p_t^{rel} of data sample.

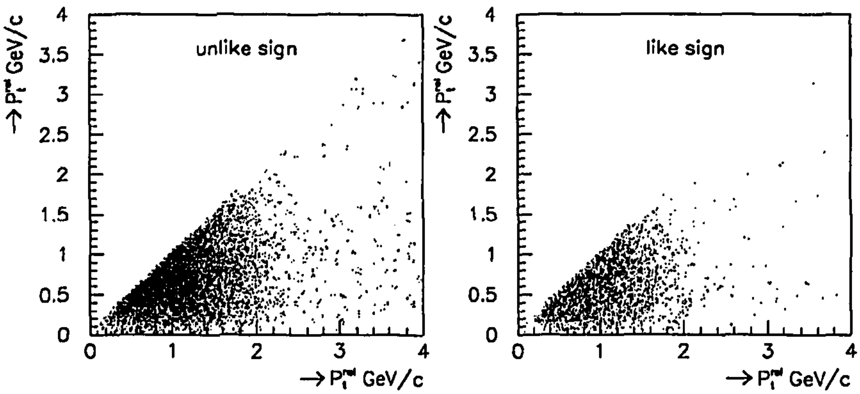

Fig. 7.22 p_t^{rel} vs. p_t^{rel} of $b\bar{b}$ Monte Carlo.

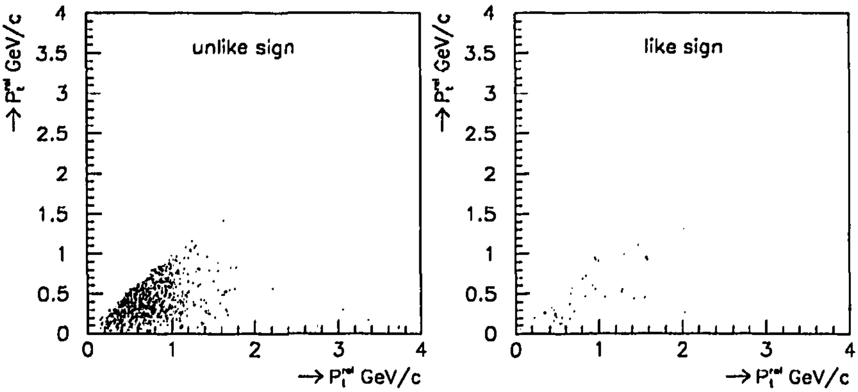

Fig. 7.23 p_t^{rel} vs. p_t^{rel} of $c\bar{c}$ Monte Carlo.

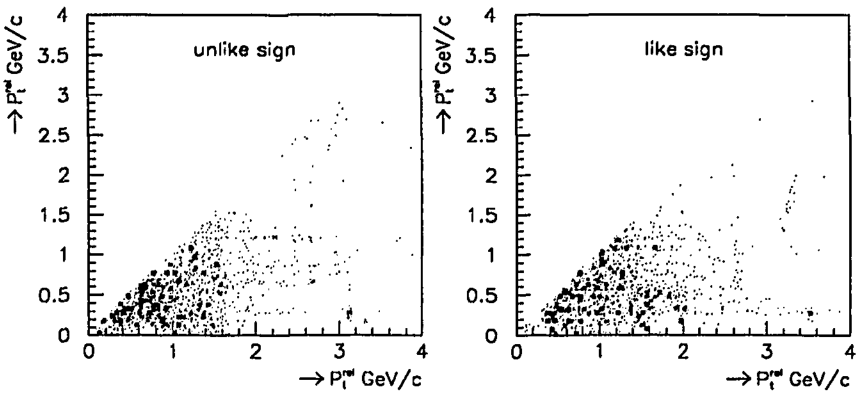

Fig. 7.24 p_t^{rel} vs. p_t^{rel} of background Monte Carlo.

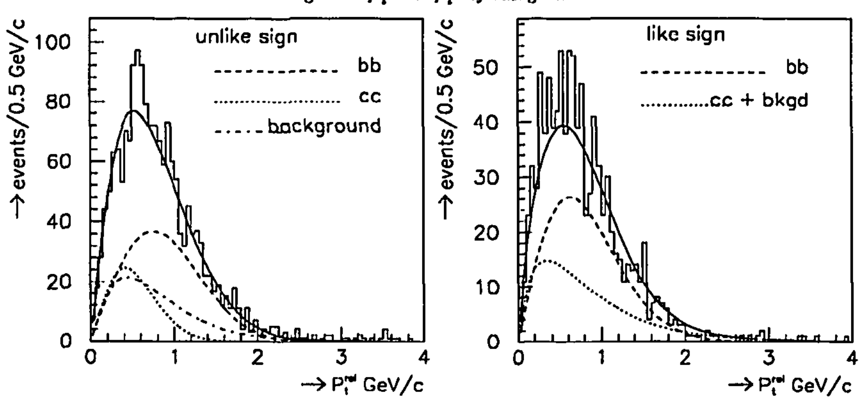

Fig. 7.25 and 7.26 Fit to p_t^{rel} spectra.

Figures 7.21 to 7.24 show distributions where the p_t^{rel} of one muon is along one axis and the p_t^{rel} of the other muon is along the other axis. They represent the data, the events from the $b\bar{b}$, $c\bar{c}$ and background Monte Carlo respectively. Like-sign dimuon and unlike-sign dimuons are shown in separate plots. It can be seen immediately that no (or almost no) like-sign dimuons can be expected from $c\bar{c}$.

In fig. 7.25 to 7.26 the distributions are shown which were used to fit the data. The distribution for events from the decay background come from a separate Monte Carlo described before. These p_t^{rel} distributions were fit to functions of the form

$$N(x,\vec{a}) = a_1 x^{a_2} \exp\frac{x^{a_3}}{a_4} \qquad x=p_t^{rel} \tag{7.12}$$

These shapes were then used to fit the data using a likelihood method, based on the MINUIT package [7.16]. The fits were done separately for like-sign and unlike-sign events because of the different characteristics for the $c\bar{c}$ contribution in both channels.

Table 7.4 Results of the fit to p_t^{rel} spectra for $f_{b\bar{b}}$.

fraction	like sign (353 events)	unlike sign (553 events)
$f_{b\bar{b}}$	0.642 ± 0.072	0.596 ± 0.036
$f_{c\bar{c}}$	0	0.104 ± 0.036
f_{bgrd}	0.358 ± 0.072	0.300 fixed

The results from the fit can be seen in table 7.4 where the fraction of events from $b\bar{b}$ ($f_{b\bar{b}}$), from $c\bar{c}$ ($f_{c\bar{c}}$) and from decay background (f_{bgrd}) are listed in percentages separately for the like-sign and unlike-sign dimuon data sample. The errors quoted are statistical errors as they come out of the MINUIT program. By varying f_{bgrd} and redoing the fit a systematic error of ± 4 % could be estimated.

The $b\bar{b}$ fraction in the subsample then follows from table 7.4 as

$$f_{b\bar{b}} = \frac{b\bar{b}}{all} = \frac{N_{like}}{N_{tot}} f_{b\bar{b}}^{like} + \frac{N_{unlike}}{N_{tot}} f_{b\bar{b}}^{unlike} = 61.4 \pm 3.6\ \% \tag{7.13}$$

Table 7.5 Results of the fit to mass spectrum of non-isolated dimuons.

fraction	central value	$f_{bgrd}+\Delta$	$f_{bgrd}-\Delta$
$f_{Drell\text{-}Yan}$	0.032 ± 0.012	0.037	0.030
f_{Υ}	0.010 ± 0.020	0.008	0.023
$f_{b\bar{b}}$	0.588 ± 0.024	0.516	0.618
f_{bgrd}	0.370 fixed	0.440	0.330

A separate study was done to establish the contribution from Drell-Yan processes and Υ decays to this subsample. For this, a fit was made to the mass spectrum of non-isolated ($S^{2\mu} \geq 9$ (GeV)^2) events. The result, shown in table 7.5, is that $\cong$ 3% (f_{DY}) of the dimuon events could still come from Drell-Yan processes and $\cong$ 1% (f_{Υ}) from the dimuons from Υ decays.

At this time only a rough estimate can be given for the beauty production cross-section at the collider. To get a more definitive number more study on the background is needed. This result is preliminary.

The cross-section can be calculated from

$$\sigma(p\bar{p} \rightarrow b \text{ or } \bar{b} + X,\ p_t^b \geq p_t^{min}) = \frac{\sigma_{MC}(p\bar{p} \rightarrow b \text{ or } \bar{b} + X,\ p_t^b \geq p_t^{min})}{\sigma_{MC}(p\bar{p} \rightarrow b\bar{b} \rightarrow \mu\mu)}\sigma_{UA1}(p\bar{p} \rightarrow b\bar{b} \rightarrow \mu\mu) \tag{7.14}$$

in which σ_{UA1} is the measured value and σ_{MC} comes from Monte Carlo calculations.

The measured dimuon cross-section is

$$\sigma_{UA1}(p\bar{p} \rightarrow b\bar{b} \rightarrow \mu\mu) = \frac{N^{observed}_{b\bar{b}\rightarrow\mu\mu}}{\int L dt} = \frac{533 \pm 34}{4.7\ pb^{-1}} = 113.4 \pm 7.2\ pb \tag{7.15}$$

with

$$N^{observed}_{b\bar{b}\rightarrow\mu\mu} = (N^{observed}_{\mu\mu} - N^{estimate}_{Drell\text{-}Yan} - N^{estimate}_{\Upsilon})\, f_{b\bar{b}} = (1 - f_{Drell\text{-}Yan} - f_{\Upsilon})\, N^{observed}_{\mu\mu}\, f_{b\bar{b}} = 533 \pm 34 \text{ events.} \tag{7.16}$$

using the numbers of table 7.5.

The values for $\sigma_{MC}(p\bar{p} \rightarrow b \text{ or } \bar{b} + X,\ p_t^b \geq p_t^{min})$ and $\sigma^{gen}_{MC}(p\bar{p} \rightarrow b\bar{b} \rightarrow \mu\mu)$ were calculated by A.Nisati and will be published shortly in a UA1 technical note. The ISAJET event generator was used for this calculation where p_t^{min} was set to 6.5 GeV/c ([34]). His predictions are

$$\sigma_{MC}(p\bar{p} \rightarrow b \text{ or } \bar{b} + X,\ p_t^b \geq 6.5) = 3.15 \pm 0.16\ \mu b. \tag{7.17}$$

$$\sigma^{gen}_{MC}(p\bar{p} \rightarrow b\bar{b} \rightarrow \mu^+\mu^-) = 133.1 \pm 1.1\ pb. \tag{7.18}$$

using the same event generator and the same detector simulation package.

To compare with the measured value, the Monte Carlo result has to be corrected for the reconstruction program (detector) efficiencies. Based on past experience we take a value of 90% for this efficiency. With this we can compute

$$\sigma^{event}_{MC}(p\bar{p} \rightarrow b\bar{b} \rightarrow \mu^+\mu^-) = \sigma^{gen}_{MC}(p\bar{p} \rightarrow b\bar{b} \rightarrow \mu^+\mu^-)\, 0.9 \left[\frac{BR(b \rightarrow \mu)}{0.12}\right]^2 = \begin{cases} 119.8 \pm 1.0\ pb & \text{for } BR(b \rightarrow \mu) = 0.120 \\ 86.5 \pm 0.7\ pb & \text{for } BR(b \rightarrow \mu) = 0.102 \end{cases} \tag{7.19}$$

in which within the brackets is corrected for different $b \rightarrow \mu$ branching ratios. LEP results suggests a $b \rightarrow \mu$ branching ratio of 10.2% compared with the collider measurements of 12%. For dimuons, this correction appears quadratically.

Substitution of the numbers in 7.14 now results in

$$\sigma(p\bar{p} \rightarrow b \text{ or } \bar{b} + X,\ p_t^b \geq 6.5\ GeV/c) = \begin{cases} 2.98 \pm 0.24^{stat} \pm 0.62^{sys}\ \mu b & \text{for } BR(b \rightarrow \mu) = 0.120 \\ 4.13 \pm 0.33^{stat} \pm 0.86^{sys}\ \mu b & \text{for } BR(b \rightarrow \mu) = 0.102 \end{cases} \tag{7.20}$$

[34] p_t^{min} is defined such that 90% of the muons satisfy this cut. For this subsample, p_t^{min} = 6.5 GeV/c.

The systematic error is estimated as follows:

Luminosity uncertainty	8%
QCD Theory (ISAJET)	15%
Isolation	10%
Decay background	2%
Efficiencies	5%
Miscellaneous	5%
$\sqrt{\sum c_i^2}$	21%

The value which was published by our collaboration [7.17] based on the data taken in and before 1985 was 2.4±1.3 μb (or 3.3±1.8 μb for BR(b → μ) = 0.102). From this it can be seen that a rough guess of the beauty production cross-section at the collider amounts to the same value as was quoted before.

Acknowledgements

Many people contributed to the work described in this thesis. I would like to mention some of them by name, at the risk of doing injustice to many others.

In the very first place I would like to thank my co-promoter Kors Bos. His support and advice have been very valuable for me and for the work I have performed. Moreover, I found it a pleasure to cooperate with him.
I thank my promoter Jos Engelen for his support and discussions.
I would like to thank Jheroen Dorenbosch, for his outstanding explanations of the experiment and the electronics.
I thank Dick Holthuizen for our discussions about physics.
I'd like to mention Bob van Eijk for his moral support and suggestions for the manuscript, Dirk Langerveld for his moral support and the exploration of other fields besides physics and our user friendly computer consultant Willem van Leeuwen, who kept smiling after my hundredth question about the systems.
It has been a pleasure to work in the UA1 collaboration and for this I would like to thank all people involved in UA1.
The FOM is gratefully acknowledged for its financial support and I would like to thank the NIKHEF(H) institute for the opportunity to participate in the UA1 experiment and to prepare this thesis.

References

[1.1] C. Rubbia, P. McIntyre and D. Cline, Proc. Int. Neutrino Conf., Aachen (1976).

[1.2] S. van der Meer, CERN ISR-PO Internal Report 72-31 (1972),
P. Bramham et al., Nucl. Instr. Methods 125 (1975) 201,
D. Möhl, G. Petrucci, L. Thorndahl and S. van der Meer, Phys. Rep. 58 (1980) 73.

[1.3] F.J. Hasert et al., Phys. Lett. 46B (1973) 121.

[1.4] S.L. Glashow, Nucl. Phys. 22 (1961) 579.

[1.5] S. Weinberg, Phys. Rev. Lett. 19 (1967) 1264.

[1.6] S. Salam, in 'Elementary Particle Theory', editors N. Svartholm, Almquist and Wiksell, Stockholm (1968) 367.

[1.7] P.W. Higgs, Phys. Lett. 12 (1964) 132.

[1.8] I.J.R. Aitchison and A.J.G. Hey, Gauge Theories in Particle Physics, Hilger, Bristol (1982),
L.B. Okun, Leptons and Quarks, North Holland Publ. Comp., Amsterdam (1981),
E.S. Abers and B.W. Lee, Phys. Reports 9C (1973) 1.

[1.9] C. Itzykson and J.B. Zuber, Quantum Field Theory, McGraw-Hill (1980),
W. Marciano and H. Pagels, Quantum Chromodynamics, Phys. Rep. 36 (1978) 137,
E. Reya, Perturbative Quantum Chromodynamics, Phys. Rep. 69 (1981) 195.

[1.10] D.P. Berger et al. (Mark J collaboration), Phys. Rev. Lett. 43 (1979) 830,
Ch. Berger et al. (Pluto collaboration), Phys. Lett. 86B (1979) 418,
R. Brandelik et al. (Tasso collaboration), Phys. Lett. 86B (1979) 243.

[1.11] ACOL (proposal), CERN/AA/LT-Note 21, 1982.

[1.12] G. Carron et al., Phys. Lett. 77B (1978) 353.

[1.13] C. Rubbia, Proceedings of the Lisbon High Energy Conference, Lisbon (1981).

[1.14] G. Arnison et al. (UA1 collaboration), Phys. Lett. 122B (1983) 103.
M. Banner et al. (UA2 collaboration), Phys. Lett. 122B (1983) 476.

[1.15] G. Arnison et al. (UA1 collaboration), Phys. Lett. 126B (1983) 398.
P. Bagnaia et al. (UA2 collaboration), Phys. Lett. 129B (1983) 130.

[1.16] G. Arnison et al. (UA1 collaboration), Phys. Lett. 158B (1985) 494.
G. Arnison et al. (UA1 collaboration), Phys. Lett. 172B (1986) 461.

[1.17] (CDF Collaboration) Phys. Rev. 64 (1990) 142.

[2.1] A. Astbury et al. (UA1 Collaboration, A 4π Solid-Angle Detector for the SPS used as a Proton-Antiproton Collider at a Centre-of-Mass Energy of 540 GeV, CERN/SPS/78-06 (1978).

[2.2] M. Banner et al. (UA2 Collaboration), Proposal to study Antiproton-Proton Interactions at 540 GeV CM Energy, CERN/SPSC/78-08 (1978),
B. Aubert et al. (UA3 Collaboration), Search for Magnetic Monopoles, CERN/SPSC/78-15 (1978),
M. Battiston et al. (UA4 Collaboration), The Measurement of Elastic Scattering and of the Total Cross-Section at CERN $\bar{p}p$ Collider, CERN/SPSC/78-105 (1978),
M.G. Albrow et al. (UA5 Collaboration), An Investigation of Proton-Antiproton Events at 540 GeV CM Energy with a Streamer Chamber Detection System, CERN/SPSC/78-70 (1978).

[2.3] M. Barranco Luque et al., Nucl. Instrum. Methods 176 (1980) 175.

[2.4] M. Calvetti et al., Nucl. Instrum. Methods 176 (1980) 255.

[2.5] M. Pimiä, Thesis University of Helsinki, HU-P-D45 Helsinki (1985).

[2.7] K. Eggert et al., Nucl. Instrum. Methods 176 (1980) 217.

[2.8] A. Astbury et al., Rutherford Report RAL-84-025 (1984).

[2.9] H. Lehmann and H. Reithler, UA1/TN81-20 (1981) (unpublished),
G. Hilgers et al., UA1/TN81-22 (1981) (unpublished).

[2.10] S. Cittolin and B. Löfstedt, Proceedings of the Topical Conference on the Application of Microprocessors to high Energy Physics Experiments, CERN Yellow Report CERN 81-07 (1981) 91.

[2.11] S. Cittolin, Proceedings of the International Conference on Instrumentation for colliding Beam Physics, SLAC, Stanford, SLAC-250 (1982) 151.

[3.1] S. Cittolin et al., MacUa1, The UA1 Macintosh-Based Development System, CERN-UA1 TN 90-01.

[3.3] L.O. Hertzberger, FAMP, NIKHEFH Technical Note TN 83-6 (unpublished).

[4.1] A. van Dijk, UA1 Technical Note TN 89-17 (unpublished).

[4.2] J.Dorenbosch, Triggers in UA1 and UA2, NIKHEFH Technical Note TN 85-14 (unpublished).

[6.1] I.J.R. Aitchison and A.J.G. Hey, Gauge Theories in Particle Physics, Hilger, Bristol (1982),
D.H. Perkins, Introduction in High Energy Physics, Addison-Wesley, Massachusetts, 1982.

[6.2] see [104], [105] and [106]

[6.3] M. Kobayashi, T.Maskawa, Prog. Theor.Phys. 49 (1973) 316

[6.4] C. Albarjar et al. (UA1 collaboration), Phys. Lett. 200B (1988) 380.

[6.5] see [1.17]

[6.6] T.D. Lee and C.S. Wu, Ann. Rev. Nucl. Sci. 16 (1966) 511.

[6.7] J. Ellis et al. Nucl. Phys. B 131 (1977) 285.
A. Ali and Z. Aydin, Nucl. Phys. B 148 (1979) 165.

[6.8] W.C. Louis et al. Phys. Rev. Lett. 56 (1986) 1027.

[6.9] V. Luth, Lifrtime of heavy flavour particles, Proc. Physisc in Collision 5 (Editions Frontieres Dreux).

[7.1] L. Pape, Basic HYDRA memory management, CERN-EP 77-6 (unpublished).

[7.2] M. Pimia, Thesis University of Helsinki, HU-P-D45 Helsinki (1985).

[7.3] K. Wacker, UA1 Technical Note TN 86-26 (unpublished).

[7.4] A.Geiser, UA1 Technical Note TN 90-59 (unpublished).

[7.5] N. Ellis and M. Jimack, UA1 Technical Note TN 86-79 (unpublished).

[7.6] M. Aguilar-Benitez et al. (Particle Data Group), Phys. Lett. 170B (1986).

[7.7] M.J. Corden and T. Markiewicz, UA1 Technical Note TN 85-59 (unpublished).

[7.8] M.J. Corden, UA1 Technical Note TN 85-60 (unpublished).

[7.9] R. Leuchs, Diplomarbeit RWTH Aachen 1982 (unpublished).

[7.10] M.J. Corden and P.M. Watkins, UA1 Technical Note TN 85-61 (unpublished).

[7.11] J/Ψ and Ψ' Production at the CERN $\bar{p}p$ Collider, will be published in Phys. Lett. B in 1990.

[7.12] C. Albarjar et al. (UA1 collaboration), Phys. Lett. B 186 (1987) 237.
C. Albarjar et al. (UA1 collaboration), Phys. Lett. B 186 (1987) 247.
C. Albarjar et al. (UA1 collaboration), Phys. Lett. B 209 (1988) 397.

[7.13] F.James, M.Roos, Computer Physics Communication 10 (1975) 343.

[7.14] H.Evans (UA1-CERN), privat communication.
C. Albarjar et al. (UA1 collaboration), Phys. Lett. B 223 (1988) 405.

Summary

In the years 1987-1989 the experiment ("UA1"), which is described in this thesis, has focused on measurements of reactions with muons. One can state that muons are a part of the 'fingerprint' of interesting reactions. In the practice of "UA1", recognizing this 'fingerprint' represents a puzzle because many (often more than one hundred) particles are produced in a collision between a proton and an anti-proton. In the experiment the properties (charge, energy, direction) of these particles are measured and subsequently the events are reconstructed. This results in several event samples corresponding to specific production mechanisms.

This thesis can be divided into two parts: the first part are the chapters 1-5 about the muon trigger of the UA1 experiment. This is a computer system that directly after a measurement reconstructs an event and checks for the presence of muons. If no muon is found the event is not considered anymore. In the other cases, the event is kept and written to magnetic tape. These tapes are used for further analysis. The necessity of a trigger follows from the fact that per second more than 250.000 interactions occur and only about 10 can be saved on tape. For this reason a trigger system is of critical importance: all events not written to tape are lost.

In chapter 2 the experiment is explained, after which in chapter 3 the ideas and constraints of the trigger are explained. Chapter 4 discusses the construction and functioning of the muon trigger and chapter 5 presents the performance.

The second part of this thesis consists of the chapters 6 and 7 containing physics analysis results from data collected with muon trigger. These results are explicitly obtained from events containing two muons. In chapter 6 the theory is briefly reviewed, after which in chapter 7 a discussion follows of the quality of the data and of the way the selections are done. Chapter 7 ends with a discussion of the J/Ψ and Υ samples and the cross-section of b-quark production.

Samenvatting

Met het experiment ("UA1"), dat in dit proefschrift beschreven wordt, heeft men zich in de jaren 1987-1989 toegelegd op het meten van reacties met muonen. Men kan stellen dat muonen een gedeelte zijn van de 'vingerafdruk' van interessante reacties. Het herkenen van die 'vingerafdruk' is in de praktijk van "UA1", een puzzel aangezien vele (vaak meer dan honderd) deeltjes worden geproduceerd in een botsing tussen een proton en een anti-proton. In het experiment worden de eigenschappen (lading, energie, richting) van deze deeltjes bepaald en vervolgens worden de gebeurtenissen gereconstrueerd. Dit resulteert in diverse samples die overeenkomen met specifieke productie mechanismes.

Dit proefschrift is in twee delen te splitsen: het eerste deel bestaat uit de hoofdstukken 1 tot 5 die gaan over de muonentrigger van het UA1 experiment. Dit is een computer systeem dat direct na een botsing de gebeurtenis doorrekent op zoek naar mogelijke muonen. Indien er geen muon gevonden wordt, dan wordt die gebeurtenis verder niet meer beschouwd. In het andere geval wordt de gebeurtenis bewaard door deze op magneetband weg te schrijven. Die magneetbanden worden dan later geanalyseerd. De noodzaak van een trigger systeem komt voort uit het feit dat er per seconde meer dan 250.000 botsingen plaats vinden terwijl er maar 10 kunnen worden bewaard. Hieruit blijkt tevens dat een triggersysteem van kritisch belang is: alle gebeurtenissen die niet naar magneetband zijn geschreven kunnen nooit meer worden gereconstrueerd.

In hoofdstuk 2 wordt het experiment toegelicht waarna in hoofdstuk 3 wordt ingegaan op de ideeën en randvoorwaarden van de dataverwerking in het algemeen en die van de trigger in het bijzonder. Hoofdstuk 4 behandelt de constructie en de werking van de muonentrigger en hoofdstuk 5 presenteert de resultaten.

Het tweede deel van dit proefschrift bestaat uit de hoofdstukken 6 en 7 die gaan over resultaten van fysica analyse van data die met de eerder beschreven muonen trigger genomen zijn. Het gaat hierbij uitsluitend over gebeurtenissen waarin twee muonen tegelijkertijd aanwezig zijn. In hoofdstuk 6 wordt de theorie toegelicht waarna in hoofdstuk 7 eerst een discussie volgt over de kwaliteit van de data en over de analyses. Verder worden in hoofdstuk 7 de J/Ψ en Υ samples besproken en de werkzame doorsnede van b-quarks productie gegeven.